1 3 MAR 2000

Fatigue of Beta Titanium Alloys

AFOSR Grant: F49620-96-1-0102

Final Technical Report
Period: 15 March 96 to 14 August 99

Principal Investigator:

Dr. K. S. Ravichandran
Associate Professor
Department of Metallurgical Engineering
412 Wm. C. Browning Building
The University of Utah, Salt Lake City, UT 84112

Submitted to:

Structural Materials Program, AFOSR/NA
Air Force Office of Scientific Research
801 N Randolph St. Rm. 732
Arlington, VA 22203-1977

20000324 045

DTIC QUALITY INSPECTED 3

REPORT DOCUMENTATION PAGE

AFRL-SR-BL-TR-00-

0078

Public reporting burden for this collection of information is estimated to average 1 hour per response, including the time for reviewing instruc ting and reviewing the collection of information. Send comments regarding this burden estimate or any other aspect of this collection of information, inclu te for Information Operations and Reports, 1215 Jefferson Davis Highway, Suite 1204, Arlington, VA 22202-4302, and to the Office of Management and Bud

1. AGENCY USE ONLY *(Leave blank)*	2. REPORT DATE	3. REPORT TYPE AND DATES COVERED
	March 2000	FINAL TECHNICAL REPORT 15 Mar 96 - 14 Aug 99

4. TITLE AND SUBTITLE
FATIGUE OF BETA TITANIUM ALLOYS

5. FUNDING NUMBERS
F49620-96-1-0102

61102F
2306/AX

6. AUTHOR(S)
K. S. RAVICHANDRAN

7. PERFORMING ORGANIZATION NAME(S) AND ADDRESS(ES)
UNIVERSITY OF UTAH
DEPARTMENT OF METALLURGICAL ENGINEERING
412 WM C BROWNING BUILDING
SALT LAKE CITY, UT 84112

8. PERFORMING ORGANIZATION REPORT NUMBER

9. SPONSORING/MONITORING AGENCY NAME(S) AND ADDRESS(ES)
AIR FORCE OFFICE OF SCIENTIFIC RESEARCH
801 N. RANDOLPH STREET, ROOM 732
ARLINGTON, VA 22203-1977

10. SPONSORING/MONITORING AGENCY REPORT NUMBER

11. SUPPLEMENTARY NOTES

12a. DISTRIBUTION AVAILABILITY STATEMENT
APPROVED FOR PUBLIC RELEASE, DISTRIBUTION IS UNLIMITED

12b. DISTRIBUTION CODE

13. ABSTRACT *(Maximum 200 words)*

A comprehensive investigation of the nature of fatigue in beta titanium alloys, especially in Ti-10V-3Fe-3Al alloy, emphasizing the crack initiation and crack growth aspects in controlled microstructural conditions, was performed. A detailed survey of literature of past work in this area, was also conducted. It has been found that the fatigue limit in this alloy is independent of the size, shape and volume fraction of the primary alpha particles. The matrix condition, as determined by the aging treatment had a strong influence on the fatigue behavior. It has been found that fatigue resistance could be improved only by controlling the aging treatment, that resulted in changes in the matrix microstructure. A mysterious fatigue behavior, exhibiting dual stress versus number of cycles to failure was also found in one microstructural condition. Aging treatments that resulted in omega phase precipitation, decreased the fatigue strength. In terms of fatigue crack growth response, omega phase increased the resistance to crack growth. Additionally, a strong sensitivity of fatigue crack growth to mean stress was also found with the omega precipitation. An evaluation of fatigue behavior of various titanium alloys was also made. It was concluded that microstructural refinement led to the minimal mean stress sensitivity in conventionally aged beta alloys, in comparison to other titanium alloys. The results are discussed in the light of microstructure, electron microscopy, fractography and quantitatitve determination of chemistry by energy-dispersive chemical analysis.

14. SUBJECT TERMS	15. NUMBER OF PAGES
	73
	16. PRICE CODE

17. SECURITY CLASSIFICATION OF REPORT	18. SECURITY CLASSIFICATION OF THIS PAGE	19. SECURITY CLASSIFICATION OF ABSTRACT	20. LIMITATION OF ABSTRACT
U	U	U	

Fatigue of Beta Titanium Alloys

AFOSR Grant: F49620-96-1-0102
(Final Technical Report, Period: 15 Mar 95 to 14 August 99)

Dr. K. S. Ravichandran (PI)
Department of Metallurgical Engineering, 412 Wm. C. Browning Building
The University of Utah, Salt Lake City, UT 84112

SUMMARY

A comprehensive investigation of the nature of fatigue in beta titanium alloys, especially in Ti-10V-3Fe-3Al alloy, emphasizing the crack initiation and crack growth aspects in controlled microstructural conditions, was performed. A detailed survey of literature of past work in this area, was also conducted. It has been found that the fatigue limit in this alloy is independent of the size, shape and volume fraction of the primary alpha particles. The matrix condition, as determined by the aging treatment had a strong influence on the fatigue behavior. It has been found that fatigue resistance could be improved only by controlling the aging treatment, that resulted in changes in the matrix microstructure. A mysterious fatigue behavior, exhibiting dual stress versus number of cycles to failure was also found in one microstructural condition. Aging treatments that resulted in omega phase precipitation, decreased the fatigue strength. In terms of fatigue crack growth response, omega phase increased the resistance to crack growth. Additionally, a strong sensitivity of fatigue crack growth to mean stress was also found with the omega precipitation. An evaluation of fatigue behavior of various titanium alloys was also made. It was concluded that microstructural refinement led to the minimal mean stress sensitivity in conventionally aged beta alloys, in comparison to other titanium alloys. The results are discussed in the light of microstructure, electron microscopy, fractography and quantitative determination of chemistry by energy-dispersive chemical analysis.

Fatigue of Beta Titanium Alloys

TABLE OF CONTENTS

	Summary	**2**
	Table of contents	**3**
I	Introduction	4
	I. 1. History of Beta Titanium Alloys	5
	I. 2. Scope of Research on Fatigue of β Titanium Alloys	5
II	Project Objectives	5
III	Results and Discussion	7
IV	References	8
V	List of Publications	9
Appendix I:	High-cycle Fatigue Resistance in Beta-Titanium Alloys	10
Appendix II:	Mechanisms of Fatigue Crack Nucleation at Surface and Subsurface Regions and Their Effect on Fatigue Life of Ti-10V-2Fe-3Al	17
Appendix III:	Fatigue Response and Micromechanisms of Crack Initiation in Ti-10V-2Fe-3Al	29
Appendix IV:	Effect of Mean Stress (Stress Ratio) and Aging on Fatigue-Crack Growth in a Metastable Beta Titanium Alloy, Ti-10V-2Fe-3Al	43
Appendix V:	Mean Stress (Tensile) Effects on Fatigue Crack Growth Behavior of Some Structural Titanium Alloys	56

I. INTRODUCTION

I. 1. History of Beta Titanium Alloys

Beta titanium alloys possess specific strength levels that are higher by at least a factor of two than those of high strength steels used in aerospace applications [1]. This advantage, combined with the better workability, strength-toughness combination, and resistance to stress corrosion cracking and hydrogen embrittlement make them contenders for critical applications such as springs, landing gear, engine nacelle structures, bolts etc. [2, 3]. In addition, β titanium alloys offer wide scope for property optimization by control of chemistry, processing and heat treatment similar to conventional α+β titanium alloys [4, 5].

With the exception of successful use in the SR-71 supersonic plane, application of beta titanium alloys in the past has been rather limited relative to other titanium alloys, owing to high manufacturing costs and the requirement of tight process control in making homogeneous alloys. These hurdles have been overcome in recent years and several beta alloys have been commercially available. These alloys possess homogeneity as well as good combination and reproducibility of properties. Notable among them are Ti-10V-2Fe-3Al (Ti-1023) and Ti-15Mo-2.7Nb-3Al-0.2Si (β–21S) produced by TIMET, Ti-3Al-8V-6Cr-4Zr-4Mo (Beta-C) introduced by RMI, Ti-11.5Mo-6Zr-4.5Sn (Beta III) introduced by Crucible, and Ti-5Al-2Sn-4Zr-4Mo-2Cr-1Fe (β-CEZ) introduced recently by CEZUS in France. These alloys reflect compositional balances that produce a desirable set of properties under selected processing/heat treatments.

I. 2. Scope of Research on Fatigue of β Titanium Alloys

From an applications perspective, damage tolerance and resistance to fatigue crack initiation as well as crack growth are the principal requirements for applications. Particularly in high strength applications, fatigue life spent in initiation and formation of a dominant small crack is relatively higher. However, there have been very few studies on fatigue [6-9] and fatigue crack growth behavior of beta alloys [10, 11]. Studies on fatigue resistance in terms of S-N behavior of smooth specimens are generally limited to examining the role of alloy chemistry and the effects of presence of notches.

From alloy design point of view, ample opportunities exist for property optimization and enhancement by microstructure control through processing and heat treatment in beta alloys. Due to restricted use in the past, only limited research [2, 3, 12, 13] has been performed in understanding the roles of processing and microstructure on the mechanical behavior of these alloys. In particular, systematic investigation of fatigue behavior including PSB formation, transition to a small crack and subsequent large crack growth, and the sensitivity of these stages to microstructural variables, is lacking. This knowledge is critical to develop alloys with improved fatigue resistance as well as to assess and predict fatigue lives of components in service, especially in high strength aerospace applications.

II. PROJECT OBJECTIVES

The general objective of the research program was to investigate the crack initiation and crack growth behavior of Ti-10V-2Fe-3Al alloy under controlled microstructural conditions. The conditions of the research were such that the overall results could be of immediate use with

respect to the application of this alloy in aerospace, yet the research was focused such that the microstructural variables could be isolated and the "cause and effect relationships" could be determined. The fatigue research in this class of alloy, in the past was largely engineering in nature, merely producing experimental data with almost no detail on the underlying mechanisms or the desirable microstructures that produced increased fatigue resistance. Such effects can be understood only by quantitative correlations between microstructural parameters and experimental data. In this regard, the specific objectives of this program were:

(i) To identify primary microstructural parameters that control endurance limit ($\Delta\sigma_e$) in fatigue, isolating the tandem effects of several microstructural variables (β grain size, size and interparticle spacing of primary alpha (α_p) or secondary alpha (α_p)) on fatigue behavior.

(ii) To determine the fatigue crack growth response under different aging conditions and mean stress levels, to see if the aging process alters the mean stress sensitivity of fatigue crack growth behavior

(iii) To review the existing literature data, including (a) smooth fatigue behavior of several β-Ti alloys and see if the general patterns found in the data correlated with the fatigue results of the present research, and (b) fatigue crack growth data of all the titanium alloys as a group and determine what microstructural variable caused the sensitivity to mean stress.

In line with the primary objectives set out above, this report summarizes the results of the basic research program conducted during the period: 15 March 1996 through 14 August 1999.

III. RESULTS AND DISCUSSION

The complete documentation of objectives, materials, experimental procedure, results and discussion as well as conclusions of specific technical aspects investigated in this program is available in detail in the publications resulting from this work. These publications are included in Appendices I through V and are listed in the following.

Appendix I **High-cycle Fatigue Resistance in Beta-Titanium Alloys**

Appendix II **Mechanisms of Fatigue Crack Nucleation at Surface and Subsurface Regions and Their Effect on Fatigue Life of Ti-10V-2Fe-3Al**

Appendix III **Fatigue Response and Micromechanisms of Crack Initiation in Ti-10V-2Fe-3Al**

Appendix IV **Effect of Mean Stress (Stress Ratio) and Aging on Fatigue-Crack Growth in a Metastable Beta Titanium Alloy, Ti-10V-2Fe-3Al**

Appendix V **Mean Stress (Tensile) Effects on Fatigue Crack Growth Behavior of Some Structural Titanium Alloys**

IV. REFERENCES

(1) R. R. Boyer, J. Met., 1980, Vol. 32, p. 61

(2) R. R. Boyer, in Beta Titanium Alloys in the 1990's, edited by D. Eylon, R. R. Boyer and D. A. Koss, TMS-AIME, Warrendale, PA, 1993, p. 335

(3) A. Takemura, H. Ohyama, T. Abumiya and T. Nishimura, in Ref. 2, P. 15.

(4) T. W. Duerig and J. C. Williams, in Beta Titanium Alloys in the 80's, edited by R. R. Boyer and H. W. Rosenberg, TMS-AIME, Warrendale, PA, 1984, p. 19

(5) S. Ankem and S. R. Seagle, in Ref. 4, p. 107

(6) W. J. Porter and D. Eylon, in Ref. 2, p. 273

(7) R. Chait and T. S. SeSisto, Metall. Trans., Vol. 8A, 1977, p. 1017

(8) G. W. Kuhlman, in Ref. 2, p. 485

(9) F. A. Crossley, in Ref. 4, p. 349

(10) T. W. Duerig, J. E. Allison and J. C. Williams, Metall. Trans., Vol. 16A, 1985, p. 739.

(11) D. Grandemange, Y. Combres and D. Eylon, in Ref. 2, p. 227.

(12) G. T. Terlinde, T. W. Duerig and J. C. Williams, Metall. Trans., Vol. 14A, 1983, p. 2101.

(13) G. T. Terlinde, H. J. Rathjen and K. H. Schwalbe, Metall. Trans., Vol. 19A, 1987, p. 1037.

V. LIST OF PUBLICATIONS

1. S. K. Jha and K. S. Ravichandran, "Effect of Aging on Mean Stress(Stress Ratio) Dependence of Fatigue Crack Growth in a Beta-Titanium Alloy: Ti-10V-2Fe-3Al", **Metallurgical and Materials Transactions, Vol. 31A, 2000, pp. 703-713**

2. S. K. Jha and K. S. Ravichandran, "High-Cycle Fatigue Resistance of Beta-Titanium Alloys," **Journal of Metals, JOM, March 2000, pp. 30-35**

3. P. S. Shankar and K. S. Ravichandran, "Effect of ω-Phase on the Tensile Deformation and Fatigue Behavior of Ti-10V-2Fe-3Al Beta-Titanium Alloy**", Submitted for Publication to Materials Science and Engineering, 2000**

4. S. K. Jha and K. S. Ravichandran, "The Mean Stress Dependence of Fatigue Crack Growth Behavior in the Beta-Titanium Alloy: Ti-10V-2Fe-3Al: The effect of aging", Presented at the ***Symposium on Fatigue of Titanium Alloys, TMS Fall Meeting, 11-15 October, 1998,*** *Chicago, Illinois, USA*, and Published in the Proceedings, "**Fatigue Behavior of Titanium Alloys**," edited by R. R. Boyer, D. Eylon and G. Lutjering, The Minerals, Metals and Materials Society, 1999, pp. 37-49

5. P. S. Shankar and K. S. Ravichandran, "Microstructural Aspects of Fatigue Crack Initiation and Growth in Ti-10V-2Fe-3Al", Presented at *the **Symposium on Fatigue of Titanium Alloys** TMS Fall Meeting, 11-15 October, 1998, Chicago, Illinois, USA*, and Published in the Proceedings, "**Fatigue Behavior of Titanium Alloys**," edited by R. R. Boyer, D. Eylon and G. Lutjering, The Minerals, Metals and Materials Society, 1999, pp. 135-147

6. K. S. Ravichandran and S. K. Jha, "Mean Stress Effects on Fatigue crack growth of titanium Alloys: Overview of mechanics and materials issues", Presented at the ***Symposium on Fatigue of Titanium Alloys, TMS Fall Meeting, 11-15 October, 1998,*** *Chicago, Illinois, USA*, and Published in the Proceedings, "**Fatigue Behavior of Titanium Alloys**," edited by R. R. Boyer, D. Eylon and G. Lutjering, The Minerals, Metals and Materials Society, 1999, pp. 57-73

7. S. K. Jha and K. S. Ravichandran, "Mechanisms of Fatigue Crack Nucleation at Surface and Subsurface Regions and Their Effect on Fatigue Life of Ti-10V-2Fe-3Al", Presented at ***Small Fatigue Cracks: Mechanics and Mechanisms Conference, 6-11 December, 1998,*** *Kona, Hawaii, USA*, and Published in the Proceedings, "**Small Fatigue Cracks: Mechanics, Mechanisms and Applications**," edited by K. S. Ravichandran, R. O. Ritchie and Y. Murakami, Elsevier, 1999, pp. 187-197

Appendix I

High-Cycle Fatigue Resistance in Beta-Titanium Alloys

High-Cycle Fatigue Resistance in Beta-Titanium Alloys

S.K. Jha and K.S. Ravichandran

A survey of high-cycle fatigue data for commercial β-titanium alloys was conducted to rationalize the wide variations in fatigue resistance even at similar tensile-strength levels. It was found that fatigue behavior, especially the endurance limits, for various alloy compositions can be roughly grouped into three classes on the basis of processing, heat treatment, and resulting microstructure. The implications of such classification on microstructure control for increased fatigue resistance is discussed.

INTRODUCTION

The use of titanium alloys in structural members in many aerospace applications has been steadily increasing.[1-3] This is not only made possible by their excellent specific stiffness (the ratio of elastic modulus to density) and specific strength (the ratio of strength to density), but also by the flexibility afforded by these alloys in terms of microstructure design and control to achieve a balance of mechanical properties. The β-titanium alloys have received increased emphasis as one of the most desirable materials for high-strength applications, such as landing gear, truck beam, springs, struts, and engine nacelle assemblies.[4,5] This is made possible by the achievement of strength and toughness levels comparable to those of high-strength steels.

The β-titanium alloys offer the ability to optimize microstructure and properties over a wide scope through various mechanical processing and heat-treatment procedures and combinations.[6-8] A β-titanium alloy is defined as an alloy in which the β-phase is retained 100% on cooling (air cooling or higher cooling rate) to room temperature from the β-phase field. The stability of the β-phase in the β-titanium alloys is measured in terms of molybdenum-equivalent,[5,9] which increases with an increase in the amount of the β-stabilizing alloying elements, such as Mo, V, Nb, Fe, Ta, and W. Typically, a β-titanium alloy is either processed (forged, extruded, or rolled) in the β-phase field (β-process) or, alternatively, β-processed followed by an α+β finish process (α+β process). Following the processing step, the alloy can be either directly aged or solution treated (either above or below the β-transus temperature of the alloy) and then aged. The degree of mechanical deformation and the time in the processing steps influence the resulting microstructure and, hence, the properties.

Fatigue resistance, particularly the endurance limit, is an important design consideration in aerospace applications. Most engineering design considerations involve either the endurance limit or some limiting stress range below which the component would not fail at some number of prescribed cycles specific to a given application. In either case, the common curve relating stress range ($\Delta\sigma$) to number of cycles to failure (N_f), known as the S-N curve, is often the first set of data that the engineer is very likely to consider. Therefore, the nature of the S-N curve, and especially the effects of processing, microstructure, notch geometry, and mean stress (stress ratio) on the curve, is of interest from the point of view of alloy development and microstructure optimization.

The β-titanium alloys offer the ability to optimize microstructure and properties over a wide scope through various mechanical processing and heat-treatment procedures and combinations.

Some fatigue data on β-titanium alloys have been developed. Much of this information is engineering data in nature, with limited attempts to control, vary, or correlate the microstructure variables to fatigue resistance. A cursory examination of some of the data indicate that there exists no simple correlation (unlike the common observation[10,11] that the endurance limit is anywhere between 0.5 to 0.8 times that of the tensile strength for structural alloys) between the endurance limit and the tensile strength in β-titanium alloys. Therefore, the motivation for this overview is to qualitatively determine the factors affecting fatigue behavior or the endurance limit. Specifically, the high-cycle fatigue (HCF) data of β-titanium alloys available in literature is rationalized from a microstructural perspective. By classifying the microstructures into three different classes, it is shown that the fatigue behavior can be qualitatively related to the general microstructural characteristics, leading to a general identification of processing/heat treatment options for increased fatigue resistance.

CLASSIFICATION

The six commercial β-titanium alloys that are considered in this overview are Ti-8V-8Mo-2Fe-3Al (Ti-8-8-2-3), Ti-10V-2Fe-3Al (Ti-10-2-3), Ti-11.5Mo-6Zr-4.5Sn (Beta III), Ti-3Al-8V-6Cr-4Mo-4Zr (Beta C), Ti-15V-3Cr-3Sn-3Al (Ti-15-3-3-3), and Ti-5Al-2Sn-2Cr-4Mo-4Zr-1Fe (Beta-CEZ). Fatigue-test data for these alloys have been reported,[12-19] mostly for R = 0.1 and R = −1. Since the data generated under R = −1 are few, only smooth-specimen fatigue data generated under R = 0.1 are considered.

The β-titanium alloys for which fatigue data[12-19] have been available were divided into three broad classes: A, B, and C (Figure 1). The division is solely based on the processing history and the resulting microstructures, so that the fatigue data can be compared in a given processing/microstructure class. These classes constitute the most common of the processing and heat-treatment combinations that are used in commercial β alloys. The classifications differed in terms of the primary processing or treatment that most affected the resulting microstructure.

Table I provides a compilation of the alloys, along with their molybdenum equivalents, β-transus temperatures, and processing and heat-treatment histories as well as the tensile properties and the endurance limits (σ_{max} at 10^7 cycles) in fatigue. For those alloys where microstructural details are not available, a qualitative estimate of the microstructure was made based on the reported processing and heat-treatment information and the literature on general microstructural studies of the alloy in question. All the microstructures have been designated A1 to A10, B1 to B13, and C1

to C14, and they will hereafter be referred to by these designations.

β-Processed and Directly Aged Microstructures

The class A microstructures in the different β-titanium alloys were mainly generated by processing (forging, rolling, and extrusion) above the β-transus, followed by air cooling (AC) or water quenching (WQ). This was followed by aging, usually at 400–600°C for up to several hours, depending on the alloy composition. While the resulting microstructures are essentially two phase (α+β), the size of α particles would be expected to depend on the cooling rate after β-processing, because the nucleation and growth of α particles would be affected by the cooling rate. In most cases, however, the resulting microstructures consist of a high volume fraction of very finely distributed α particles (Figure 1a).[16] Since the ultimate tensile strength (UTS) data for A1 were not available, a UTS value of 1,050 MPa was assumed from the given yield strength (Table I).

α+β Solution-Treated and Aged Microstructures

The class B microstructures were generated by processing (forging, rolling, or extrusion) above the β-transus with or without the α+β finish process and cooling to room temperature by AC or WQ. This was followed by a solution treatment below the β-transus temperature (i.e., in the α+β phase field [sub-β field]) for 0.5–2 h, followed by AC or WQ, then aging at 400–600°C for several hours. The resulting microstructures generally consist of coarse primary-α (α_p) and uniformly distributed, fine, secondary-α (α_s) in transformed β-matrix (Figure 1b).[20]

For a given alloy in this class, the distribution of α_s is expected to be coarser as compared to that obtained by the class A treatment. This is due to a relatively lower degree of supersaturation of β-matrix with respect to α-stabilizing elements at the aging temperature as well as the reduction in the driving force for nucleation caused by the primary-α formation. In some cases, depending on the processing and the α+β solution-treatment conditions, a heterogeneous distribution of α_s may also occur by preferential nucleation at the α_p-matrix interface and at the β-grain/subgrain boundaries.

Super-β Heat-Treated and Aged Microstructures

The class C microstructures were generated by processing (forging, rolling, or extrusion) above the β-transus and cooling to room temperature by AC or WQ. This was followed by a solution treatment above the β-transus for 0.5–2 h followed by AC or WQ, then aging at 400–600°C for several hours. The resulting microstructures generally consist of a nonuniform distribution of α phase in the transformed β matrix as well as continuous-grain-boundary α[6,19,21] in some alloys (Figure 1c). There are a few exceptions to this generality, depending on the degree of recovery/recrystallization that occurred during the β-solution treatment. For example, in the case of Ti-15-3-3-3,[22] a very uniform distribution of α was found after solution treatment at 790°C followed by air cooling and aging at 540°C for 8 h, due to negligible recovery/recrystallization at the solution-treatment step. Similar results were reported in another study on an alloy of similar composition.[23] Since the UTS data for the microstructure C1 were unavailable, a UTS of 1,000 MPa was assumed from the given yield strength (Table I).

S-N FATIGUE BEHAVIOR

The reported fatigue data for Ti-10-2-3, Beta-III, and Ti-8-8-2-3 are compiled in Figure 2a, b, and c, respectively, in terms of the maximum stress (σ_{max}) versus the number of cycles to failure (N_f). The corresponding UTS levels are also indicated. In the case of Beta-CEZ, Beta C, and Ti-15-3-3-3, only the fatigue limits were available, and these are included in Table I. From Figure 2, it is evident that there is the possibility of varying HCF behavior over a wide range by varying microstructure. For example, in Figure 2a, the fatigue limit (σ_{max} at 10^7 cycles) varied from 725 MPa to 1,000 MPa, a change of about 38%.

Ti-10-2-3

In Ti-10-2-3, the microstructures belonging to class A (A3, A4, and A5) show the highest fatigue limits (Figure 2a), followed by those belonging to class B (B1, B2, B3, B4, B5, and B6). The processing and available microstructural information for A2 through A4 (Table I) indicate that these were given identical β-processing treatments prior to aging. Therefore, these specimens had identi-

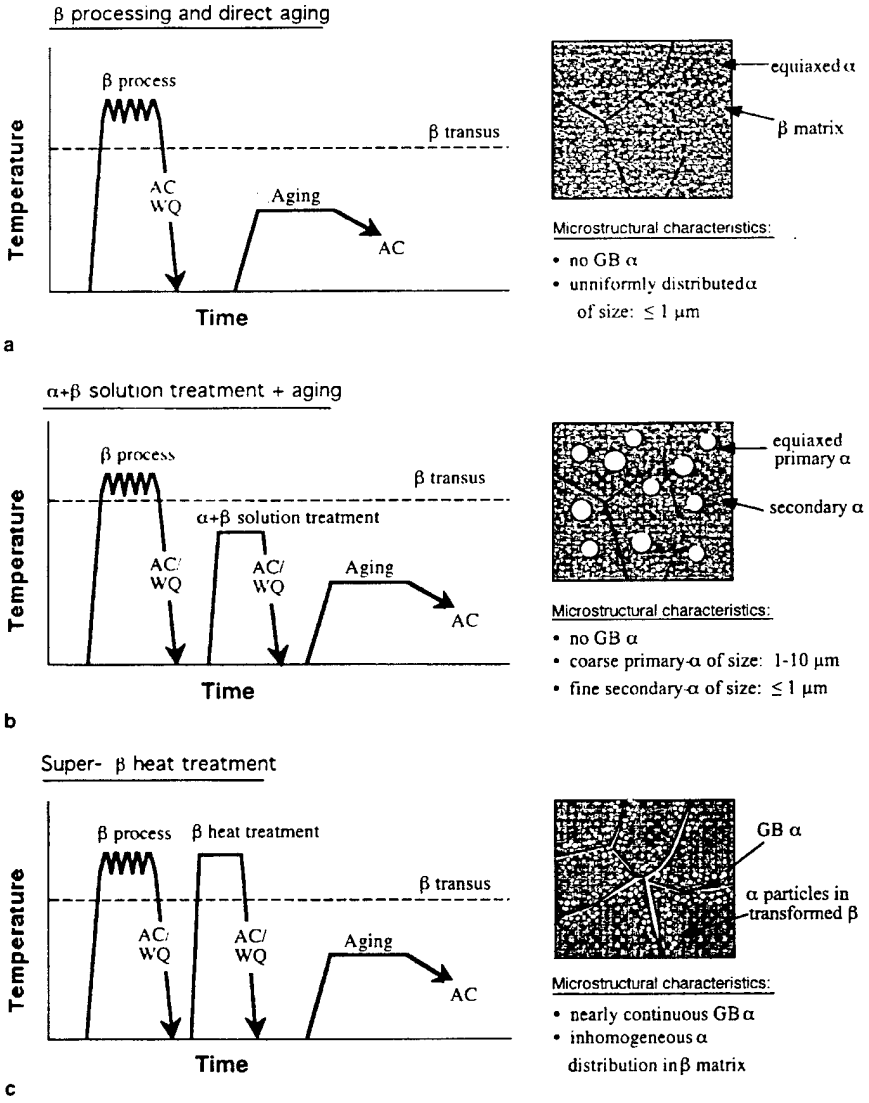

Figure 1. Processing, heat treatment, and microstructure of β-titanium alloys in (a) class A, (b) class B, and (c) class C.

cal β-grain structures, except for the difference in size and distribution of α caused by the differences in the aging treatments. [In this study, when α particles were formed in a single-step heat treatment, they are denoted as α, but when they were formed in two steps (primary/secondary α+β heat treatment) they are denoted as primary-α (α_p) and secondary-α (α_s).] Thus, it seems reasonable to infer that the variations in fatigue limits corresponded to the variations in the characteristics of α particles.

On the other hand, microstructures B1 and B3 showed similar fatigue limits in spite of the different aging treatments (Table I) and the consequent difference in strength levels. However, these microstructures had identical processing and solution-treatment steps. This indicates that the α_p distribution (the size and the spacing of α_p) or the β-grain size, which are expected to be identical in B1 and B3, controlled the fatigue limits of these cases. However, such a rationalization could not be applied to B4, B5, and B6 because they showed different fatigue limits, even though their primary treatments were nearly the same. Since aging-treatment temperatures varied for these microstructures, the only way to explain the variations in fatigue behavior is on the basis of α_s characteristics. Therefore, either the characteristics of α_p or α_s can control fatigue behavior in this class of microstructures, depending on heat treatment. Regardless of this duality, all of the class B microstructures of this alloy showed relatively lower fatigue limits when compared to the class A microstructures.

Beta-III

There were only two classes (A and C) of microstructures in this alloy for which fatigue data were reported. The microstructures belonging to class A (A6 and A7) showed relatively higher fatigue limits (Figure 2b) than those belonging to class C (C5, C6, C7, and C8). A6 and A7 had slightly different fatigue limits (Figure 2b), even though their aging treatments were similar. However, the same aging treatment can produce differences in the characteristics of α due to the differences in the extrusion temperature, as noted for these microstructures (Table I). Therefore, fatigue behavior can still be considered controlled by the characteristics of α particles, including distribution, size, and interparticle spacing.

All of the microstructures in Beta-III belonging to class C were given super-β+A treatments. In this class, C5 and C7, on one hand, and C6 and C8, on the other, showed comparable fatigue behaviors (Figure 2b). These four microstructures were given identical solution and aging treatments. The comparable strength levels of these four cases (Table I) are also consistent with the heat treatment. However, there is a difficulty in classifying all four microstructures in class C. It appears that with the exception of C5, the others (C6, C7, and C8) could reasonably be classified in C, because they either had a high extrusion temperature or were air cooled after extrusion at low temperature (815°C). In either case, it is very likely that these microstructures had a nonuniform distribution of α, due to a relatively low driving force for nucleation. On the other hand, C5 seems to belong to class A, due

Table I. Microstructures Belonging to Class A, Class B, and Class C

I.D.	Alloy (Mo-Equivalent/ β-transus)	Processing and Heat Treatment	YS (MPa)	UTS (MPa)	Microstructure	Fatigue Limit** (MPa)	Ref.
A1	Ti-8-8-2-3 (15/740)	Hot working + direct aging at 510°C for 8 h	931–955	1,050	Fine α in transformed β-matrix*	860	12
A2	Ti-8-8-2-3 (15/740)	Extrusion at 927°C (84% reduction) + direct aging at 510°C for 8 h followed by AC	NA	1,315	β-grains of size 56–113 μm + α in transformed β-matrix*	930 930	13 13
A3	Ti-10-2-3 (9.5/800)	Forged at (β_t + 15°C) (reduction 4:1) followed by controlled cooling at 5°C/s + direct aging to 1,193 MPa UTS	1,172	1,193	Elongated β-grains (width ~ 32 μm), very low v.f. of α_p, fine α_s in transformed β-matrix*	1,000	14
A4	Ti-10-2-3 (9.5/800)	Processing same as for A3 + direct aging to 1,138 MPa UTS	1,069	1,138	Same as in case A3 except for the difference in size and distribution of α_s*	1,000	14
A5	Ti-10-2-3 (9.5/800)	Processing same as in case A3 + direct aging to 1,006 MPa UTS	958	1,006	Same as in case A3 except for the difference in size and distribution of α_s*	900	14
A6	Beta III (12/760)	Extrusion (10.9:1 reduction) at 760°C followed by WQ + direct aging at 482°C for 8 h followed by AC	1,280	1,394	α particles in transformed β-matrix'	876	15
A7	Beta III (12/760)	Extrusion (10.9:1 reduction) at 982°C followed by WQ + direct aging at 482°C for 8 h followed by AC	1,159	1,283	Same as in case A6 except for the relatively coarser distribution of α due to higher extrusion temperature'	860	15
A8	Beta C (16/732)	Forged at (β_t + 85°C) + direct aging at 535°C for 8 h	1,123	1,179	α particles in transformed β-matrix'	790	16
A9	Ti-15-3 (12/760)	Forging at (β_t + 30 to 65°C) + direct aging at 510°C for 8 h	1,165	1,234	α particles in transformed β-matrix'	830	16
A10	Ti-15-3 (12/760)	Forging at (β_t + 30 to 65°C) + direct aging at 535°C for 8 h	1,096	1,158	α particles in transformed β-matrix'	810	16
B1	Ti-10-2-3 (9.5/800)	Forged at (β_t + 15°C) (reduction 3:1) followed by AC + ST at (β_t – 30°C) followed by WQ + aged to 1,027 MPa UTS	938	1,027	α_p and α_s in transformed β-matrix*	825	14
B2	Ti-10-2-3 (9.5/800)	Forged at (β_t + 15°C) (reduction 3:1) followed by AC + ST at (β_t – 30°C) + aged to 1,227 MPa UTS	1,117	1,227	α_p and α_s in transformed β-matrix*	725	14
B3	Ti-10-2-3 (95/800)	Processing and ST same as in case B1 + aged to 1,131 MPa UTS	1,034	1,131	Same as in case B1, except for the difference in size and distribution of α_s*	825	14
B4	Ti-10-2-3 (9.5/800)	β-forge + ST at 745 to765°C for 0.5 h followed by AC or WQ + aging at 480–510°C for 8 h followed by AC	NA	1,217	α_p and α_s in transformed β-matrix'	911	17

to its microstructural condition; the low extrusion temperature (815°C) in the β-field followed by WQ and aging could have resulted in a relatively uniform distribution of α, giving a relatively high fatigue limit of all the four cases.

Ti-8-8-2-3

As in Ti-10-2-3 and Beta-III alloys, the microstructures of class A (A1 and A2) exhibited a relatively higher fatigue limit (Figure 2c). However, A2 had a higher fatigue limit than A1, even though both had a similar aging treatment. The fatigue limits scaled with strength levels in these two microstructures. It is possible that the different fatigue response arose from the different β-processing treatments employed (Table I). As with A6 and A7 of the Beta-III alloy (Table I), different primary treatments can result in different characteristics of α even under an identical aging condition. Therefore, it is reasonable to infer that the characteristics of α controlled the fatigue behavior in this class, consistent with the classification.

C2 had the highest fatigue limit of all the alloys in class C (Figure 2c). However, even though the general processing/heat treatment is consistent with the definition of class C, this microstructure was produced after an unusually high reduction (84%) during processing in the β-field. It is possible that this process actually led to uniform α precipitation due to a relatively higher driving force for the $\beta \rightarrow \alpha$ transformation. Therefore, C2 may as well belong to class A. On the other hand, the α distribution in C3 is expected to be relatively nonuniform due to the low degree of work (30%) in the β-field. Because of this, when compared to C2, C3 would be expected to show a lower fatigue limit, since fatigue limit is likely to be controlled by β-grain or subgrain structure due to nonuniform α. C1 had a fatigue limit slightly higher than that of C3. Although the complete processing information was not available, it is clear that a difference in β-processing will result in different β-grain structure, leading to different fatigue limits for the two microstructures. This is consistent with their classification into class C.

Beta-CEZ

The four sets of data presented in Table I for microstructures B7 to B10 in this alloy provide further support to the suggestion that either α_p or α_s can control the fatigue limit in class B microstructures (see the discussion for Ti-10-2-3). In spite of different aging temperatures (leading to the production of different α_s distributions) causing widely different strength levels in B7 and B8, these microstructures had nearly the same fatigue limit. Similarly, B9 and B10 had similar fatigue limits even though the aging treatments and strength levels were different. This clearly indicates that the fatigue limit depended only on the α+β solution-treatment temperature and not the aging temperature. The only parameters that can change under these heat-treatment conditions are the size and interparticle spacing of α_p. The α_p particles are expected to be relatively larger and farther spaced for the higher α+β treatment temperature and relatively smaller and more closely spaced for the lower α+β treatment temperature. This

I.D.	Alloy (Mo-Equivalent/ β-transus)	Processing and Heat Treatment	YS (MPa)	UTS (MPa)	Microstructure	Fatigue Limit** (MPa)	Ref.
B5	Ti-10-2-3 (9.5/800)	β-forge + ST at 745–760°C for 0.5 h followed by WQ+ aging at 510–540°C for 8 h followed by AC	NA	1,103	α_p and α_s in transformed β-matrix'	811	17
B6	Ti-10-2-3 (9.5/800)	β-forge + ST at 745–760°C for 0.5 h followed by WQ + aging at 565–620°C for 8 h followed by AC	NA	965	α_p and α_s in transformed β-matrix'	759	17
B7	Beta-CEZ (5.1/890)	ST at 830°C for 1 h followed by WQ + aging at 550°C for 8 h followed by AC	1,518	1,601	Equiaxed α_p + α_s in β-matrix*	900	18
B8	Beta-CEZ (5.1/890)	ST at 830°C for 1 h followed by WQ + aging at 600°C for 8 h followed by AC	1,208	1,283	Equiaxed α_p + α_s in transformed β-matrix*	900	18
B9	Beta-CEZ (5.1/890)	ST at 860°C for 1 h followed by WQ + aging at 550°C for 8 h followed by AC	1,478	1,557	Equiaxed α_p + α_s in transformed β-matrix*	825	18
B10	Beta-CEZ (5.1/890)	ST at 860°C for 1 h followed by WQ + aging at 600°C for 8 h followed by AC	1,304	1,370	Equiaxed α_p + α_s in transformed β-matrix*	825	18
B11	Ti-10-2-3 (9.5/800)	β hot die forged or β block followed by α+β finish + ST at (β_t – 30°C) + aging	1,100	1,195	α_p and α_s in transformed β-matrix'	895	16
B12	Ti-10-2-3 (9.5/800)	β hot die forged or β block followed by α+β finish + ST at (β_t – 30°C) + aging	1,000	1,100	α_p and α_s in transformed β-matrix'	860	16
B13	Ti-10-2-3 (9.5/800)	β hot die forged or β block followed by α+β finish + ST at (β_t – 30°C) + overaging	895	965	α_p and α_s in transformed β-matrix'	830	16
C1	Ti-8-8-2-3 15 / 740)	Hot working + ST at 800°C for 1.5 h followed by WQ + aging at 540°C for 8 h	862–931	1,000	Heterogeneous α_s in transformed β-matrix*	720	12
C2	Ti-8-8-2-3 (15/740)	Extrusion at 927°C (84% reduction) + ST at 802°C for 1.5 h followed by WQ + aging at 538°C for 8 h followed by AC	NA	1,210	β-grain size = 56–113 μm, α in transformed β-matrix*	880	13
C3	Ti-8-8-2-3 (15/740)	Extrusion at 927°C (30% reduction) + ST at 802°C for 1.5 h followed by WQ + aging at 538°C for 8 h followed by AC	NA	1,231	β-grain size = 319 μm, α in transformed β-matrix*	680	13
C4	Beta III (12/760)	Extrusion at 760°C (10.9:1 reduction) followed by AC + ST at 760°C for 0.5 h followed by WQ + aging at 482°C for 8 h followed by AC	1,166	1,211	α in transformed β-matrix'	624	15

explains the higher fatigue limits (900 MPa) in B7 and B8 ($\alpha+\beta$ solution-treated at 830°C) and relatively lower fatigue limits (825 MPa) in B9 and B10 ($\alpha+\beta$ solution-treated at 860°C). Hence, it is clear that fatigue limit is influenced by the characteristics of α_p in this class of Beta-CEZ alloy.

Ti-15-3-3-3

The details of the four microstructures of this alloy are presented in Table I (A9, A10, C13, and C14). The fatigue limits of A9 and A10 are consistent with the earlier suggestion that the characteristics of uniform α control the fatigue behavior in class A microstructures. Although microstructures A9 and A10 were given the identical β-processing treatment, the aging temperature (510°C) of A9 is lower than that of A10 (535°C), thus resulting in a slightly higher fatigue limit in A9 relative to A10.

The fatigue data for C13 and C14 (Table I) suggest that the fatigue limit was controlled by the α particles distribution, since these microstructures were given identical β-processing and β-solution treatments. Hence, the small difference between their fatigue limits can only be explained on the basis of the small difference in their aging-treatment temperatures. However, a close examination of the processing and heat-treatment details of C-13 and C-14 indicates that their microstructures are closer to class A than class C.

It was shown[22] in Ti-15-3-3-3 that negligible recovery/recrystallization occurred below 800°C, and a very uniform precipitation of α occurred on subsequent aging. Therefore, the solution-treatment temperature of 785°C, in the case of C13 and C14, would result in a uniform distribution of α on aging.[22] It would then be expected that the characteristics of α would affect the fatigue behavior. As a result of the uniform precipitation of α from a nonrecovered/nonrecrystallized β-matrix, the microstructural characteristics of C13 and C14 are expected to be similar to A9 and A10, respectively, allowing their classification into class A. The similarity in fatigue limits of A9 and C13 and those of A10 and C14 thus appears to be meaningful.

Beta C

The four microstructures (C9, C10, C11, and C12) of this alloy belonging to class C are presented in Table I; however, only one microstructure in class A was available (A8). The fatigue limits of C9, C10, C11, and C12 seemed to be controlled by β-grain dimensions or the size of the α particle-free regions in the β-grains, consistent with the characteristics of this class of microstructures. It was shown[21] that almost complete recrystallization occurred after 843°C solution treatment (held for 1 h followed by air cooling) and that the subsequent aging at 482°C for 24 h produced a nonuniform α distribution with regions free from α particles in the matrix. Thus, it is reasonable to assume that a solution treatment at 910°C in the case of C10 and C11 would result in the microstructure described above.[21] Further, relatively higher fatigue limits of C10 and C12 relative to that of C1 are consistent with the behavior of class C microstructures. This is because the β-grain/subgrain dimensions in C11 are expected to be larger when compared to that in C10 and C12 due to the higher forging temperature employed for the production of C11 (Table I).

CLASSIFYING FATIGUE BEHAVIOR

From the above discussion of smooth fatigue data for various alloys, it is rea-

Table I. Microstructures Belonging to Class A, Class B, and Class C

I.D.	Alloy (Mo-Equivalent/ β-transus)	Processing and Heat Treatment	YS (MPa)	UTS (MPa)	Microstructure	Fatigue Limit** (MPa)	Ref.
C5	Beta III (12/760)	Extrusion at 815°C (10.9:1 reduction) followed by WQ + ST at 760°C for 0.5 h followed by WQ + aging at 482°C for 8 h followed by AC	1,145	1,249	α in transformed β-matrix*	828	15
C6	Beta III (12/760)	Extrusion at 815°C (10.9:1 reduction) followed by AC + ST at 760°C for 0.5 h followed by WQ + aging at 482°C followed by AC	1,166	1,201	α in transformed β-matrix*	655	15
C7	Beta III (12/760)	Extrusion at 982°C(10.9:1 reduction) followed by WQ + ST at 760°C for 0.5 h followed by WQ + aging at 482°C for 8 h followed by AC	1,138	1,256	α in transformed β-matrix*	783	15
C8	Beta III (12/760)	Extrusion at 982°C(10.9:1 reduction) followed by AC + ST at 760°C for 0.5 h followed by WQ + aging at 482°C for 8 h followed by AC	1,156	1,190	α in transformed β-matrix*	690	15
C9	Beta-C (16/732)	Hot rolled (about 90% reduction) + ST at 815°C for 1 h followed by AC + aging at 496°C for 20 h followed by AC	1,188	1,324	α in transformed β-matrix†	645	19
C10	Beta-C (16/732)	Forged at (β_t + 85°C) + ST at 910°C followed by AC + aging at 535°C for 8 h	1,199	1,262	α in transformed β-matrix†	800	16
C11	Beta-C (16/732)	Forged at (β_t + 195°C) + ST at 910°C followed by AC + aging at 535°C for 8 h	1,190	1,258	α in transformed β-matrix†	700	16
C12	Beta-C (16/732)	Forged at (β_t + 85°C) + ST at 815°C followed by AC + aging at 565°C for 8 h	1,151	1,192	α in transformed β-matrix†	780	16
C13	Ti-15-3 (12/760)	Forged at (β_t + 30 to 65°C) + ST at 785°C followed by AC + aging at 510°C for 8 h	1,192	1,275	α in transformed β-matrix†	840	16
C14	Ti-15-3 (12 /760)	Forged at (β_t + 30 to 65°C) + ST at 785°C followed by AC + aging at 535°C for 8 h	1,055	1,151	α in transformed β-matrix†	810	16

N.A. Data not available. YS: Yield strength. UTS: Ultimate tensile strength. AC: Air cool; WQ: Water quench; β_t: β-transus temperature.
* Reported/observed microstructure information
† Inferred microstructure information based on alloy chemistry and β-transus.
** σ_{max} at 10^7 cycles

sonable to conclude that microstructures of class A show a relatively superior HCF behavior compared to the class B and the class C microstructures, because the fatigue limit invariably seems to be controlled by the matrix structure (α particles size and spacing) in class A. On the other hand, in class B microstructures, the fatigue behavior seems to be controlled by either the matrix structure (the characteristics of α_s, which, for a given alloy, is coarser in class B than in class A microstructures) or the primary microstructure (the characteristics of α_p). The fatigue limits of the microstructures in class C seem to be controlled by the β-grain or subgrain dimensions, which are expected to be relatively larger in size, when compared to any other microstructural variable. However, there were some cases in class C (C2, C5, C13, and C14) that had microstructures similar to those in class A. As a result, it is not surprising to find that these showed fatigue limits comparable to that of class A microstructures.

The fatigue limits of all the alloys and microstructures compiled in Table I are plotted in Figure 3 as a function of UTS. On the basis of the above discussion, the three classes (A, B, and C) are demarcated into different regions. Since the microstructures C2 (Ti-8-8-2-3), C5 (Beta III), and C13 and C14 (Ti-15-3-3-3) were classified into class A, these have been identified separately by the closed triangles in Figure 3; this reclassification reaffirms the grouping of fatigue behavior into three classes.

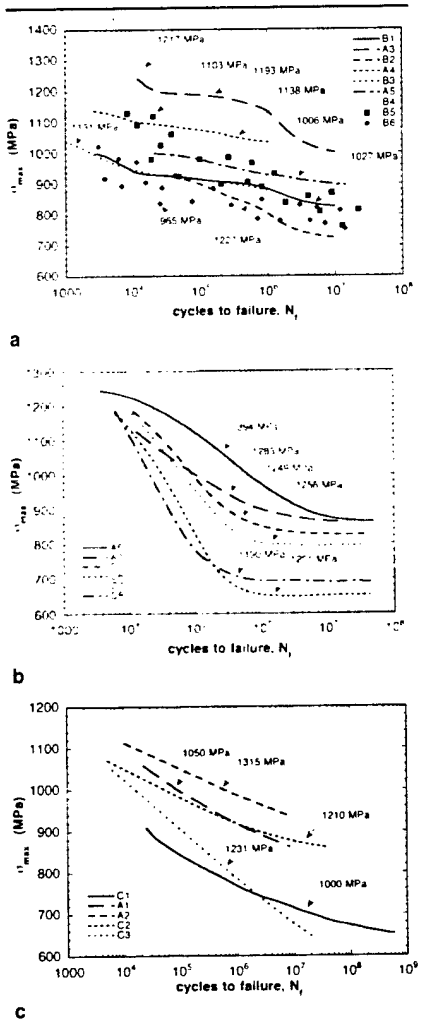

Figure 2. Smooth fatigue data at R = 0.1 for (a) Ti-10V-2Fe-3Al, (b)Ti-11.5Mo-6Zr-4.5Sn (Beta III), and (c) Ti-8V-8Mo-2Fe-3Al.

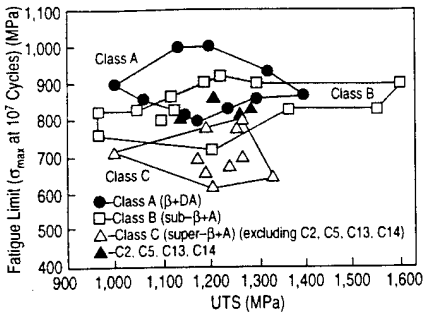

Figure 3. A classification of the fatigue behavior of β-titanium alloys.

Two important observations are clear from Figure 3. First, the class A microstructures that generally possess uniformly distributed fine α particles show medium to high fatigue limits over a range of strength levels. The class B microstructures that contain duplex sizes of α particles possess medium levels of fatigue limits, again over a wider range of strength levels. The class C microstructures, generally containing grain-boundary α and relatively nonuniform distribution of α particles, possess low levels of fatigue limits. Second, the present data do not agree with the general supposition that the fatigue limit empirically scales with UTS by some factor (anywhere from 0.5 to 0.8), on the basis of generally observed fatigue-limit-strength correlations observed for structural metals.[10,11] This deviation is most striking for the class B microstructures having duplex sizes of α particles. Figure 3 indicates that in this microstructural condition, the fatigue limits vary over a narrow range (750–880 MPa) even when the ultimate strength levels varied from 960 MPa to 1,600 MPa.

Further, the shaded regions indicate that there is no general trend between fatigue limit and tensile strength in the other classes of microstructures that were considered in this study. Even in class A, which showed the highest fatigue limit levels, there is no correlation between fatigue limit and strength. It should be noted that fatigue behavior is also affected by surface condition and that the observed lack of correlation may be aggravated by the varied surface conditions that are employed in the tests in different studies. Notwithstanding this factor, the general microstructural condition that could result in the highest fatigue resistance is that having a uniform distribution of fine α particles in the transformed β matrix.

ACKNOWLEDGEMENT

This overview was made possible by the financial support of the U.S. Air Force Office of Scientific Research through grant F49620-96-1-0102, with C.H. Ward and S. Wu as program monitors. We thank them for this support and encouragement.

References

1. R.R. Boyer, "An Overview on the Use of Titanium in the Aerospace Industry," *Materials Science and Engineering*, A213 (1996), pp. 103–114.
2. Yves Honnorat, "Issues and Breakthrough in the Manufacture of Turboengine Titanium Parts," *Materials Science and Engineering*, A213 (1996), pp. 115–123.
3. D.P. Davies and B.C. Gittos, "Titanium Usage in Modern Helicopter Designs," *Titanium '95: Science and Technology*, ed. P.A. Blenkinsop, W.J. Evans, and H.M. Flower (London: IOM, 1995), pp. 1609–1637.
4. R.R. Boyer, "Applications of Beta Titanium Alloys in Airframes," *Beta Titanium Alloys in the 1990's*, ed. D. Eylon, R.R. Boyer, and D.A. Koss (Warrendale, PA: TMS, 1993), pp. 335–346.
5. P.J. Bania, in Ref. 4, pp. 3–14.
6. T.W. Duerig and J.C. Williams, "Overview: Microstructure and Properties of Beta Titanium Alloys," *Beta Titanium Alloys in the 80's*, ed. R.R. Boyer and H.W. Rosenberg (Warrendale, PA: TMS, 1984), pp. 19–67.
7. G. Terlinde, T.W. Duerig, and J.C. Williams, "Microstructure, Tensile Deformation and Fracture in Aged Ti-10V-2Fe-3Al," *Metall. Trans. A*, 14A (1983), pp. 2101–2115.
8. G. Terlinde, H.J. Rathjen, and K.H. Schawalbe, "Microstructure and Fracture Toughness of the Aged β-Titanium Alloy Ti-10V-2Fe-3Al," *Metall. Trans. A*, 14A (1983), pp. 1037–1049.
9. J.K. Gregory, "Fatigue Crack Propagation in Titanium Alloys," *Handbook of Fatigue Crack Propagation in Metallic Structures*, ed. Andrea Carpinteri (Dordrecht, Netherlands: Elsevier Science Publications, 1994), pp. 281–321.
10. A.D. Wilson, "Fracture and Fatigue Properties of Structural Steels," *ASM Handbook*, vol. 19 (Materials Park, OH: ASM, 1996), pp. 591–604.
11. R.J. Bucci, G. Nordmark, and E.A. Starke, Jr., "Selecting Aluminum Alloys to Resist Failure by Fracture Mechanisms," *ASM Handbook*, vol. 19 (Materials Park, OH: ASM, 1996), pp. 771–812.
12. R. Chait and R.E. Pasternak, "The Stress Controlled High Cycle Fatigue Response of a Metastable Beta Titanium Alloys as Influenced by Several Test Variables," *J. Engineering Materials and Technology*, 100 (1978), pp. 426–428.
13. R. Chait and F.S. DeSisto, "The Influence of Grain Size on the High Cycle Fatigue Crack Initiation of a Metastable Beta Titanium Alloy," *Metall. Trans. A*, 8A (1977), pp. 1017–1020.
14. G.W. Kuhlman et al., "LCF, Fracture Toughness and Fatigue/Fatigue Crack Propagation Resistance of Optimization in Ti-10V-2Fe-3Al Alloy, through Microstructural Modification," *Microstructures, Fracture Toughness and Fatigue Crack Growth Rate in Titanium Alloys*, ed. A.K. Chakrabarti and J.C. Chesnutt (Warrendale, PA: TMS, 1987), pp. 171–191.
15. A.M. Adair, W.H. Reimann, and R.F. Klinger, "The Influence of Thermomechanical Processing on the Fatigue Behavior of Extruded Beta-III Titanium," *Titanium Science and Technology*, ed. R.I. Jaffee and H.M. Burte (New York: Plenum Press, 1973), pp. 1801–1812.
16. G.W. Kuhlman, "A Critical Appraisal of Thermomechanical Processing of Structural Titanium Alloys," *Microstructure/Property Relationships in Titanium Aluminides and Alloys*, ed. Y-W. Kim and R.R. Boyer (Warrendale, PA: TMS, 1991), pp. 465–491.
17. G.W. Kuhlman, in Ref. 4, pp. 477–483.
18. Y. Combres and B. Champin, in Ref. 4, 477–483.
19. J.G. Ferrero, J.R. Wood, and P.A. Russo, in Ref. 4, pp. 211–226.
20. M.H. Campagnac and A. Vassel, "Influence of Microstructure on Tensile and Fracture Toughness Properties of Ti-10V-2Fe-3Al Alloy," *Designing with Titanium* (London: Institute of Metals, 1986), pp. 261–266.
21. G.A. Bella et al., "Effects of Processing on Microstructure and Properties of Ti-3Al-8V-6Cr-4Mo-4Zr (Beta-C™)," *Microstructure/Property Relationships in Titanium Aluminides and Alloys*, ed. Y-W. Kim and R.R. Boyer (Warrendale, PA: TMS, 1991), pp. 493–510.
22. E. Breslauer and A. Rosen, "Relationship between Microstructure and Mechanical Properties in Metastable β-Titanium 15-3 Alloy," *Materials Science and Technology*, 7 (1991), pp. 441–446.
23. P.J. Bania, G.A. Lenning, and J.A. Hall, "Development and Properties of Ti-15V-3Cr-3Sn-3Al (Ti-15-3)," *Beta Titanium Alloys in the 80's*, ed. R.R. Boyer and H.W. Rosenberg (Warrendale, PA: TMS, 1983), pp. 209–229.

S.K. Jha and K.S. Ravichandran are with the University of Utah.

For more information, contact K.S. Ravichandran, University of Utah, Department of Metallurgical Engineering, 135 South, 1460 E, Rm. 412, Salt Lake City, Utah 84112; (801) 581-7197; fax (801) 581-4937; e-mail ravi@mines.utah.edu.

Appendix II

Mechanisms of Fatigue Crack Nucleation at Surface and Subsurface Regions and Their Effect on Fatigue Life of Ti-10V-2Fe-3Al

Small Fatigue Cracks: Mechanics, Mechanisms and Applications
K.S. Ravichandran, R.O. Ritchie and Y. Murakami (Editors)
© 1999 Elsevier Science Ltd. All rights reserved.

MECHANISMS OF FATIGUE CRACK NUCLEATION AT SURFACE AND SUBSURFACE REGIONS AND THEIR EFFECT ON FATIGUE LIFE OF Ti-10V-2Fe-3Al

S. K. JHA and K. S. RAVICHANDRAN
Department of Metallurgical Engineering,
135 South, 1460 East, Rm. 412, University of Utah,
Salt Lake City, UT 84112

ABSTRACT

The nature of fatigue crack nucleation at surface and subsurface regions in smooth fatigue specimens and its effect on fatigue life was investigated in a β-titanium alloy, Ti-10V-2Fe-3Al. Four microstructures of the alloy, with nearly similar strength levels were considered. The microstructures varied in terms of the volume fraction of primary-α particles (α_p), the aspect ratio of α_p and the nature of transformed β-matrix (α-aged versus ω-aged). In three α-aged microstructures, both subsurface as well as surface crack nucleation were observed. In case of ω-aged microstructure having a high volume fraction of α_p, only subsurface crack nucleation was seen. Subsurface crack nucleation sites were found to be associated with α_p particles in all microstructures. All of the α-aged microstructures showed similar fatigue limit, with similar critical crack sizes as determined from the Kitagawa diagram. The ω-aged microstructure, on the other hand, showed a lower fatigue limit and a larger critical crack size compared to the α-aged microstructures. It was concluded that the nature of the matrix as determined by aging, controlled the slip characteristics in these alloys, which in turn controlled the fatigue life spent in subsurface crack nucleation and small crack growth.

KEYWORDS

Fatigue crack nucleation, small crack, beta-titanium alloy, Kitagawa Diagram, fatigue life, subsurface initiation, surface initiation

INTRODUCTION

Total life in fatigue is thought to be distributed over four stages, viz., nucleation of a crack of certain size, small-crack growth, large-crack growth and unstable fracture [1,2]. It has been pointed out that a large percentage of fatigue life of a smooth specimen may be expended in crack

nucleation and small-crack growth, especially in high-cycle fatigue [3,4]. In this regard, it becomes important to develop a clear understanding of crack nucleation characteristics and early crack growth. A component fatiguing in service may have spent a large portion of its life in nucleating and growing a crack to a size that can be detected by non-destructive techniques. This is even more critical when a fatigue crack originates subsurface and remains undetected until it grows to the surface. There are studies showing that subsurface crack nucleation need not always be associated with defects such as inclusions or pores but can occur purely as a consequence of dislocation-microstructure interaction during fatigue, especially in titanium alloys [5–7]. Several mechanisms have been proposed in these studies based on dislocation pile-up or localized deformation.

In the present study, fatigue crack nucleation behavior as well as total fatigue life of smooth specimens of the β-titanium alloy, Ti-10V-2Fe-3Al, in various microstructural conditions, were studied. There have been some fatigue studies on this alloy [4,8] but there is a lack of understanding of aspects governing fatigue crack nucleation. The specific objective was to understand the effect of microstructure on crack nucleation behavior. It has been found that the characteristics of transformed β-phase (α-aged versus ω-aged) determined the microstructural variable that affected the fatigue life. The location of crack origin (surface versus subsurface) was found to be strongly dependent on the microstructure as well as the stress level.

EXPERIMENTAL PROCEDURE

The Ti-10V-2Fe-3Al (wt. %) alloy was supplied by TIMET (Henderson, Nevada) in the form of plates of size: 267 mm x 210 mm x 38 mm. The plates were made from cast ingots by the following processing routes: Plate I was β-forged and air-cooled followed by 25% reduction in α+β rolling (at 760° C) and air cooled; Plate II was β-forged and air cooled followed by 65% reduction in α+β rolling (at 760° C) and air-cooled. Smooth fatigue test specimens, oriented in LT direction, were machined from the plates. The specimens were then heat treated to produce different microstructural conditions. The heat treatment schedules, microstructure details and the tensile properties are presented in Table 1. Smooth fatigue specimens with a rectangular cross section were electropolished (electrolyte: 4 : 1 of acetic acid and 65% perchloric acid; voltage: 30 V; time: about 40 minutes) prior to testing. Fatigue tests were conducted in a MTS 810 servohydraulic fatigue test system equipped with a TESTSTAR II controller. Fatigue tests were performed in tension-tension at a stress ratio (R) of 0.1 and a frequency of 35 Hz at room temperature. The volume fractions of phases in the microstructure were measured using point-counting technique [9] and interparticle spacings as well as grain sizes were measured using linear-intercept method [9]. Fracture surfaces were examined in a Cambridge S240 scanning electron microscope (SEM) at an accelerating voltage of 20 KV. Energy dispersive spectroscopic (EDS) analyses of initiation sites were performed using a Kevex X-ray detector. Thin foils of microstructures were observed in a JEOL JEM-2000 FX II transmission electron microscope (TEM) at an accelerating voltage of 200 KV.

RESULTS AND DISCUSSION

Microstructures

The four microstructures are shown in Fig. 1 and their tensile properties are summarized in Table 1.

Table 1. Heat Treatment, Microstructures and Tensile Properties

Microstructure	Heat Treatment	Microstructure Description	0.2%Y.S. (MPa)	UTS (MPa)	% El.
A	Plate I: ST, 700C, 2h, WQ + Aging, 525C, 8h, WQ	45% HAR α_p and α_s particles in β	988	1066	13
B	Plate I: ST, 780C, 2h, WQ + Aging, 580C, 8h, WQ	10% HAR α_p and α_s in β	1057	1085	10
C	Plate II: ST, 700C, 2h, WQ + Aging, 525C, 8h, WQ	45% LAR α_p and α_s in β	980	1021	14
D	Plate I: ST, 700C, 2h, WQ + Aging, 260C, 6h, WQ	45% HAR α_p and ω particles in β	1028	1047	9

ST=solution treatment; WQ=water quench; HAR=high aspect ratio (l:w = 15:1; l=length and w=width of α_p particles); LAR=low aspect ratio (l:w = 2.5:1)

1. Microstructures A and D had approximately 45% of high aspect ratio (length ~ 10 μm ; width ~ 0.7 μm) α_p phase (Figs. 1(a) and (d)). Microstructure B consisted of approximately 10% of high aspect ratio α_p (Fig. 1(b)) and microstructure C had approximately 45% of low aspect ratio (length ~ 4μm; width ~ 1.4 μm) α_p (Fig. 1(c)). The interparticle spacings between α_p in microstructures A, C and D were approximately 2 μm. In microstructure B, the α_p interparticle spacing was approximately 10 μm. Owing to aging treatment, the transformed matrices of microstructures A, B and C (all were α-aged) consisted of secondary α (α_s) particles while that of microstructure D (ω-aged) consisted of ω particles. The dark field TEM images of matrix microstructures of A and D are shown in Fig. 2. The size of α_s platelets and their spacing are on the order of 0.06 μm (width) x 0.3 μm (length) and 0.2 μm, respectively. On the other hand, the size and the spacing of ω particles are on the order of 0.006 μm (diameter) and 0.01 μm, respectively. It has been shown [10] that the primary microstructural aspects of Ti-10V-2Fe-3Al such as α_p size and spacing had negligible influence on the strength levels. However, strength levels were found to be largely controlled by the matrix structure, which depended on the aging treatment [10]. Thus, aging conditions were chosen in the present study to achieve similar strength levels in the microstructures studied (Table 1).

Fatigue Behavior

Results of smooth specimen fatigue tests are presented in Fig. 3. Fatigue crack nucleation sites were identified by fractography and the specimens in which subsurface crack nucleation or surface nucleation occurred are shown by open or filled symbols, respectively. The fatigue limits of microstructures A, B and C were similar ($\sigma_{max,e}$ ~ 850 MPa). On the other hand, the fatigue

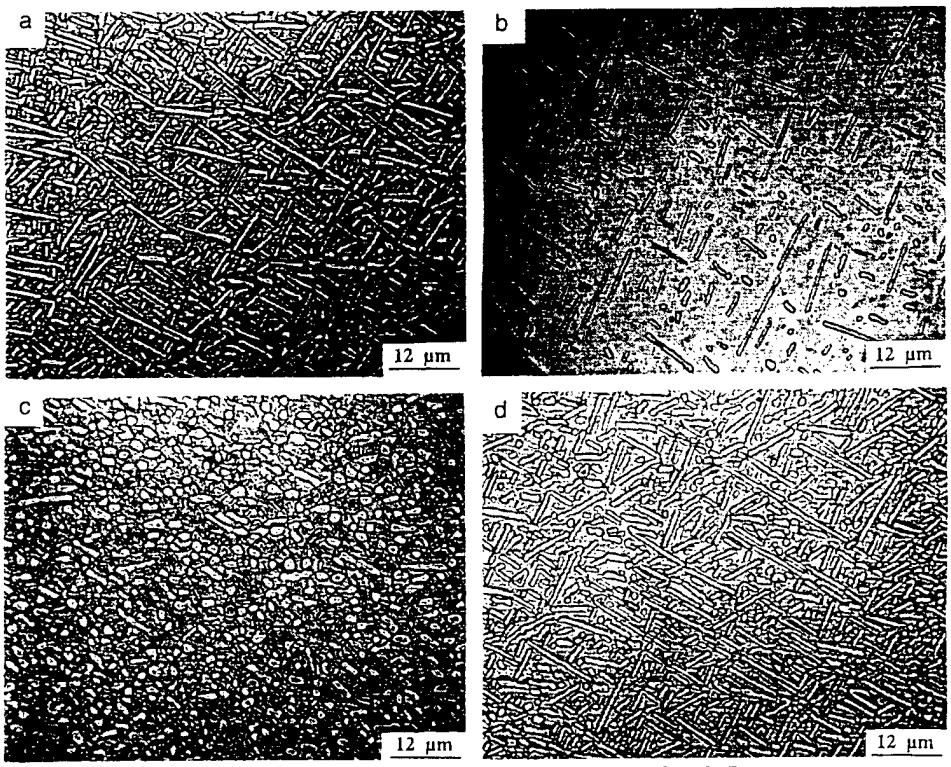

Fig. 1. Optical micrographs of microstructure (a) A; (b) B; (c) C; (d) D

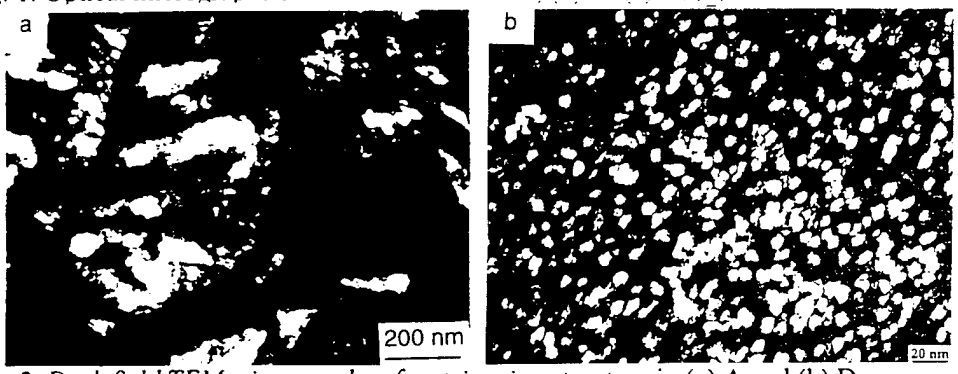

Fig. 2. Dark field TEM micrographs of matrix microstructure in (a) A and (b) D

limit of microstructure D was relatively lower ($\sigma_{max,e}$ ~ 790 MPa) compared to the other microstructures. While fatigue tests at all stress levels in D showed subsurface crack nucleation, both subsurface and surface crack nucleation were observed in A through C. Also, portions of fatigue curves of A through C, that represented subsurface crack nucleation, overlapped at low stress levels (σ_{max} < ~ 920 MPa). It is also interesting to note that for A and C there existed a particular stress level (about 910 MPa for A and 890 MPa for C) above which all specimens showed surface nucleation. Below these stress levels, only subsurface crack nucleation was observed. Such a critical stress level also existed for B (~ 920 MPa). However, unlike A and C, in B, both subsurface and surface crack nucleation were seen below this stress level with more than 50% of specimens tested in the lower stress level range showing surface crack nucleation. Additionally, at the same stress level, the surface nucleation resulted in lower total life compared to the subsurface nucleation. The data points formed two separate fatigue curves, one for surface and the other for subsurface nucleation (Fig. 3).

Fatigue crack growth data for the microstructures are presented elsewhere [11]. While microstructures A through C showed nearly the same crack growth behavior, microstructure D showed relatively lower rates of crack growth and a higher crack propagation threshold, ΔK_{th}.

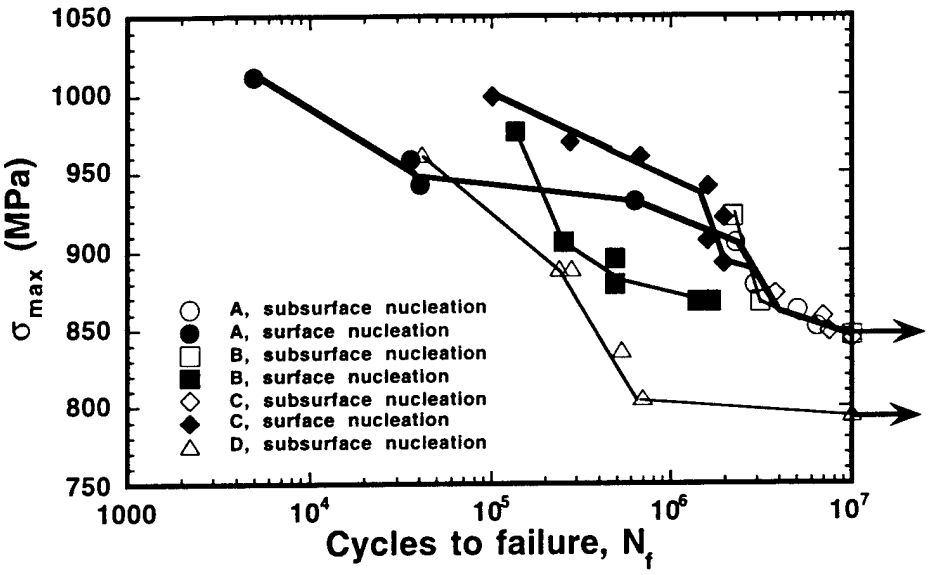

Fig. 3. Fatigue behavior of the four microstructures investigated

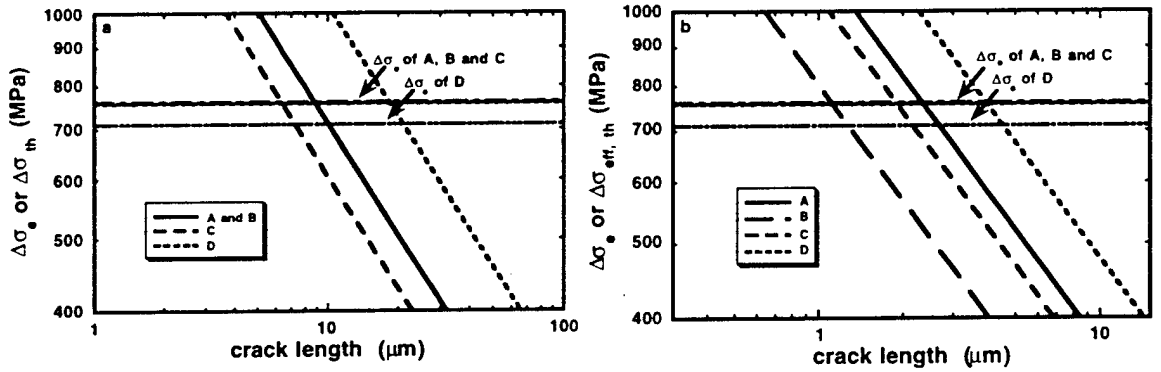

Fig. 4. Kitagawa diagrams for the four microstructures A through D: (a) on the basis of ΔK_{th} and (b) on the basis of $\Delta K_{eff,th}$

Critical Small Crack Sizes

In order to estimate the critical sizes (a_{cr}) of non-propagating cracks, Kitagawa diagrams [12] were constructed for the four microstructures and are shown in Fig. 4. The horizontal lines are the lines drawn using the fatigue limit, $\Delta\sigma_e$, which is independent of crack size. The inclined lines were constructed using the threshold condition for the propagation of large cracks:

$$\Delta\sigma_{th} = \frac{\Delta K_{th}}{\sqrt{\pi a} F(a/w)} \quad \text{.....(1)}$$

Where a is the crack size and F(a/w) is the geometric-correction factor. The crack size at which these two lines intersect is identified as the critical crack size. The critical crack size is the size below which small cracks are considered to be non-propagating, which has been consistent with experimental observations [12,13]. At crack sizes larger than this, cracks are found to obey the fracture mechanics-based characterization. Results from the Kitagawa diagrams in Fig. 4 are summarized in Table 2. It is to be noted that generally, the critical crack sizes have been found to correspond to either the grain size or the size of the controlling microstructural unit [12,14] in many materials. From Table 2, it can be seen that comparable critical crack sizes were obtained for microstructures A through C (5.2 to 7 μm) suggesting a common controlling microstructural unit in these microstructures. However, a relatively larger critical crack size for D (23 μm) suggests a larger controlling microstructural unit size in this microstructure. However, these sizes are much smaller than the prior β grain size, which was approximately 150 μm in microstructures A, B and D and about 100 μm in microstructure C. All the critical crack sizes, seem to be not related to either the size of α_p, or the aspect ratio of α_p or the interparticle spacing between α_p.

It was shown [15,16] that the Kitagawa diagram plotted using $\Delta K_{eff,th}$ instead of ΔK_{th}, more closely predicted the non-propagating critical crack size in some materials. Here, $\Delta K_{eff,th}$ is the effective threshold stress intensity range after taking crack closure into account ($\Delta K_{eff,th} = K_{max,th} - K_{cl,th}$; where $K_{max,th}$, $K_{min,th}$ and $K_{cl,th}$ are the maximum, the minimum and the closure stress intensity factors at threshold). A detailed discussion of crack closure in these microstructures is presented elsewhere [11]. The Kitagawa diagrams plotted using $\Delta K_{eff,th}$ are shown in Fig 4(b). Once again, similar critical crack sizes were obtained for the microstructures A, B and C (~2 μm) while relatively a larger critical crack size (~5 μm) was predicted in microstructure D. These crack

Table 2. The large-crack threshold levels and estimates from Kitagawa diagrams

Microstructure	ΔK_{th} (Mpa$\sqrt{m}$)	a_{cr} using ΔK_{th} (μm)	$\Delta K_{eff,th}$ (Mpa$\sqrt{m}$)	a_{cr} using $\Delta K_{eff,th}$ (μm)
A	3.9	7.1	1.8	2.2
B	3.9	7.1	1.4	1.3
C	3.4	5.2	1.9	2.0
D	5.7	23.0	2.75	5.0

sizes are quite different from the estimates based on ΔK_{th} and may be considered as closely representing non-propagating crack sizes in these four microstructures. Clearly, these critical crack sizes are much smaller than the prior β grain sizes in these microstructures. Although the α_p interparticle spacing varied from about 2 μm in microstructures A and C to 10 μm in B, the predicted crack sizes were similar in the three microstructures. Thus, the α_p interparticle spacings do not seem to influence the critical crack sizes. Also, the critical crack sizes were similar in microstructures A through C in spite of the size variations of α_p platelets seen these microstructures. For example, the dimensions of α_p varied from a length of 10 μm and a width of 0.7 μm in microstructures A and B, to a length of 4 μm and a width of 1.4 μm in microstructure C, thus eliminating the possibility of α_p size as the controlling microstructural unit. The other

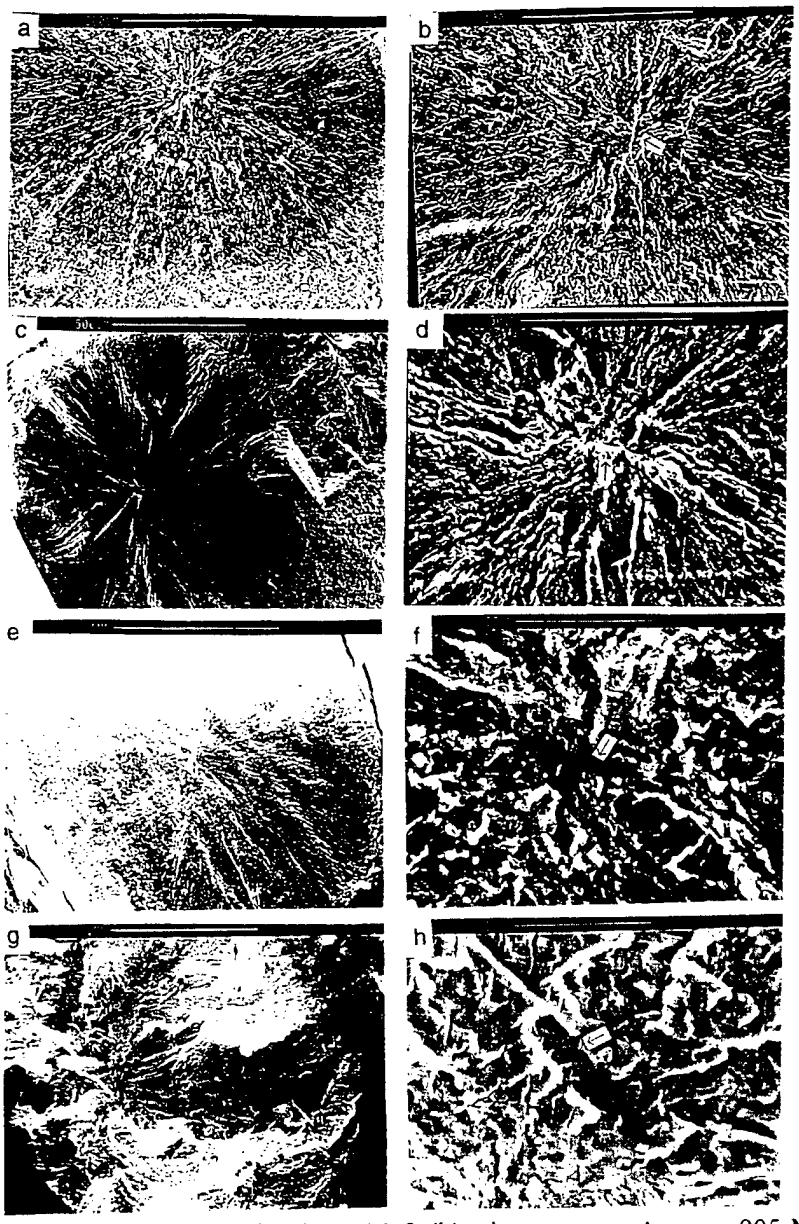

Fig. 5. Fracture surfaces at two magnifications: (a) & (b) microstructure A, σ_{max}=905 MPa; (c) & (d) microstructure B, σ_{max}=922 MPa; (e) & (f) microstructure C, σ_{max}=858 MPa; (g) & (h) microstructure D, σ_{max}= 890Mpa

possibilities for the controlling microstructural unit can be the size or the spacing of secondary particles in transformed β matrix. Although in other studies [1,6,7,17] the sizes of the α_p, the α_p platelet colonies or the prior β grains were suggested to be controlling microstructural units, the data in the present study indicate altogether a different type of "controlling microstructural unit". As discussed in a later section, the α_s spacing in the transformed β-matrix of microstructures A

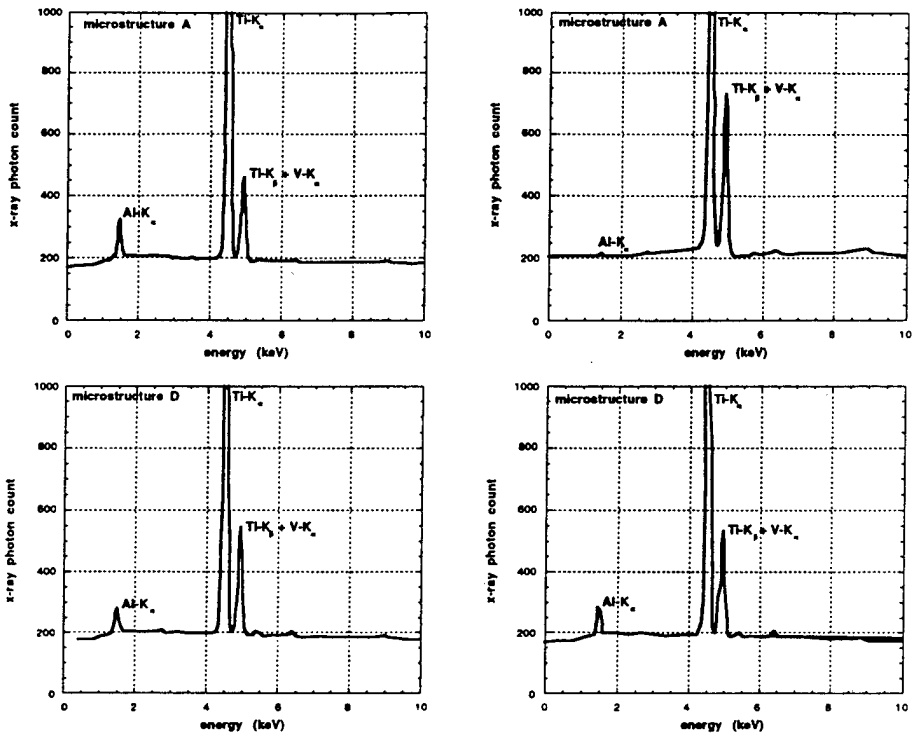

Fig. 6. EDS analysis results from the opposite faces of fracture surfaces of microstructures A and D

through C, seems to be the controlling microstructural unit in these microstructures. The spacing of α_s particles was found to be on the order of 0.1 μm in microstructure A (Fig. 2(a)). It is also reasonable to expect that the distribution of α_s to be similar in microstructures A through C due to similar aging conditions and strength levels. The sizes of the controlling microstructural units were found to be approximately one tenth of the critical small crack sizes [18] estimated from the Kitagawa diagrams. Thus, in the present study, the data (Fig. 4(b)) suggest that the spacing of α_s particles are the controlling unit size in microstructures A through C. In microstructure D, the nature of ω-aged matrix seems to promote inhomogeneous deformation leading to a relatively larger critical crack size. This is discussed in more detail later.

Fracture Surface Analysis

Fractographs of subsurface crack nucleation sites for microstructures A, B, C and D are presented in Figs. 5 (a) to (h). A faceted fracture morphology was observed at the crack origins in all the cases, as indicated by the arrows in the figures (Fig. 5(b), (d), (f) and (h)). The morphologies and the sizes of these facets roughly corresponded to the morphologies and the sizes of α_p in microstructures A through D. However, the facet size and morphology remained independent of the stress level. This is in contrast to other studies in α+β titanium alloys which indicated that the facet dimensions increased with a decrease in the stress level [17].

It was considered important to establish whether the facets represented cleaved α_p platelets or corresponded to the α_p-matrix interface. To resolve this issue, EDS analyses on the fracture facets were done and results are presented in Fig. 6. The EDS results were similar for microstructures A through C. The result from one of these microstructures (microstructure A) is produced in Fig. 6 (a & b). For microstructures A through C, the difference in Al-K_α and V-K_α

signals in the EDS spectra of the opposite faces of fracture surface indicates that facets corresponded to the interface between α_p and the transformed β matrix. In case of microstructure D, however, intensity of Al-K_α and V-K_α signals from the opposite faces of fracture surface are similar (Fig. 6 (c & d)) indicating that the facet did not correspond to the interface but to a plane through the α_p particle.

A few examples of fracture surfaces for stress levels corresponding to surface crack nucleation are presented in Fig. 7 (a) to (f) for the microstructures A, B and C. The sizes and the morphologies of the facets at crack origin (Fig. 7), roughly corresponded to that of α_p particle, although this was not very clear in case of microstructure B (Fig. 7(d)).

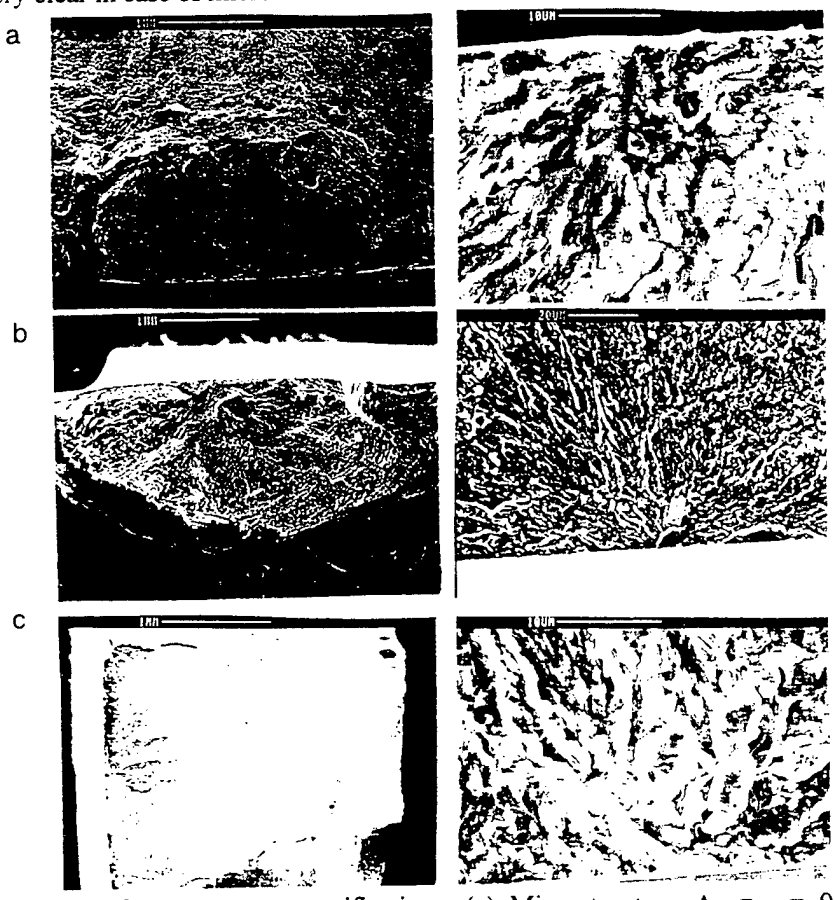

Fig. 7. Fracture surfaces at two magnifications: (a) Microstructure A, σ_{ma} = 932 MPa; (b) Microstructure B, σ_{max} = 895 MPa; (c) Microstructure C, σ_{max} = 970 MPa

Mechanisms of Fatigue Crack Nucleation

As indicated earlier, the large-crack growth behavior in terms of da/dN vs ΔK was found to be similar in microstructures A, B and C. Thus, the observation of similar fatigue limit and the overlap of S-N data in the regime where subsurface nucleation occurred, indicates that approximately the same number of cycles were spent in crack nucleation and small-crack growth in microstructures A through C. Additionally, similar values of the controlling microstructural

unit size in these microstructures (Table 2) suggest that the fatigue lives involved in subsurface crack nucleation are comparable.

As discussed before, the controlling microstructural unit size seems to be independent of the dimensions of α_p or the interparticle spacing of α_p. However, it appears that the nature of slip in the transformed β-matrix, as determined by the aging conditions, controlled crack nucleation and small-crack growth in this alloy. It is known that α-aging of β-titanium alloys leads to homogenous distribution of deformation in matrix [19]. Thus, the distribution of deformation and more specifically the dislocation densities in slip bands would be controlled by the α_s distribution in these microstructures. Also, the effective slip-band length is expected to be of the order of average α_s spacing in the matrix. On the other hand, in the ω-aged microstructure, the ω particles induce inhomogeneous deformation or planar slip [20,21]. Due to the reduced cross-slip in this condition (microstructure D), higher dislocation densities are expected in the slip bands. This can cause the crack to nucleate in a fewer number of cycles in microstructure D [22] compared to the other microstructures. Also, the larger effective slip band length in this microstructure can lead to a relatively lower number of cycles spent in small-crack growth regime. The combined effect of the reduction in cycles for crack nucleation and the faster small-crack growth rates seems to exceed the beneficial effect on fatigue life brought about by the lower large-crack growth rates [11] in this microstructure.

CONCLUSIONS

1. Fatigue limit in Ti-10V-2Fe-3Al alloy is independent of the size, shape and volume fraction of primary-α (α_p) particles, in the range studied.
2. The matrix condition, as determined by the aging treatment had a strong influence on the fatigue behavior. For example, ω-aged microstructure showed lower fatigue limit and poorer fatigue life over most of stress level range, compared to the α-aged microstructures.
3. Comparable values of critical crack sizes were predicted for the α-aged microstructures from the Kitagawa diagrams. However, a relatively larger critical crack size was estimated for the ω-aged microstructure.
4. It is suggested that the nature of slip in the transformed β-matrix controlled the fatigue crack nucleation process in these microstructures.

REFERENCES

1. Hall, J. A. (1997) Int. J. Fatigue, **19**, S23
2. Kaynak, C., Ankara, A. and Baker, T. J. (1996) Int. J. Fatigue, **18**, 25
3. Ruppen, J. A., Eylon, D. and McEvily, A. J. (1980) Metall. Trans. A, **11A**, 1072
4. Chait, R. and DeSisto, T. S. (1997) Metall. Trans. A, **8A**, 1017
5. Ruppen, J., Bhowal, P., Eylon, D. and McEvily, A. J. (1979) *Fatigue Mechanisms*, Proceedings of an ASTM-NBS-NSF symposium, Kansas City, Mo, May 1978, J. T. Fong, ed., ASTM STP 675, 47
6. Yokoyama, H., Umezawa, O., Nagai, K. and Suzuki, T. (1997) ISIJ International, **37**, 1237
7. Neal, D. F. and Blenkinsop, P. A. (1976) Acta Metall., **24**, 59
8. Chait, R. and Pasternak, R. E. (1978) Trans. ASME, J. Engng. Mater. Tech., **100**, 426

9. *Quantitative Microscopy* (1968) DeHoff, R. T. and Rhines, F. N., eds., McGraw-Hill Book Company
10. Boyer, R. R. and Kuhlman, G. W. (1987) Metall. Trans., **18A**, 2095
11. Jha, S. K. and Ravichandran, K. S., (1999) Metall. Trans., in review
12. Miller, K. J. (1982) Fat. Engng. Mater. Struct., **5**, 223
13. Lucas, P. and Kunz, L. (1992) *Short Fatigue Cracks*, ESIS publication 13, K. J Miller and E. R. de los Rios, eds., Mechanical Engineering Publications, London, 265
14. Lankford, J. (1985) Fatigue Fract. Engng. Mater. and Struct., **8**, 161
15. Kendall, J. M., James, M. N. and Knott, J. F. (1986) *The Behavior of Short Fatigue Cracks*, EGF Pub 1, K. J. Miller and E. R. De Los Rios, eds, Mechanical Engineering Publications, London, 241
16. Mei, Z., Krenn, C. R. and Morris Jr., J. W. (1995) Metall. Trans., **26A**, 2063
17. Umezawa, O. and Nagai, K. (1997) ISIJ International, **37**, 1170
18. Taylor, D. and Knot, J. F. (1981) Fat. Engng. Mater. and Struct., **4**, 147
19. Niinomi, M. and Kobayashi, T. (1996) Mater. Sci. and Engng., **A213**, 16
20. Hickman, B. S. (1969) Trans. Met. Soc. AIME, **245**, 1329
21. Duerig, T. W., Terlinde, G. T. and Williams, J. C. (1980) Metall. Trans., **11A**, 1987
22. Venkatraman, G., Chung, Y. W. and Mura, T. (1991) Acta Metall. Mater., **39**, 2631

Appendix III

Fatigue Response and Micromechanisms of Crack Initiation in Ti-10V-2Fe-3Al

FATIGUE RESPONSE AND MICROMECHANISMS OF CRACK INITIATION IN Ti-10V-2Fe-3Al TITANIUM ALLOY

P. S. Shankar and K. S. Ravichandran

Department of Metallurgical Engineering
The University of Utah
135 South 1460 East Room 412, Salt Lake City, UT 84112

ABSTRACT

Fatigue response of three beta annealed microstructures of Ti-10V-2Fe-3Al, having comparable strength levels was studied. The effect of microstructure on fatigue resistance has been rationalized in terms of size, location & origin of fatigue crack initiation site. The resistance to fatigue crack growth was almost similar in all microstructures. However, the σ_{max}-N_f behavior of ω-aged microstructures was relatively poor compared to the furnace cooled and α-aged microstructures. In all these microstructures, subsurface crack initiation was observed at low stress levels while surface crack initiation was observed at higher stress ranges. Subsurface crack initiation appears to occur by a process of crystallographic cleavage. The mechanism of cleavage seems to determine the fatigue crack initiation site size. The ω-aged microstructure exhibited a stress dependence on the crack initiation site size. On the contrary, the crack initiation site size is independent of the stress range in the furnace cooled & α-aged microstructures. This appears to extend the crack initiation life in both these microstructures, relative to the ω-aged microstructure.

Fatigue Behavior of Titanium Alloys
Edited by R.R. Boyer, D. Eylon, and G. Lütjering
The Minerals, Metals & Materials Society, 1999

INTRODUCTION

Beta titanium alloys offer a variety of microstructural morphologies and associated mechanical property variations thus giving considerable latitude in microstructure design. These alloys offer the highest strength to weight ratio and deepest hardenability among titanium alloys[1]. They also possess excellent hot workability and good strength-toughness-ductility combinations surpassing that of conventional two phase ($\alpha+\beta$) alloys[2,3]. These attributes have over the years increased their use in high strength aerospace applications[4]. Fatigue resistance is a critical requirement that cannot be overlooked in aircraft applications because of obvious safety reasons. The capability to achieve high strength levels in beta alloys is generally limited by the need to maintain a minimum fatigue resistance. Thus, characterizing the fatigue behavior of any potential alloy is important in this class of titanium alloys. Only a few attempts[5-10] have been made to characterize the fatigue behavior of beta alloys. Generally, it was observed[11,12] that changes in the characteristics of primary alpha do not have a pronounced effect on the fatigue crack growth (FCG) response of beta alloys. An exception[11] is the effect brought about by the presence of omega (ω) precipitates. On the contrary, fatigue crack initiation (FCI) behavior of beta alloys varies with microstructure[6,7,13] even at equal strength levels. The micromechanisms responsible for the varied fatigue behavior are not clear.

Generally, heat treatment of the beta alloys is performed in the $\alpha+\beta$ field because β-solution treatment followed by quenching resulted in high strengths and concomitant low ductility and toughness[2]. An alternative is to slowly cool from β-field instead of quenching. Slow cooling generally results in high aspect ratio α-plates, which could enhance toughness significantly. A variation in the subsequent aging treatments should provide a good strength-toughness combination. There has been very little work done to understand the fatigue behavior of β-annealed microstructures of Ti-10V-2Fe-3Al alloy.

The objective of the present work is to investigate the FCG & FCI behavior of beta (β) heat treated microstructures. The microstructures were aged differently so as to obtain almost similar strength levels. The micromechanisms of FCI and the consequent fatigue behavior were analyzed

EXPERIMENTAL PROCEDURE

The starting material for the study was 1.5" thick Ti-10V-2Fe-3Al alloy plates. Prior processing involved β forging followed by water quenching[14]. Subsequently the alloy was $\alpha+\beta$ forged and rolled into plate form in the $\alpha+\beta$ region. Three microstructures, *viz.*, furnace cooled, α-aged & ω-aged were obtained by β heat treatment. The β-transus temperature of this alloy is 805°C ± 3°C[11]. The furnace cooled microstructure was obtained by annealing at 815°C for 1/2 hr followed by furnace cooling. The two aged microstructures were obtained by initially β-heat treating as above which was followed by $\alpha+\beta$ solution treatment at 700°C for 10hrs. Subsequently α-aging was performed at 525°C for 8 hrs to precipitate α_s and ω-aging was performed at 260°C for 10 hrs to precipitate ω. Aging temperatures were determined from the time-temperature-transformation diagram[15] such that secondary alpha (α_s) and ω-phase are precipitated. Aging times were chosen such that the Vickers hardness levels of all three microstructures were almost similar.

Tensile testing was performed using specimens of 1" gage length, 0.25" width and 0.1" thick at a strain rate of 2.76×10^{-3} /sec. Fatigue crack growth tests were performed on compact tension (CT) specimens of 8 mm thickness and 50 mm width. After heat treatment, the specimens were sequentially polished upto 1 μ alumina. Experiments were performed

according to ASTM E647 at a stress ratio R=0.1 and frequency 35 Hz on MTS 810 servohydraulic test system equipped with TESTAR II controller and an automated crack growth testing procedure. Crack growth was monitored using a COD gage.

Fatigue tests to construct σ_{max}-N_f curves were performed on smooth fatigue specimens shown in figure 1. Specimens were initially electric discharge machined (EDM) from the plate and then subsequently heat treated. After heat treatment they were mechanically polished using 240 emery paper to remove the surface layers affected by heat treatment. Subsequently electropolishing was performed using a solution of 80% glacial acetic acid and 20% perchloric acid at a temperature of ~ 5°C and at around 35-40 volts. Tests were conducted at R=0.1 and frequency 35 Hz. The maximum cyclic stress was typically between 60% and 100 % of the tensile strength. Fatigue fracture were surfaces observed under a Cambridge scanning electron microscope (SEM) to identify the location and mechanisms of crack initiation. The areas of the crack initiation sites were measured from SEM micrographs by tracing the outline on a transparent graph sheet.

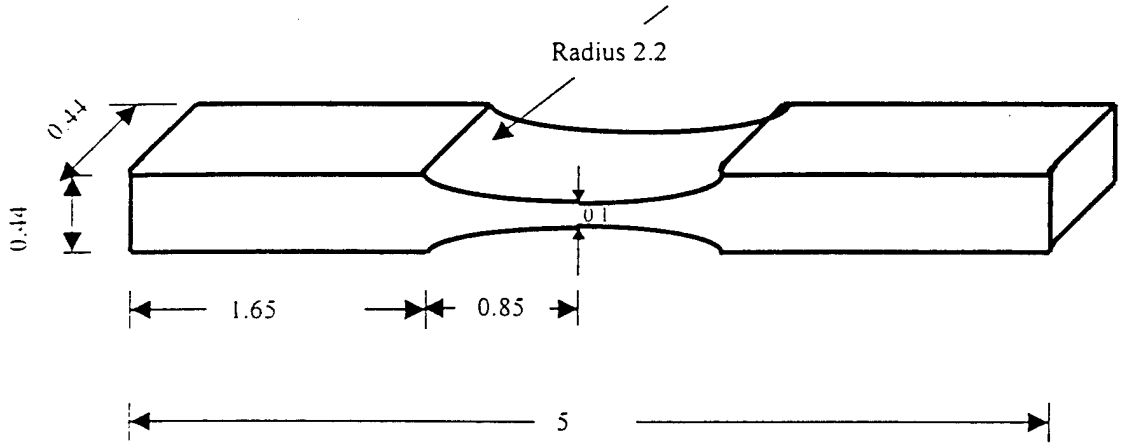

NOTE: Dimensions in inches

Fig. 1. Specimen geometry of smooth fatigue sample

RESULTS AND DISCUSSION

Microstructure and Tensile Behavior

Furnace cooling from the β-field produced a Widmanstatten basketweave microstructure as shown in figure 2(a). The prior β-grain size was 155 μ as measured by the linear intercept method. Figures 2(b) & 2(c) illustrate the microstructures after the α+β solution heat treatment followed by α- and ω-aging respectively. The volume fraction of α_p in both these microstructures was about 40% as measured by the point count method. It is to be noted that the aging conditions result in α_s and ω in the α-aged and ω-aged microstructures[15]. However, due to the fine size scale of α_s and ω phases, these are not visible in these micrographs. The mechanical properties are given in table 1.

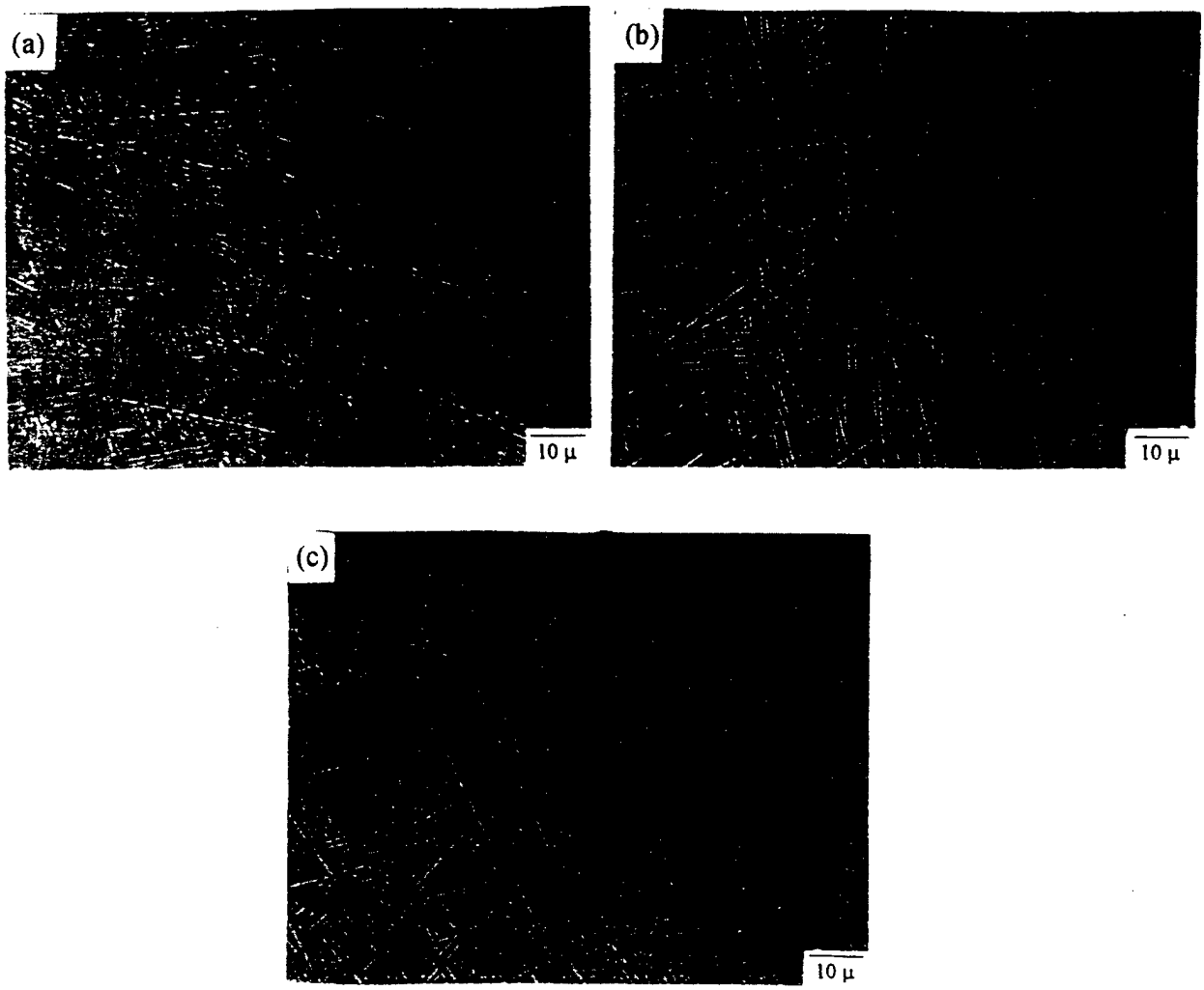

Fig. 2. β heat treated microstructures of Ti-10V-2Fe-3Al
(a) Furnace cooled (b) α-aged (c) ω-aged

Table 1: Mechanical properties of Ti-10V-2Fe-3Al after heat treatment

No.	Heat Treatment	Microstructure	0.2%YS (MPa)	UTS (MPa)	% Elongation	n	$\Delta\sigma_f$ (MPa)
1	815°C ½ h FC	Furnace cooled	880	978	13.78	0.45	700
2	815°C ½ h FC; 700°C 10 h WQ; 525°C 8h WQ	FC + (α+β) solution treated + α_s aged	925	997	10.53	0.44	700
3	815°C ½ h FC; 700°C 10 h WQ; 260°C 10 h WQ	FC + (α+β) solution treated + ω-aged	978	990	5.73	0.38	630

$\Delta\sigma_f$ = fatigue limit at 10^7 cycles; FC – Furnace cooled; WQ – Water Quenched; YS – Yield stress; UTS – Ultimate tensile strength; n – strain hardening exponent.

Fatigue Crack Growth (FCG) behavior

FCG responses of the three microstructures are shown in figure 3. It is clear that the FCG behavior is independent of the microstructure. In addition, there is almost no difference in the ΔK_{th} values among the microstructures. This shows that the presence of ω-phase does not influence either the FCG rates or the threshold stress intensity factor range, ΔK_{th}. On the contrary, past work by Duerig et.al.[11] showed a distinct change in the fatigue crack propagation rate in the microstructure containing ω-phase when compared to the non-ω microstructures. It should be noted that Duerig et.al.[11] employed microstructures with high strength (UTS ranging between 1250 – 1450 MPa) compared to those studied here (UTS ~ 1000 MPa). Further investigation is necessary to explain the absence of microstructural effect between the ω and the non-ω conditions in terms of their FCG behavior.

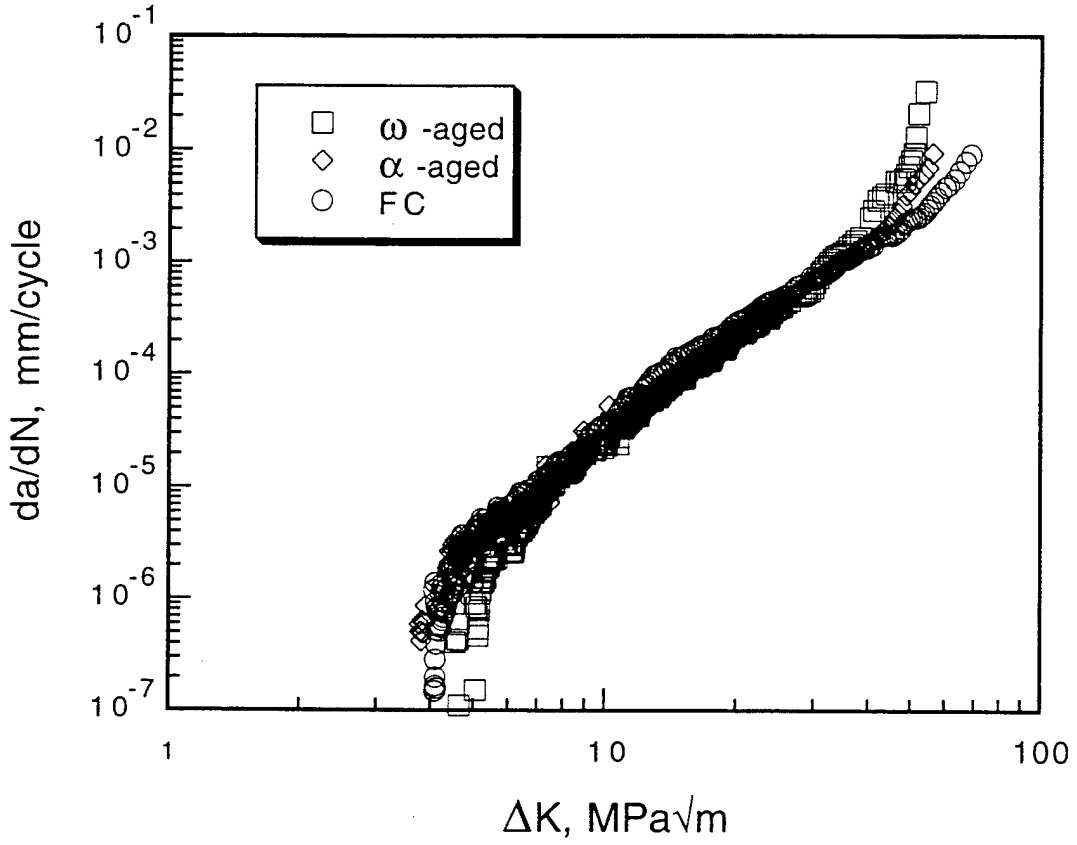

Fig. 3. Fatigue Crack Growth curves of FC, α-aged & ω-aged microstructures at R=0.1

Fatigue Crack Initiation behavior

The σ_{max}-N_f curves of all the three microstructures are shown in figure 4. The ω-aged microstructure clearly exhibits relatively poor resistance to fatigue compared to the other two microstructures. The influence of ω appears to be more pronounced in the lower stress high cycle fatigue (HCF) domain of the curve. The fatigue limit of these microstructures is given in Table 1. From figure 4, it can also be seen that in the case of ω-aged & α-aged, crack initiated at the surface from stress levels 850 MPa and above while it was subsurface/interior below 850 MPa. In FC, a mixed trend is observed though there is a tendency for surface crack initiation at higher stresses. There is no significant difference between the fatigue behavior of FC and α-aged microstructures.

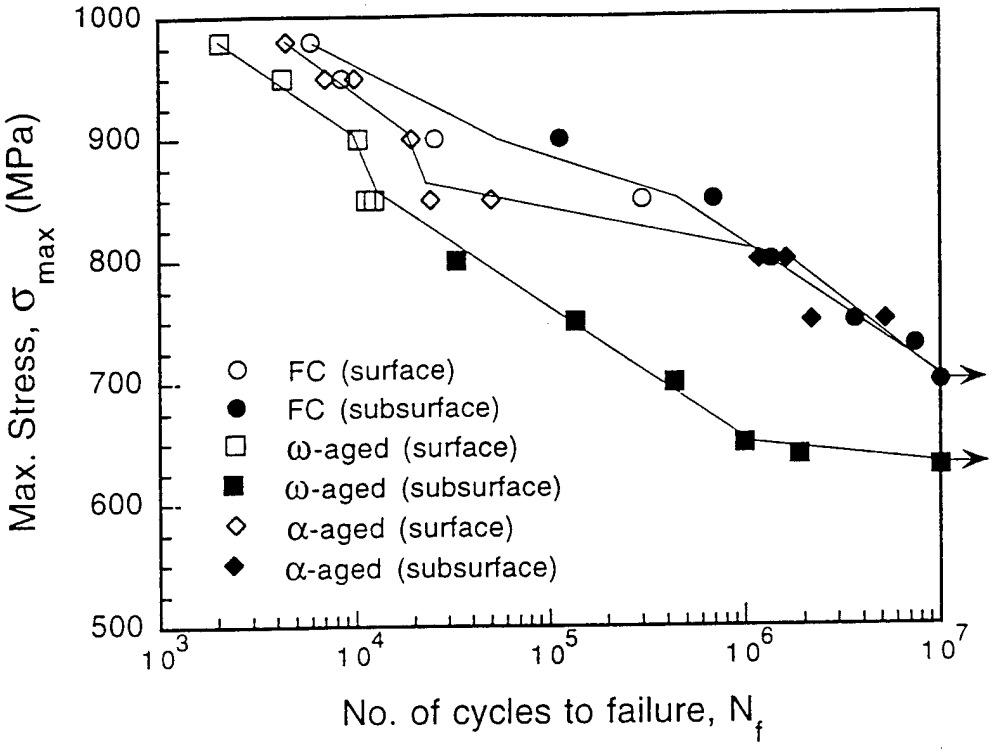

Fig. 4. σ_{max} – N_f behavior of FC, α-aged & ω-aged at R=0.1. The initiation locations (surface or subsurface) are identified in the captions.

Characteristics of interior/subsurface crack initiation

Figures 5(a) & (b) show the crack initiation site in the furnace cooled microstructure at a maximum cyclic stress of 730 MPa. Figure 5(c) indicates the measured area of the crack initiation site. From 5(b) it is clear that the initiation site is a flat faceted region consisting of a number of aligned α-plates. At all stress levels of subsurface initiation, the presence of α-plates could be clearly seen at the initiation sites. This indicates a cleavage mode of crack initiation. Fatigue crack initiation by cleavage was initially observed in an earlier study[16]. A similar explanation may be applied for the cleavage features observed at the initiation sites in this study.

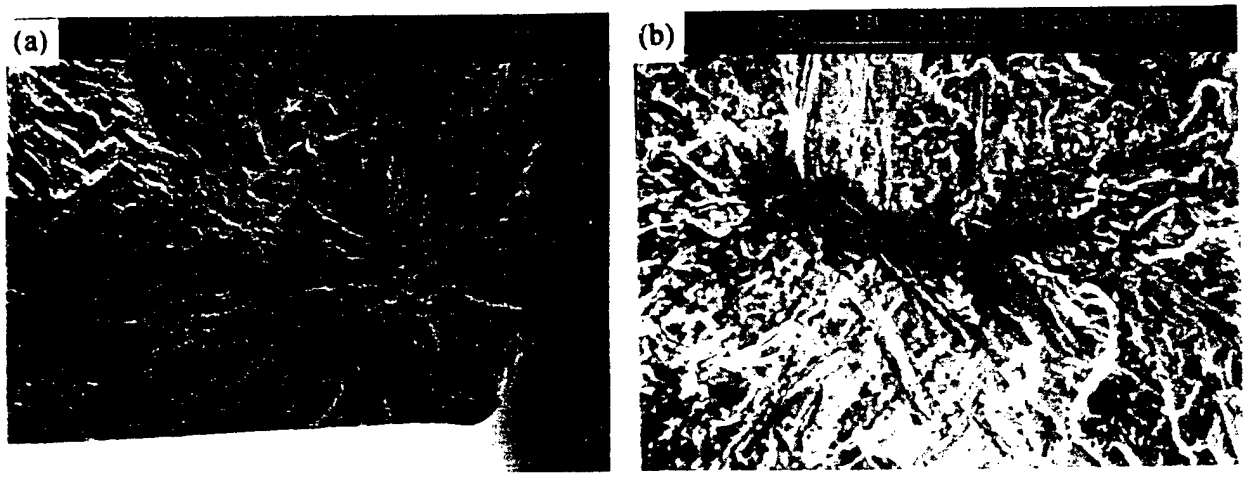

Fig. 5. Subsurface crack initiation in FC at σ_{max} = 730 MPa (a) Low magnification (b) High magnification

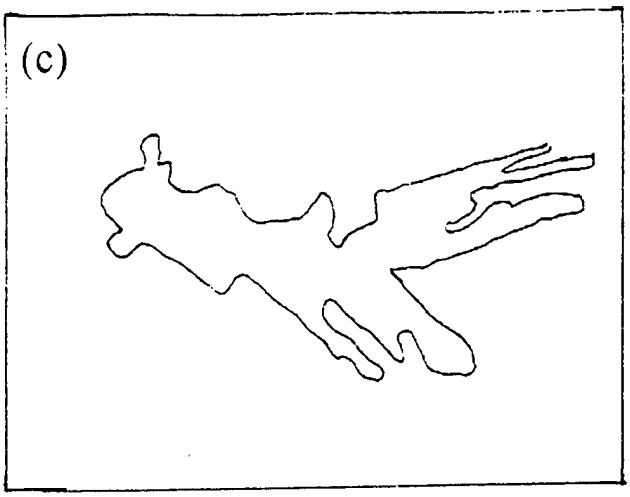

Fig. 5 (c) Area of the crack initiation site in FC at σ_{max} = 730 MPa

Figures 6(a) & 6(b) show a typical subsurface crack initiation site in the ω-aged microstructure. As in the furnace cooled microstructure, there is a flat faceted region indicative of cleavage fracture. Figure 7(a) shows a large faceted region at the initiation site in the ω-aged condition at σ_{max} = 640 MPa. Figure 7(b) shows the area of the corresponding initiation site. In figure 7(a) a step like appearance can be observed in the faceted region. This probably happens due to the presence of ω-precipitates in this microstructure. It is well known[2] that dislocations cut through ω-precipitates leading to a planar slip mode. Slip is localized in these planes which appear as coarse slip steps. This localization of slip appears to initiate the cleavage process. Thus the microstructural feature controlling the fatigue behavior in the ω-aged condition is suggested to be the ω-precipitates.

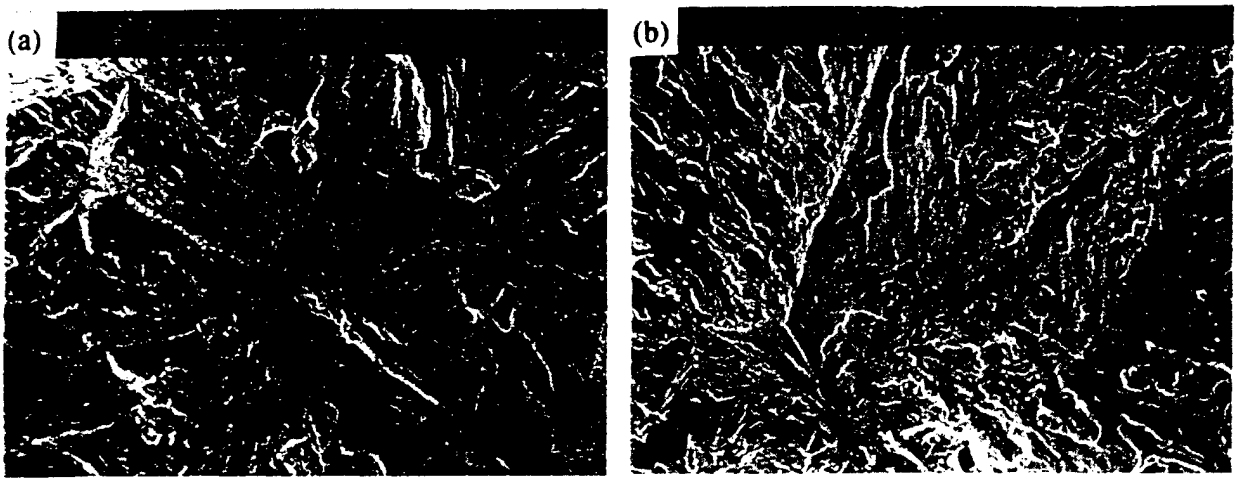

Fig. 6. Subsurface crack initiation site in ω-aged microstructure at σ_{max} = 650 MPa
(a) Low Magnification (b) High Magnification

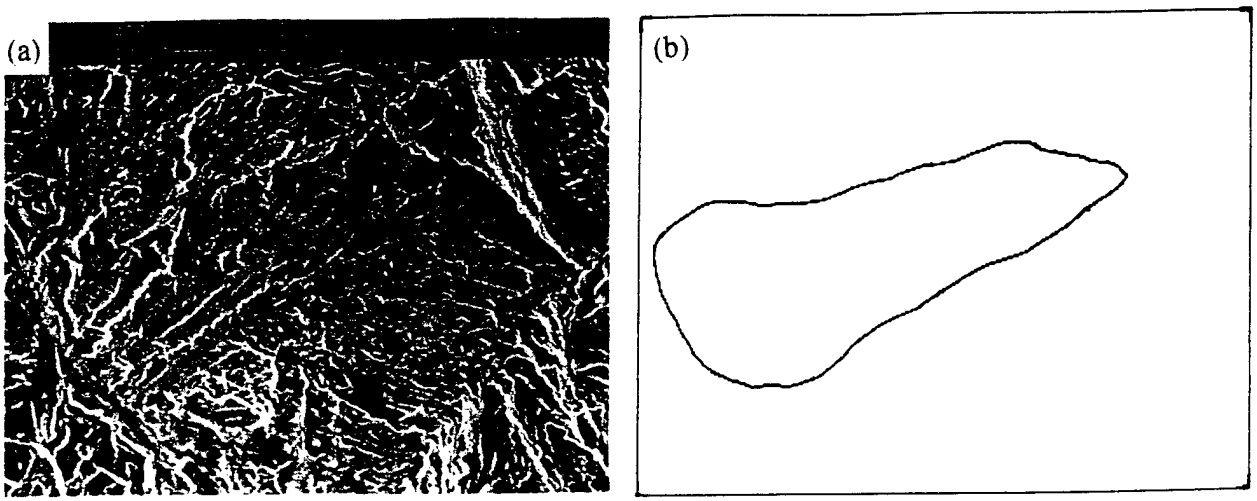

Fig. 7. (a) Cleavage facets in ω-aged microstructure at σ_{max} = 640 MPa
(b) Area of the crack initiation site

Figure 8(a) shows a subsurface crack initiation site in the α-aged microstructure. The corresponding area of the crack initiation site is shown in figure 8(b). The initiation site shows featureless α-plates with a dominant grain boundary alpha (GB_α) but there also appear cleavage markings on the site. It appears that the process of cleavage initiated from the GB_α. Figure 9(a) also shows an initiation site with cleavage of α_p plates with the appropriate area in figure 9(b). Here no GB_α is seen. Recent work by Kiese and Wagner[10] on this alloy stressed the importance of the strength of GB_α with respect to the matrix that leads to the formation of GB_α cracks. In the present case, though one would expect a strength differential between the aged matrix and GB_α regions, the probability of crack initiation at GB_α and in the interior seems equal as demonstrated by figures 8 & 9. Thus in the α-aged microstructure, the initiation mechanism appears to be controlled by the α_p plates.

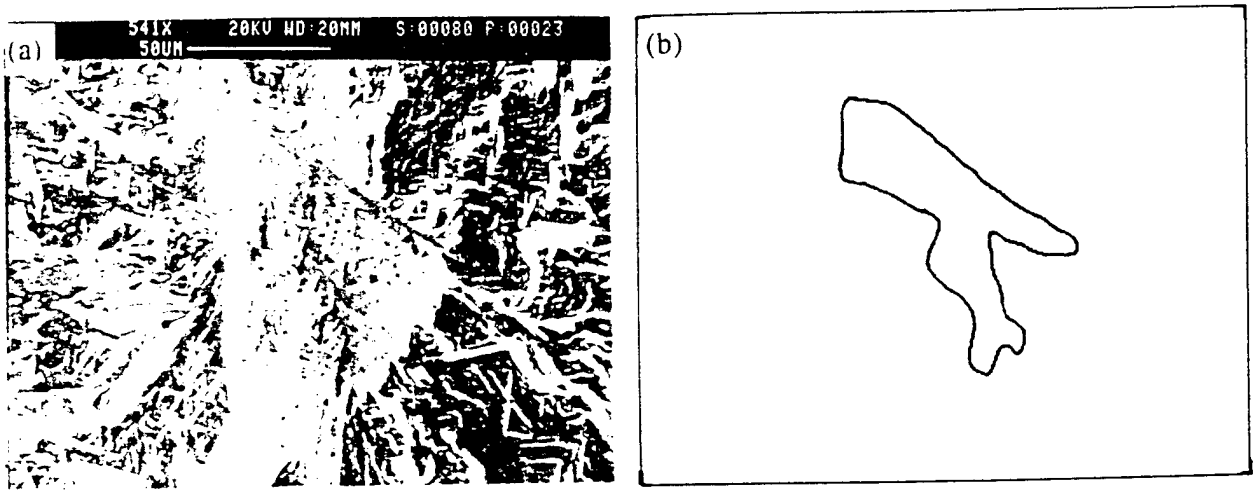

Fig. 8 (a) Subsurface crack initiation site in α-aged at σ_{max} = 800 MPa
(b) Crack Initiation site area

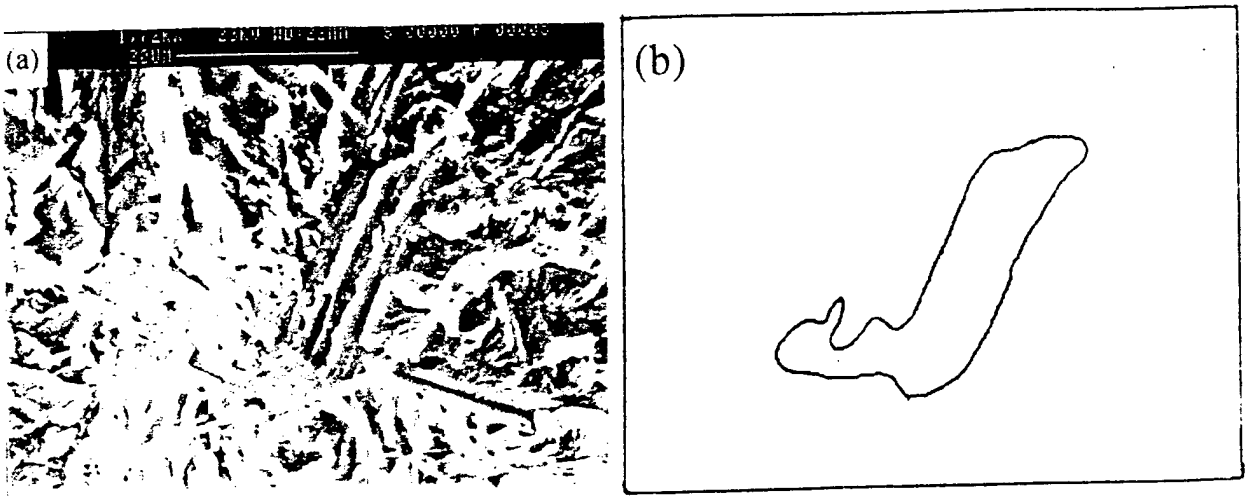

Fig. 9 (a) Subsurface crack initiation site in α-aged at σ_{max} = 800 MPa
(b) Crack Initiation site area

Characteristics of surface crack initiation

Figures 10-12 are typical surface crack initiation sites in FC, ω-aged & α-aged respectively. All the three microstructures exhibit a flat faceted initiation site. No significant difference in the initiation site can be observed between these microstructures. There are two mechanisms, which have been proposed for surface initiation in titanium alloys. One is the conventional persistent slip band (PSB) approach[17] which deals with the formation of intrusions and extrusions at the specimen surface. At lower stresses, the intrusion-extrusion mechanism becomes less distinct because the formation of PSBs needs a plastic strain amplitude of over 10^{-5}[18]. At higher stresses, since this strain amplitude is achieved surface crack initiation occurs. The other mechanism was proposed for Ti-6Al-4V by Ruppen et.al.[19]. According to them, if slip compatibility between α & β phases can occur on pyramidal planes, then surface initiation results at high stresses. The mechanism of surface crack initiation is unclear at this time.

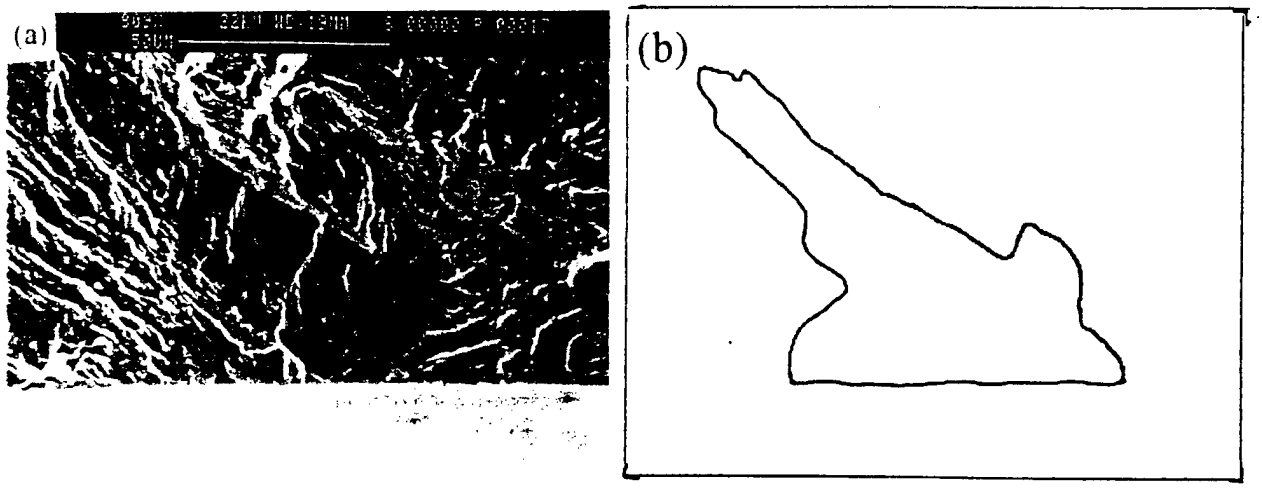

Fig. 10 (a) Surface crack initiation site in FC at σ_{max} = 980 MPa
(b) Area of the initiation site

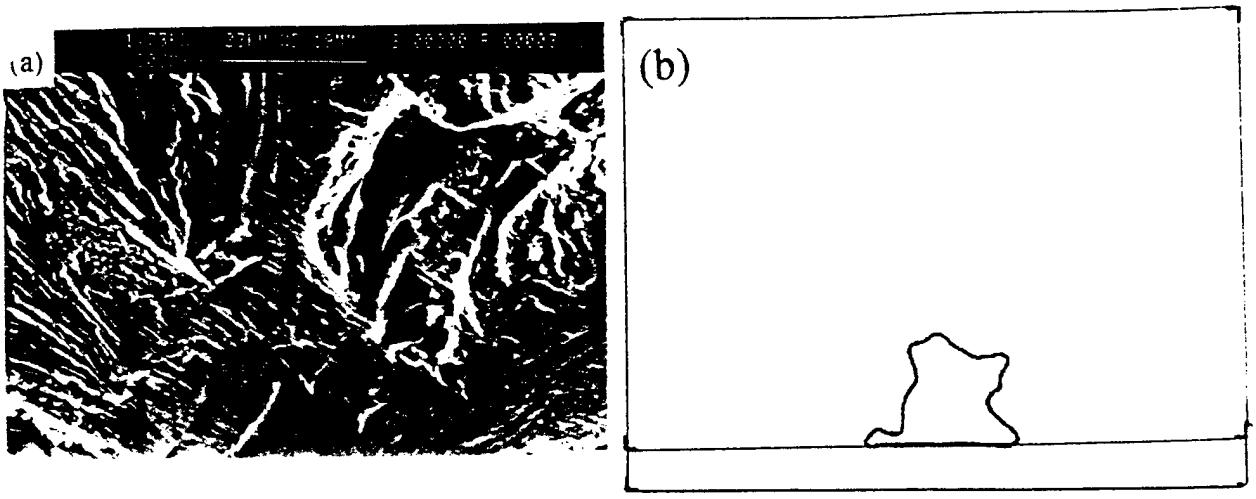

Fig. 11 (a) Surface crack initiation site in ω-aged at σ_{max} = 980 MPa
(b) Area of the initiation site

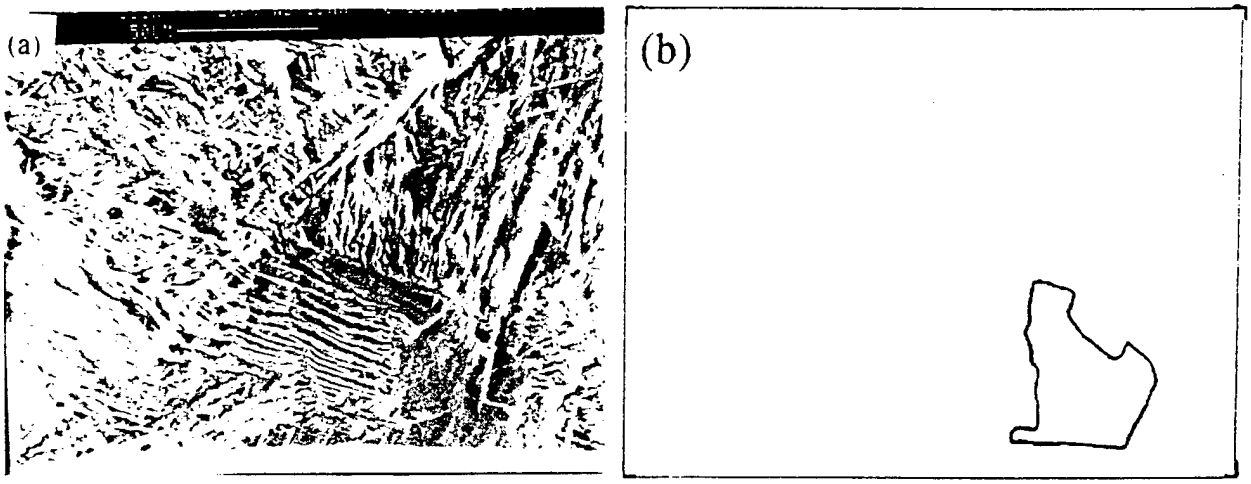

Fig. 12 (a) Surface crack initiation site in α-aged at σ_{max} = 980 MPa
(b) Area of the initiation site

Crack initiation site size and its relevance in S-N fatigue behavior

Assuming an equivalent embedded circular crack of diameter '2a', the diameter of the crack initiation site was calculated from the total area of the crack initiation site and has been plotted against the maximum cyclic stress as shown in figure 13. From the figure it is clear that at lower stress levels, the crack initiation site size in ω-aged microstructure is bigger compared to the other two microstructures. This difference in site size appears to be consistent with the mechanism of cleavage in these microstructures. Figure 14(a) shows the initiation site of the ω-aged microstructure observed at 750 MPa at a high magnification. Very fine cleavage features are seen with no deflection. In the ω-aged microstructures, the planarity of slip leads to slip

localization that initiates the cleavage process resulting in large facets. On the contrary, figure 14(b) shows the cleavage mechanism in the FC microstructure. Cleavage features are seen in every α-platelet and it looks like there is deflection/arrest across α-β interfaces. The pronounced α-β interface is an indication of this. Cleavage in FC microstructure is clearly controlled by individual α_p plates that appear to reduce the size of the initiation site.

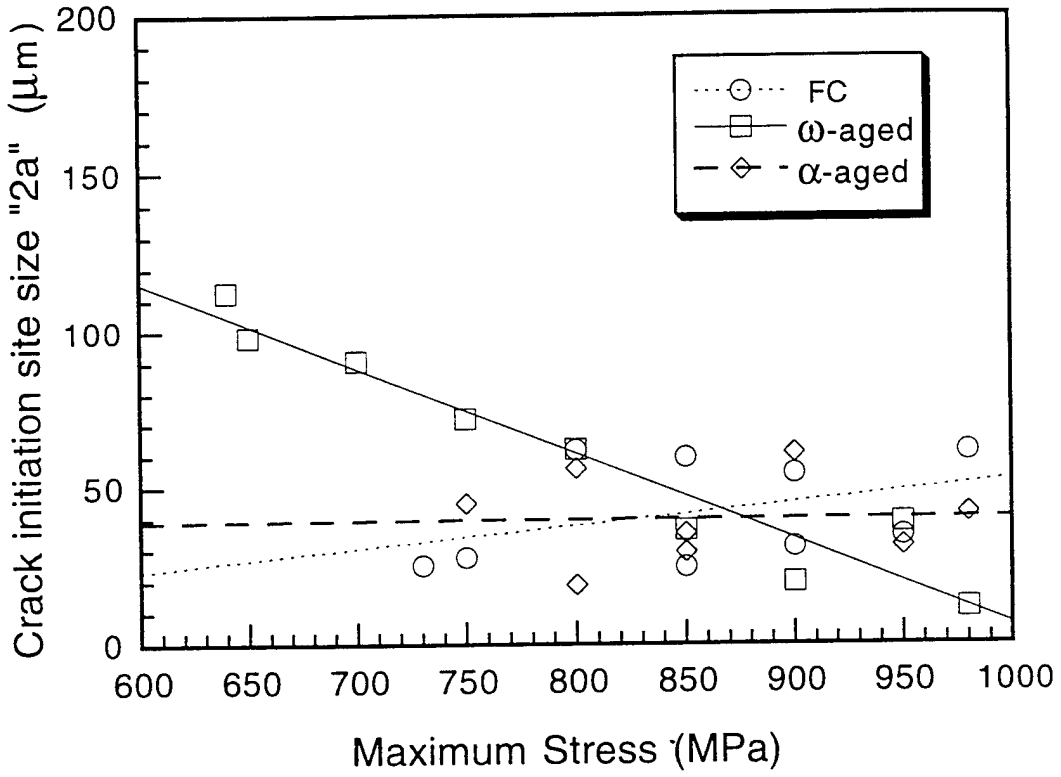

Fig. 13. Variation of crack initiation site size with maximum cyclic stress

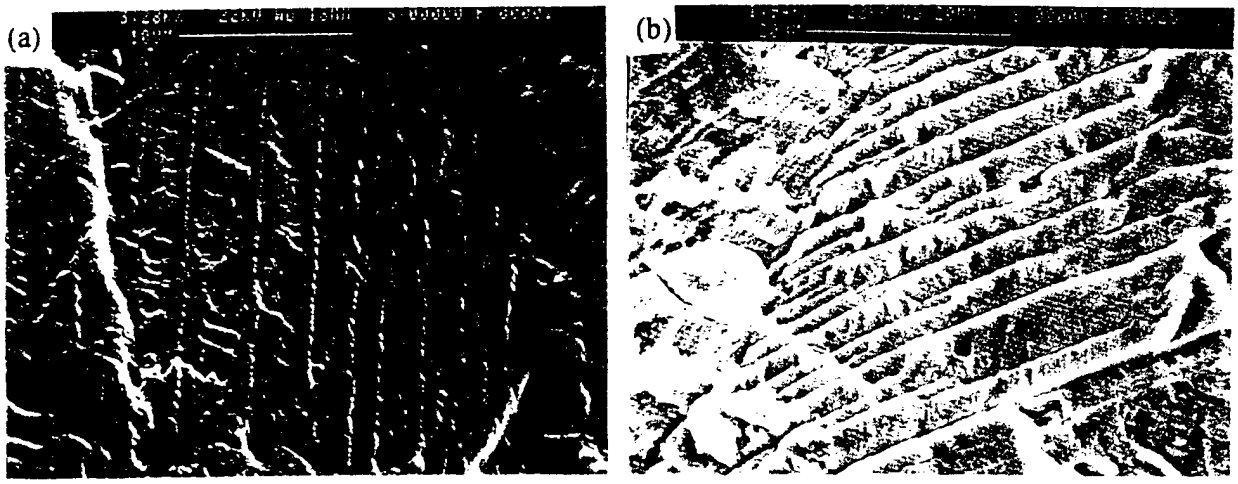

Fig. 14. Mechanism of cleavage in (a) ω-aged microstructure (b) FC microstructure

It can also be observed from figure 13 that in the ω-aged microstructure, the site size decreases linearly with increasing maximum stress whereas in the other two microstructures, the site size

is more or less a constant. The presence and absence of such a stress dependence in the ω and non-ω microstructures respectively, can be interpreted following manner. After crack initiation has taken place, the rest of the fatigue life is all crack propagation and thus the equation $\Delta K = \Delta\sigma\sqrt{\pi}\sqrt{(2a)}\ f(a/w)$ is assumed to be valid. When all the microstructures are subjected to the same stress, the ΔK in the ω microstructure at the beginning of the crack propagation phase is much higher than the other two because the crack initiation site size is higher in the ω-microstructure. Due to this higher ΔK, failure occurs in a lesser number of cycles. From an alternate perspective, since the site size is higher in ω-aged microstructure, if it were to fail at the same number of cycles as the other two microstructures, then it would need a lower cyclic stress range to be applied. This is the primary reason for the poor response of the ω-aged microstructure in the high cycle fatigue domain of the S-N curve, i.e., below 850 MPa. At higher stress, this rationale doesn't work as it predicts a higher life to failure in the ω-aged condition. At higher stresses since the crack initiates from the surface rather than interior, the mechanism of its formation is likely to dictate the fatigue life in these microstructures. Also, since the crack propagation behavior is almost same for all the three microstructures, the initiation life in the ω-aged microstructure is relatively short when compared to the non-ω microstructures.

CONCLUSIONS

Fatigue response and crack initiation mechanisms have been evaluated for three beta heat treated microstructures of Ti-10V-2Fe-3Al titanium alloy. The specific conclusions that can be drawn are as follows.

1. Fatigue Crack Growth resistance of all three microstructures is almost same.
2. ω-aged microstructure has the poorest σ_{max}-N_f behavior among all the three microstructures. The two non-ω microstructures do not show a significant difference between their σ_{max}-N_f behavior.
3. Subsurface crack initiates by a process of cleavage in all the three microstructures. ω precipitates resulting in slip localization appear to control the cleavage process in the ω-aged whereas α_p plates seem to be the controlling microstructural feature in the non-ω aged.
4. There is a stress dependence of the initiation site size in the ω-aged microstructure whereas the site size is independent of microstructure.
5. In the high cycle fatigue regime, the bigger fatigue crack initiation site size in the ω-aged condition compared to the non-ω aged microstructures seems to be related to the mechanism of cleavage.
6. The crack initiation phase in the furnace cooled and the α-aged microstructure is relatively greater than the ω-aged microstructure.

ACKNOWLEDGEMENT

This research was performed under the support of the Air Force Office of Scientific Research (AFOSR) of the U.S. Air Force through a grant: F49620-96-1-0102. The authors are thankful for the interest and encouragement of program managers: Drs. S. Wu & C.H. Ward. The supply of material by TIMET, Inc., Henderson, Nevada, USA is gratefully acknowledged.

REFERENCES

1. P.J. Bania, Beta titanium alloys in the 1990s, TMS-AIME (1993), D.Eylon, R.R. Boyer & D.A. Koss (Eds) 3
2. T.W. Duerig & J.C. Williams, Beta titanium alloys in the 80's, TMS-AIME (1984), R.R. Boyer & H.W. Rosenberg (Eds) 19
3. C.C. Chen & R.R. Boyer, J. Metals, 31, (1979) 33
4. R.R. Boyer, Beta titanium alloys in the 1990s, TMS-AIME (1993), D.Eylon, R.R. Boyer & D.A. Koss (Eds) 335
5. R. Chait & T.S. DeSisto, Metall. Trans., 8A, (1977) 1017
6. R.R. Boyer & G.W. Kuhlman, Metall. Trans., 18A, (1987) 2095
7. L. Wagner & J.K. Gregory, Beta titanium alloys in the 1990s, TMS-AIME (1993), D.Eylon, R.R. Boyer & D.A. Koss (Eds) 199
8. E. Awade, J. Mendez, J.M. Rongvaux, Intl. Workshop on "Beta Titanium Alloys, (1994) A. Vassel, D. Eylon & Y. Combres (Eds) 143
9. K. Shiozawa & H. Matsushita, Fatigue '96, Proc. Sixth Intl. Fatigue Cong. Pergamon Press (1996) G. Luthering & H. Nowack (Eds) 301
10. J. Kiese & L. Wagner, Fatigue '96, Proc. Sixth Intl. Fatigue Cong. Pergamon Press (1996) G. Luthering & H. Nowack (Eds) 959
11. T.W. Duerig, J.E. Allison & J.C. Williams, Metall. Trans. 16A, (1985) 739
12. D. Grandemange, Y. Combres & D. Eylon, Beta titanium alloys in the 1990s, TMS-AIME (1993), D.Eylon, R.R. Boyer & D.A. Koss (Eds) 227
13. Fatigue Data Book: Structural Alloys ASM, 356
14. Unpublished work
15. T.W. Duerig, G.T. Terlinde & J.C. Williams, Metall. Trans., 11A, (1980) 1987
16. D.F. Neal & P.A. Blenkinshop, Acta Metall., 24, (1976) 59
17. P. Neumann, Acta Metall., 17, (1969) 1219
18. O. Umezawa & K. Nagai, ISIJ Intl., 37, (1997) 1170
19. J. Ruppen, P. Bhowal, D. Eylon & A.J. McEvily, ASTM STP 675, Published by ASTM (1979) 47

Appendix IV

Effect of Mean Stress (Stress Ratio) and Aging on Fatigue-Crack Growth in a Metastable Beta Titanium Alloy, Ti-10V-2Fe-3Al

Effect of Mean Stress (Stress Ratio) and Aging on Fatigue-Crack Growth in a Metastable Beta Titanium Alloy, Ti-10V-2Fe-3Al

S.K. JHA and K.S. RAVICHANDRAN

The effect of mean stress, or the stress ratio (R), on the fatigue-crack growth (FCG) behavior of α-aged and ω-aged microstructures of the beta titanium alloy Ti-10V-2Fe-3Al was investigated. While the mean stress had a negligible effect on the FCG behavior of the α-aged microstructure, a strong effect was observed in the ω-aged microstructure. In particular, the values of the threshold stress-intensity range (ΔK_{th}) exhibited a strong dependence on R in the ω-aged microstructure, while this dependence was weak in the α-aged microstructure. These effects seem to arise primarily from fracture-surface roughness-induced crack closure. The crack closure levels for the α-aged microstructure were found to be very low compared to those for the ω-aged microstructure. Transmission electron microscopy and scanning electron microscopy studies of microstructures and fracture surfaces were performed to gain insight into the deformation characteristics and crack propagation mechanisms, respectively, in these microstructures. The microstructure-induced differences in FCG behavior are rationalized in terms of the effect of aging on slip and crack closure.

I. INTRODUCTION

Ti-10V-2Fe-3Al (Ti-10-2-3), a metastable β-titanium alloy, is a widely used material for high-strength applications in the aerospace industry, owing to its relatively high strength, excellent strength/toughness combination, good fatigue strength, and enhanced processing characteristics.[1–6] A number of microstructural variations can be produced in this alloy by employing different combinations of thermomechanical processes and heat treatments.[1,2,3] Typically, the alloy is heat treated either by quenching from the $\alpha + \beta$ or the β field and is subsequently aged at a lower temperature. During aging, the β phase decomposes into a β phase enriched in β-stabilizing elements, secondary α particles (α_s), and/or ω particles, depending on the aging temperature and time.[7,8,9] By varying these parameters during aging, the strength and ductility of this alloy can be varied significantly.[1]

There are studies[1,6,8,10] indicating that fatigue crack growth (FCG) characteristics are little affected by microstructural parameters that can be varied by primary heat treatment, such as volume fraction, size, or shape of primary α in β-titanium alloys. However, there have been very few studies on the FCG behavior of Ti-10-2-3 as influenced by the secondary heat treatment, that is, the aging condition. In particular, the effect of ω-phase formation at lower aging temperatures has not been fully understood. The issue of the presence or absence of ω phase in the microstructure is significant, since it has been suggested[3,8] that ω phase formation significantly decreases the ductility of β titanium alloys. Therefore, it is considered important to systematically investigate the effect of ω phase formation on the FCG response of Ti-10-2-3, including its effect on the stress-ratio dependence of FCG behavior.

Duerig *et al.*[8] first observed a significant increase in FCG resistance at growth rates less than 5×10^{-4} mm/cycle, in the case of an ω-aged microstructure, when compared to an α-aged microstructure of comparable strength, at the stress ratio (R) of 0.1. It was suggested that planar slip induced by the ω phase led to increased mode II displacements at the crack tip, causing asperity mismatch and, thus, leading to crack closure.[11,12,13] There was no attempt, however, to show conclusively that crack closure was, indeed, responsible for the differences in the FCG behavior of ω-aged and α-aged microstructures. In the aforementioned work, at growth rates greater than 5×10^{-4} mm/cycle, the ω-aged microstructure showed higher growth rates relative to those of the α-aged microstructure. It is not obvious why a microstructure with planar deformation characteristics should show different responses above and below 5×10^{-4} mm/cycle, as indicated previously. The limited data (only one FCG test was reported) also raise concerns with regard to the dependence of FCG on R in ω-aged and ω-free microstructures in Ti-10-2-3. A study clarifying this issue is needed, since, in conventional $\alpha + \beta$ and α titanium alloys,[14–20] weak and strong effects of the stress ratio on FCG rates have been found, seemingly depending on composition and microstructures.

There are two different explanations given for the observation of a stress-ratio effect in conventional titanium alloys. First, earlier studies[14,15,16] suggested that the higher growth rates at high R levels were due to the contribution from static modes of crack extension to cyclic crack extension. Second, crack closure, due to the interference in the crack wake at low ΔK levels, has been suggested in recent studies[17,18,19] to cause lower growth rates at low R values than at high R values. However, there are also studies[20] which show that crack closure does not completely explain the stress-ratio effect on FCG rates. Further, more-recent interpretations[21] suggest an altogether different explanation for

S.K. JHA, Graduate Research Assistant, and K.S. RAVICHANDRAN, Associate Professor, are with the Department of Metallurgical Engineering, 135 South, 1460 East, Rm. 412, University of Utah, Salt Lake City, UT 84112.

Manuscript submitted May 11, 1999.

Table I. Chemical Composition of the Ti-10V-2Fe-3Al Alloy

Element	H (Max)	O (Max)	N (Max)	Fe	Al	V	Ti
Wt pct	0.01	0.03	0.03	1.93	2.95	10.15	balance

the dependence of FCG on the stress ratio. The intent of the present study is not to resolve the varied observations of stress-ratio effect and their interpretation in different classes of titanium alloys; rather, the principal objectives of this research are to investigate the effect of R on FCG in ω-aged and α-aged microstructures in Ti-10-2-3 and to identify the relevant mechanisms responsible for such an effect. Therefore, the effect of α aging *vs* ω aging on FCG was studied by maintaining a constant primary solution heat treatment and varying the nature of the secondary heat treatment. It has been found that there is only a small effect of R upon FCG in the near-threshold region, but almost none in the Paris-law regime, in the case of the α-aged microstructure. However, in the case of the ω-aged microstructure, a significant effect of the R ratio over the entire FCG regime was observed. The mechanisms responsible for these effects have been identified from fractography and crack-path observations.

II. MATERIAL AND EXPERIMENTAL PROCEDURE

A. *Material*

The Ti-10-2-3 alloy was supplied by TIMET (Henderson, NV) in the form of plates of 267 × 210 × 38 mm in size. The chemical composition of the plates is given in Table I. The β-transus temperature for the alloy was about 800 °C. The plates were made from cast ingots by the following processing routes: β forging at 850 °C, followed by air cooling, then rolling in the $\alpha + \beta$ region at 760 °C to a 25 pct reduction in thickness, followed by air cooling. The microstructures in the plates were found to be uniform through the thickness, except in the near-surface regions, to a depth of about 2 mm. These regions were removed by electrodischarge machining (EDM). Blanks cut from the plates by EDM were heat treated to obtain the desired microstructures and aged conditions. The heat-treatment schedules are given in Table II. Since the strength of the Ti-10-2-3 alloy is largely influenced by aging, the aging periods were appropriately chosen to obtain similar strength levels at different aging temperatures. This was done to minimize the variation in FCG behavior due to differences in the strength level. Since the objective was to have comparable strength levels, the ω aging period was restricted to 6 hours. This may not correspond to complete transformation of β at this temperature. However, microhardness studies indicated that the change in Vickers hardness after 6 and 32 hours of aging treatment was less than 17 pct, suggesting that most of the transformation had occurred within 6 hours. Therefore, the microstructure can be considered to be almost in equilibrium. Compact-tension (CT) specimens of 63.5 × 61 × 8 mm in size, oriented in the longitudinal-transverse direction, were machined from the heat-treated blanks. The specimen surfaces were metallographically polished down to 1 μm alumina to enable the observation of crack growth.

B. *Experiments*

The FCG tests were conducted in an MTS 810 servohydraulic fatigue test system equipped with a TESTSTAR II digital controller, a personal computer, and the associated test-control software. Tests were done following the ASTM E647-93 FCG test standard.[22] The samples were precracked at ΔK levels of about 10 to 15 MPa$\sqrt{\text{m}}$. Following precracking, a decreasing ΔK test and, subsequently, an increasing ΔK test were conducted on a given sample. The ΔK gradients[22] of −0.08 and 0.2 were employed in the decreasing and increasing ΔK tests, respectively. Tests were performed at three stress ratios ($R = 0.1, 0.5$, and 0.8) at the frequency of 35 Hz, at room temperature in a laboratory air environment. Crack lengths were continuously monitored during testing using a crack-opening displacement (COD) gage* mounted at the mouth of the notch. The COD gage also enabled continuous recording of the load *vs* displacement traces, from which the closure loads were determined. The point of initial deviation from the linear-elastic part of the unloading curves was taken to be the closure load. These closure loads were used to determine ΔK_{eff} and K_{cl} values. The FCG tests were repeated at each R ratio to ensure reproducibility of the FCG data. In the case of the ω-aged microstructure, in addition to tests on regular CT samples, tests were also conducted using side-grooved CT samples. This was because, in regular CT samples, crack-plane deviations of about 10 deg occurred sometimes when cracks grew out of the notch. The K calculations for side-grooved specimens

*Model No. MTS 632.02F-20.

Table II. Heat Treatments, Microstructural Descriptions, and Tensile Properties for the Microstructures Investigated

Designation	Heat Treatment	Microstructure	0.2 Pct Yield Strength (MPa)	UTS (MPa)	Pct Elongation
α-aged	solution treatment at 700 °C for 2 h followed by water quenching; aging treatment at 525 °C for 8 h followed by water quenching	45 pct α_p + α_s particles in β-matrix	987	1065	13
ω-aged	solution treatment at 700 °C for 2 h followed by water quenching; aging treatment at 260 °C for 6 h followed by water quenching	45 pct α_p + ω particles in β-matrix	1028	1047	9

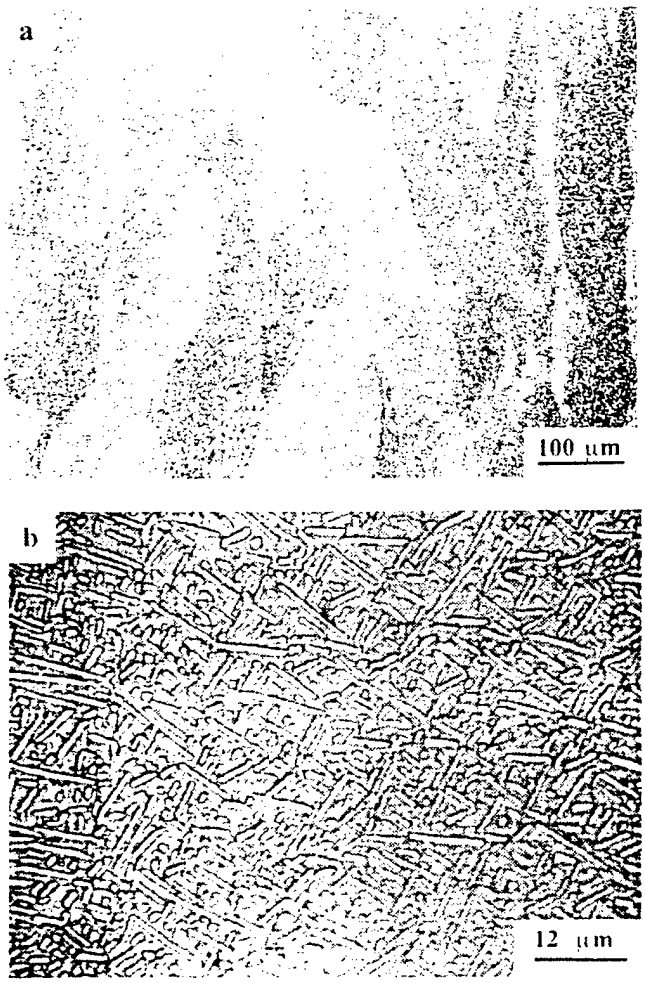

Fig. 1—Optical micrographs of the α-aged microstructure (*a*) showing prior-β grains and (*b*) showing distribution of α_p particles.

were done following ASTM E813-89 standards. Since there was no difference between the FCG behavior as determined by CT and side-grooved CT specimens, it was concluded that neither the side grooves nor the small out-of-plane crack extensions affected the FCG behavior of the ω-aged microstructure. The fracture surfaces, as well as crack-path profiles of FCG samples obtained by sectioning the fracture surface along the plane parallel to the specimen broad surface, were observed in a Cambridge S240 scanning electron microscope at an accelerating voltage of 20 kV. Thin-foil specimens, for observations of microstructure in a transmission electron microscope (TEM), were prepared by dimpling followed by ion milling. The foils were observed in a JEOL** JEM-2000 FX II TEM, at an accelerating voltage of 200 kV.

**JEOL is a trademark of Japan Electron Optics Ltd., Tokyo.

III. RESULTS AND DISCUSSION

A. *Microstructural and Tensile Properties*

Optical micrographs of the α-aged microstructure are shown in Figures 1(a) and (b). Figure 1(a) illustrates the structure of the β grains, which are elongated in the rolling direction. Figure 1(b) shows the morphology and the distribution of primary α (α_p) particles. Since the primary α heat treatment was the same, both the α-aged and the ω-aged microstructures appeared similar in optical micrographs. The volume fraction and the average interparticle spacing of α_p particles were estimated to be 0.45 and 1.8 μm, respectively, using point-counting and linear-intercept methods.[23] The microstructures, however, differed in terms of the constituents in the transformed β matrix. In Figure 2, TEM micrographs of the transformed β microstructure in the α-aged condition are presented. The bright-field micrograph and the $(110)_\beta$ diffraction pattern of this region are presented in Figures 2(a) and (b), respectively. The schematic of the diffraction pattern, presented in Figure 2(c), indicates that the (0001) pattern of secondary α (α_s) particles in the transformed β matrix is superimposed on the β-phase pattern. This is consistent with the established orientation relationship[7,24] between the α and β phases in titanium alloys, *viz.*, $(0001)_\alpha // \{110\}_\beta$ and $\langle 11\bar{2}0\rangle_\alpha // \langle 111\rangle_\beta$. Campagnac and Vassel[7] observed a slight arcing of the α_s diffraction spots in the diffraction pattern of an α-aged matrix. They concluded that this occurred due to superposition of two $(0001)_{\alpha_s}$ patterns. However, arcing was not very evident in the present study (Figure 2(b)). Dark-field imaging using the $(1\bar{1}00)_{\alpha_s}$ spot revealed the presence of relatively coarse α_s particles in the matrix (Figure 2(d)). In Figure 3, TEM micrographs of the ω-aged microstructure are presented, showing the distribution of ω phase in the ω-aged microstructure. The bright-field micrograph and the $(110)_\beta$ pattern of this region are presented in Figures 3(a) and (b), respectively. It is clear from Figure 3(b) that the $(11\bar{2}0)_\omega$ pattern is superimposed on the β-phase pattern (Figure 3(c)). This also is consistent with the established orientation relationship[7,24] between the ω and β phases in titanium alloys, *viz.*, $(0001)_\omega // \{111\}_\beta$ and $\langle 11\bar{2}0\rangle_\omega // \langle 110\rangle_\beta$. The dark-field image formed using the $(10\bar{1}0)_\omega$ spot revealed the distribution of ω phase in the matrix (Figure 3(d)).

B. *Effect of Stress Ratio on FCG*

Figures 4(a) and (b) show the FCG data for the stress ratios of $R = 0.1$, 0.5, and 0.8, in the form of *da/dN vs* ΔK plots, for the α-aged and ω-aged microstructures, respectively. From repeated tests, the FCG behavior was found to be very reproducible for both microstructures. For the α-aged microstructure, a smaller effect of R was observed in the near-threshold region, and very little R effect was present in stage II (Paris-law regime) of FCG. Such a pattern is commonly seen in high-strength materials, including 2.25Cr-1Mo steel[25] and some Al alloys.[26] Additionally, these data are consistent with the reported FCG data on the Ti-10-2-3 alloy.[27] In contrast, a significant R effect was observed, both in the threshold regime and in the Paris-law regime of FCG, for the ω-aged microstructure. Figure 5 shows the FCG data in terms of *da/dN vs* ΔK_{eff} for the two microstructures. It can be seen that the stress-ratio effect vanishes when the FCG data are plotted in terms of ΔK_{eff}, although, for the ω-aged microstructure at R equal to 0.8, the crack growth rates are slightly higher at *da/dN* levels greater than 10^{-4} mm/cycle. This suggests that the observed stress-ratio effect in most of the FCG region in the two microstructures is due to crack closure. It then follows that the ω-aged microstructure exhibited a

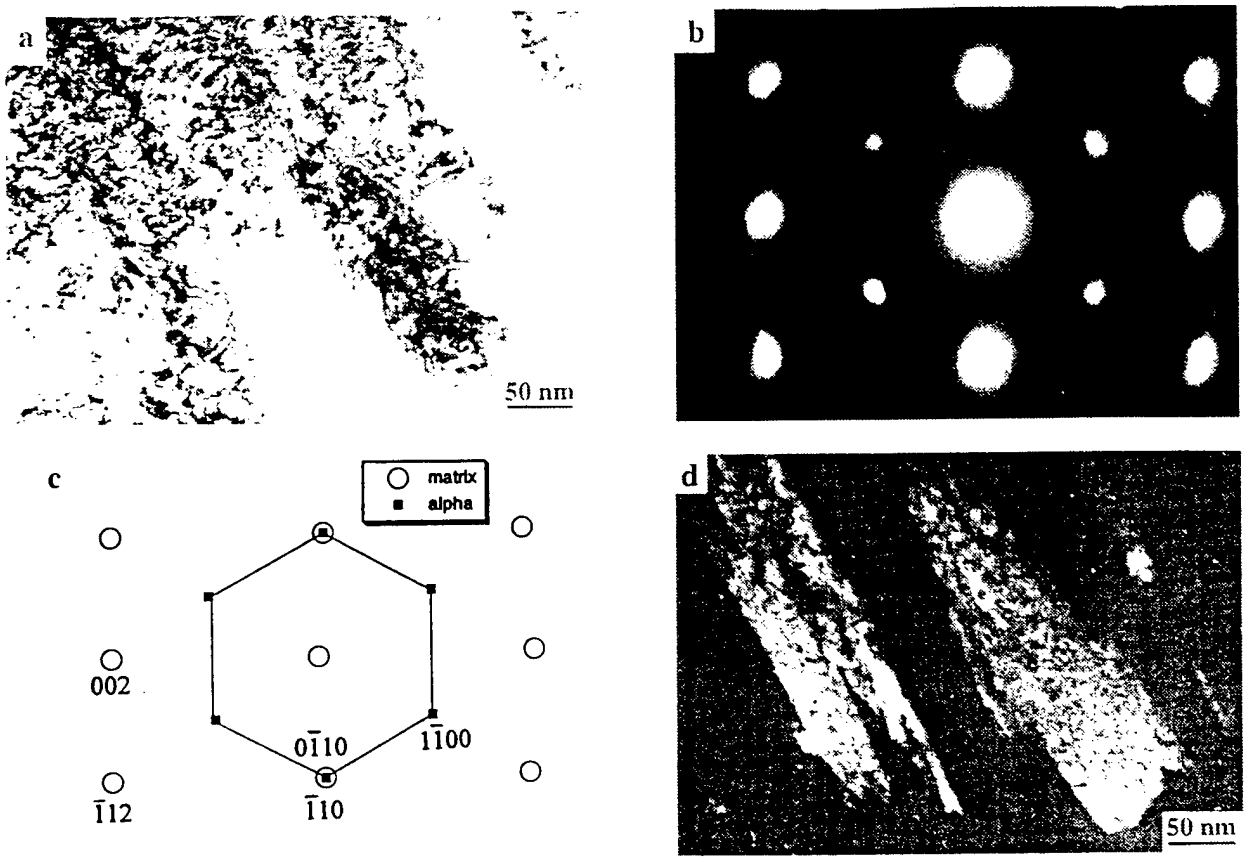

Fig. 2—TEM micrographs of the α-aged microstructure: (*a*) bright-field image, (*b*) $[110]_\beta$ zone diffraction pattern, (*c*) indexed diffraction pattern, and (*d*) dark-field image using the $(1\bar{1}00)_\alpha$ spot.

greater degree of crack closure compared to the α-aged microstructure. It also follows that there is very little difference between the FCG behavior of the α-aged and ω-aged microstructures once closure is accounted for.

C. *Effect of Stress Ratio on* ΔK_{th}

The effect of stress ratio on the threshold condition for FCG in the two microstructures is summarized in Figure 6 in the form of ΔK values at threshold (ΔK_{th}) and ΔK_{eff} values at threshold ($\Delta K_{\text{eff},th}$), plotted as a function of R. It is clear from Figure 6 that there is a greater effect of stress ratio on ΔK_{th} in the ω-aged microstructure than in the α-aged microstructure. The effect of the stress ratio vanishes when $\Delta K_{\text{eff},th}$ is considered instead of ΔK_{th}. In order to compare the closure levels at $R = 0.1$ in the two microstructures, the closure stress-intensity levels (K_{cl}) are plotted as a function of $K_{\min}$ in Figure 7. It is clear that considerably higher K_{cl} values were observed in the ω-aged microstructure than in the α-aged microstructure. While no crack closure was observed for ΔK levels greater than about 19 MPa$\sqrt{\text{m}}$ ($K_{\min}$ greater than about 2.1 MPa$\sqrt{\text{m}}$) in the α-aged microstructure at $R = 0.1$, substantial closure levels were observed even at higher ΔK values in the ω-aged microstructure. At $R = 0.5$, while no crack closure was observed in the α-aged microstructure, considerable closure was observed in the ω-aged microstructure (Figure 7). At $R = 0.8$, the *da/dN vs* ΔK_{eff} data were the same as the *da/dN vs* ΔK curve, for both microstructures, because of the absence of crack closure at $R = 0.8$.

D. *Effect of Microstructure on FCG Behavior*

A comparison of FCG behavior at $R = 0.1$ for the two microstructures is made in Figure 8. In Figure 8(a), the FCG data are presented in terms of *da/dN vs* ΔK. The relatively lower crack growth rates in the ω-aged microstructure (Figure 8(a)) are due to higher levels of crack closure in this microstructure, as discussed in the previous section. In Figure 8(b), comparison is made between the two microstructures in terms of *da/dN vs* ΔK_{eff} data. Once closure is accounted for, the data for the two microstructures come together, except for some difference in the threshold region of FCG (Figure 8(b)). Figure 9 shows the *da/dN vs* ΔK data at $R = 0.8$ for the two microstructures. As one would expect, in the absence of fatigue-crack closure, the two curves agree well, although there is a small difference in the threshold region of FCG. This difference must be due to microstructural effects. It has been suggested[28] that crack deflection at the microstructural level leads to the realization of a mode I ΔK that is smaller than the applied ΔK. The FCG rate differences observed only in the near-threshold region of FCG are also consistent with the fact that crack deflections from the mode I growth plane become significant only in the near-threshold regime, where increased mode II displacements become operative at the crack tip, due to localization

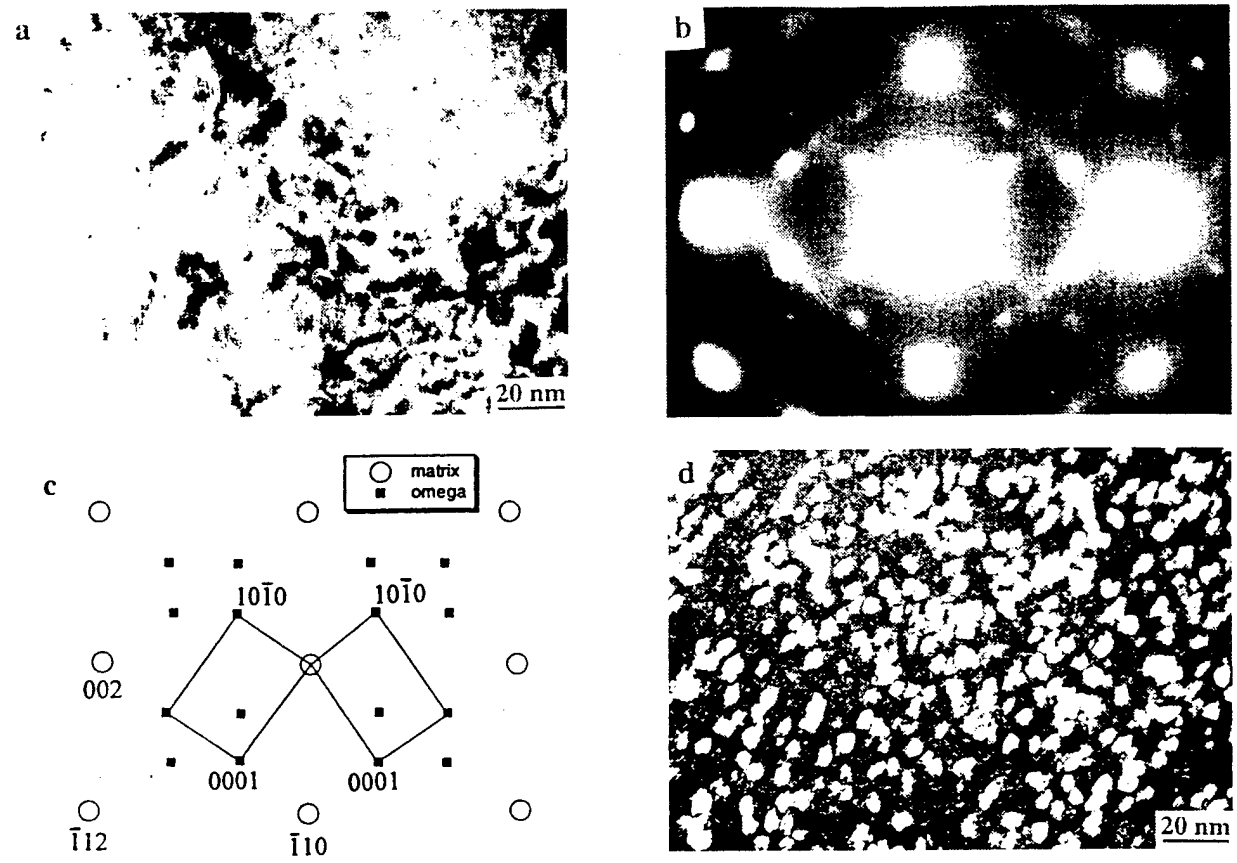

Fig. 3—TEM micrographs of the ω-aged microstructure: (*a*) bright-field image, (*b*) $[110]_\beta$ zone diffraction pattern, (*c*) indexed diffraction pattern, and (*d*) dark-field image using the $(10\bar{1}0)_\omega$ spot.

of crack-tip deformation along slip bands. In any case, this effect could not be attributed to the macroscopic crack-plane deviations observed in the FCG tests of the ω-aged microstructure. This is because of the fact that the FCG test data from regular CT and side-grooved CT specimens agreed well with each other

E. *Fatigue Fracture Mechanisms in the Near-Threshold Region*

The fracture morphologies observed in the near-threshold region are shown in Figures 10 and 11 for the α-aged and ω-aged microstructures, respectively. At a relatively low magnification, a flat, transgranular fracture surface was observed in the α-aged microstructure (Figure 10(a)) tested at $R = 0.1$. At a higher magnification, well-defined traces of α_p particles were seen (Figure 10(b)). In addition, a fracture morphology consisting of microscopically small features, the size of which roughly corresponded to the average α_p interparticle distance (1.86 μm), was seen (Figure 10(c)). In contrast, in the ω-aged microstructure, a rough fracture-surface topography was evident even at a low magnification level (Figure 11(a)). The sizes of these roughness features nearly corresponded to the average prior-β grain size (Figure 1(a)). At a higher magnification, however, traces of α_p particles were seen in these regions. These traces were not very well defined, but appeared to be irregular and discontinuous and seem to consist of secondary cracks (Figure 11(b)).

It is now well known[11–13,29,30] that, in the near-threshold FCG region, crack propagation is accomplished by dislocation movement by mode II shear at the crack tip. Generally, a single slip system is suggested to be active,[11,12,30] promoting a zigzagged crack path in polycrystalline materials.[11,12,30] In this study, the relatively high fracture-surface roughness observed in the ω-aged microstructure suggests that the dislocation pileup lengths were on the order of the prior-β grain size, with the crack deflecting at the prior-β grain boundaries, during crack growth. To verify this in the ω-aged microstructure, profiles of the crack path were examined in detail in the three regimes of ΔK, *viz.*, the decreasing ΔK regime, the near-threshold regime, and the increasing ΔK regime. Figures 12(a) through (d) illustrate the crack-path profiles in each of these regimes and the corresponding normalized crack closure levels (K_{cl}/K_{max}) plotted as a function of crack length. The crack length and the ΔK levels corresponding to the crack-tip positions at the centers of the figures are also indicated. While the crack-path profiles in the decreasing ΔK (Figure 12(a)) and in the increasing ΔK regimes (Figure 12(c)) appeared flat, the profile in the threshold regime was found to be rough (Figure 12(b)). Evidence of crack deflections at grain boundaries is seen, as indicated by the points marked as A in Figure 12(b). At the points marked as B however, cracks deflected within a grain. This kind of deflection seemed to occur in a relatively larger grain. In Figure 12(d), the closure level increased during the decreasing ΔK test, reached a maximum at the threshold region ($da/dN \sim 10^{-7}$ mm/cycle), and then decreased during the increasing ΔK test. In contrast, the

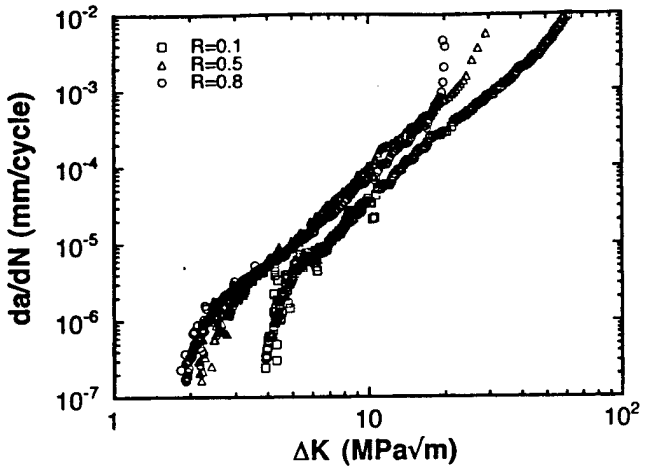

(a)

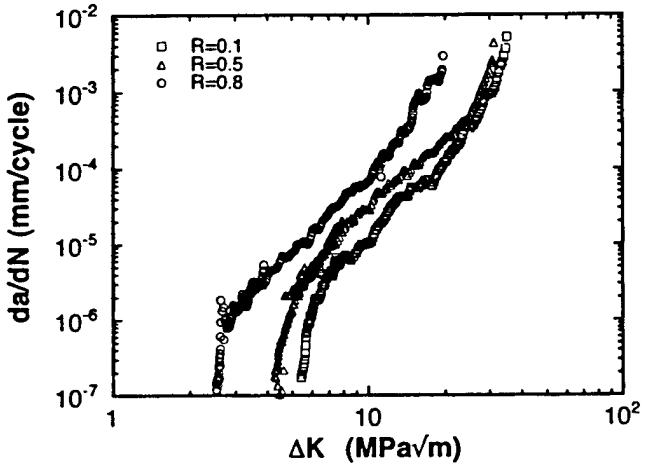

(b)

Fig. 4—The effect of stress ratio on the FCG behavior of (*a*) α-aged microstructure and (*b*) ω-aged microstructure.

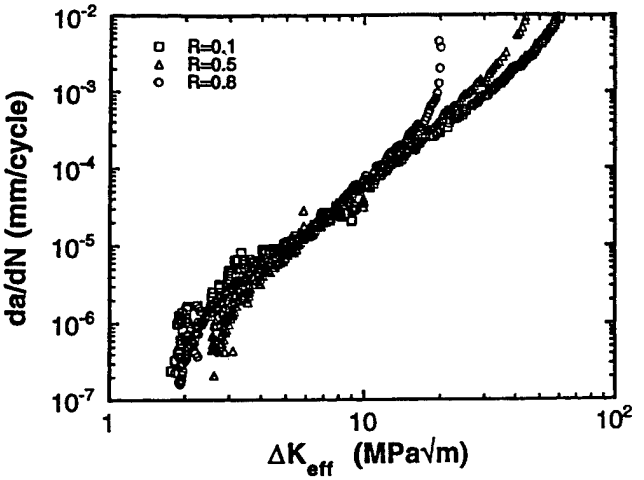

(a)

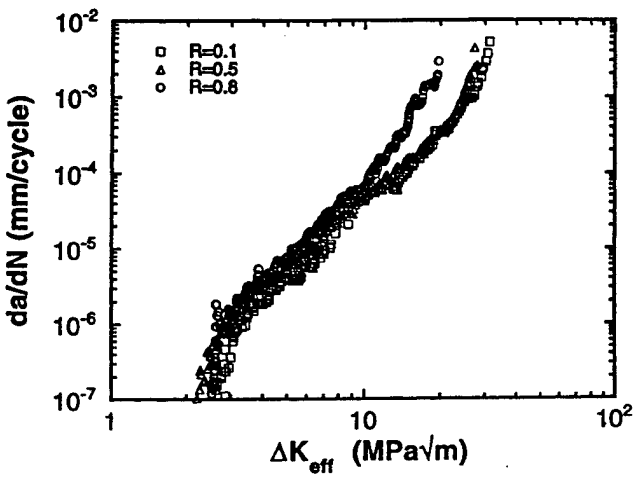

(b)

Fig. 5—The FCG data plotted in terms of ΔK_{eff} for (*a*) α-aged microstructure and (*b*) ω-aged microstructure.

crack-path profile in the α-aged microstructure (not presented here) was flat throughout the entire ΔK regime. This is expected, based on observations made on the fracture surfaces of the α-aged microstructure (Figure 10(a)). A flat crack-path profile over the entire range of applied ΔK and the observation of well-defined traces of α_p (Figure 10(b)), as well as the presence of features corresponding to the α_p interparticle spacing (Figure 10(c)), suggest that crack deflections on the order of α_p interparticle spacing occurred during crack growth in the α-aged microstructure.

F. *Effect of Microstructure on Crack Closure*

It is important to rationalize the fracture-surface roughness levels on the basis of crack-tip deformation, controlled by the interactions between dislocations and microstructural features. As has been documented in many studies,[31,32,33] small, coherent and shearable ω particles tend to produce planar slip during deformation at relatively low temperatures. It appears that the increased fracture-surface roughness in the ω-aged microstructure is caused by planar slip. It is evident from Figures 2(d) and 3(d) that the ω particles in the ω-aged microstructure are relatively smaller than the α_s

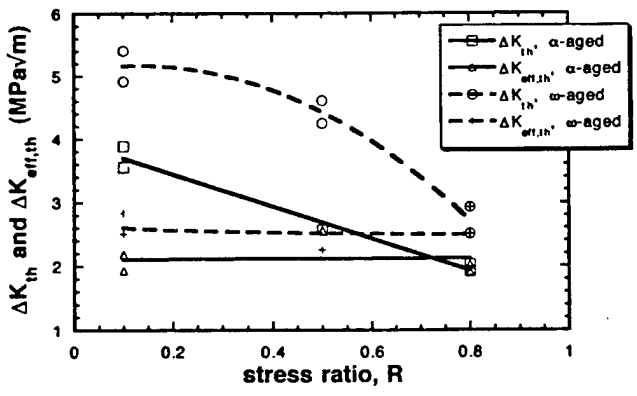

Fig. 6—The effect of stress ratio on ΔK_{th} and $\Delta K_{eff,th}$ for the α-aged and ω-aged microstructures.

particles in the α-aged microstructure. Furthermore, the ω phase has an ordered hcp crystal structure.[34,35,36] These ordered ω particles would be expected to dominate the deformation behavior due to their high density in the matrix

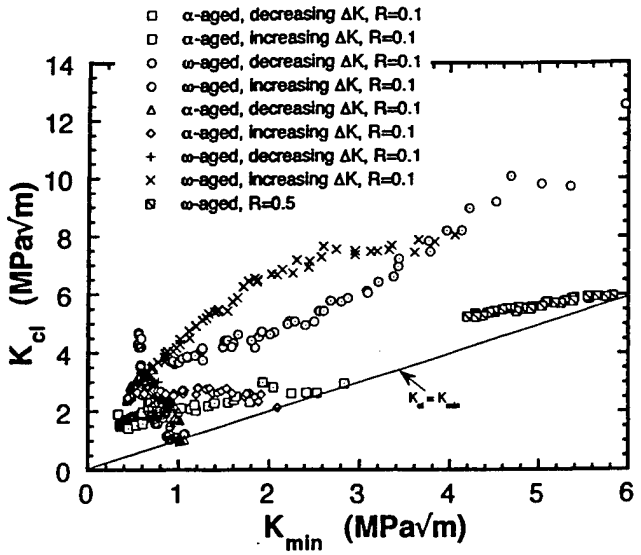

Fig. 7—The crack closure data, K_{cl}, plotted as a function of K_{min}, for the α-aged and ω-aged microstructures.

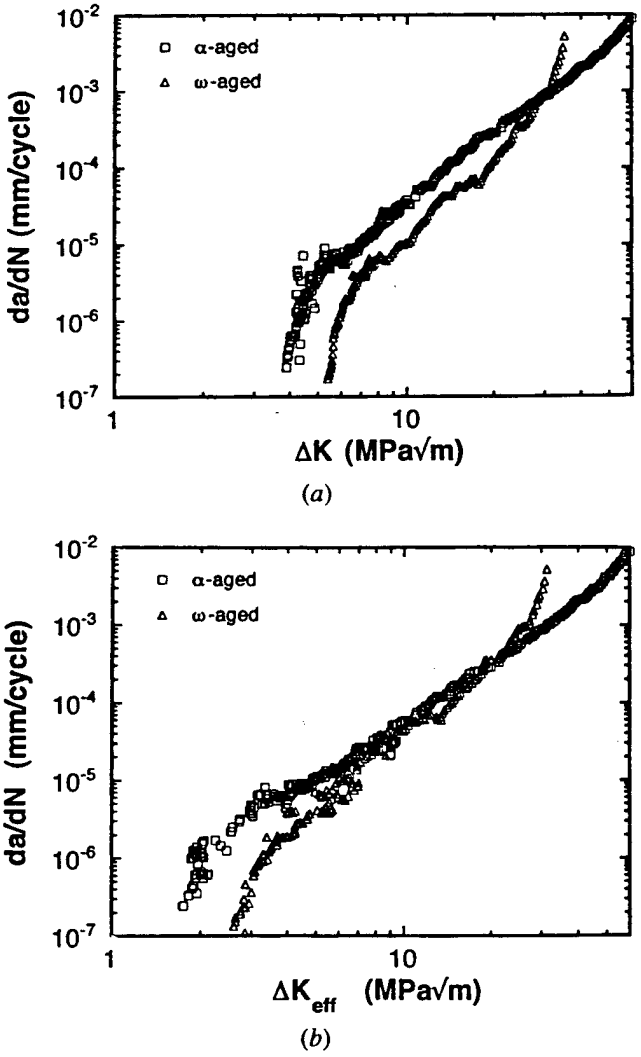

Fig. 8—A comparison of FCG behavior of α-aged and ω-aged microstructures at $R = 0.1$: (*a*) in terms of *da/dN vs* ΔK and (*b*) in terms of *da/dN vs* ΔK_{eff}

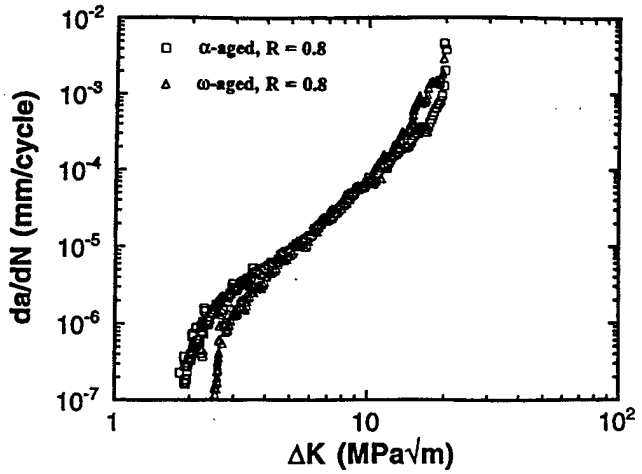

Fig. 9—A comparison of FCG behavior of α-aged and ω-aged microstructures at $R = 0.8$.

(Figure 3(d)). This is expected to cause an enhanced localization of dislocation motion in the ω-aged matrix when compared to the α-aged matrix. It seems that such localized deformation causes shearing of α_p particles in the ω-aged microstructure (Figure 11(a)). In the α-aged microstructure, however, only homogenous slip is expected to occur, thus leading to a more homogenous distribution of deformation in the matrix. This seems to result in crack growth by cleavage either through the α_p particles or along the α_p-matrix interfaces (Figure 10(b)). On the basis of this reasoning, the mechanisms of crack propagation are illustrated schematically for the α-aged and ω-aged microstructures in Figures 13(a) and (c), respectively. The crack-path profiles in the near-threshold region of the α-aged and the ω-aged microstructures are presented in Figures 13(b) and (d), respectively. The presence of large-sized asperities in the crack path of the ω-aged microstructure (Figure 13(b)) supports the suggested FCG mechanism. The crack-path profile appears to be more or less flat for the α-aged microstructure (Figure 13(d)), even at a magnification level higher than that of Figure 13(b), indicating the very small sizes of fracture-surface asperities in the α-aged case, relative to the ω-aged microstructure.

On the basis of the fracture mechanisms discussed previously, it is possible to conclude that crack closure was primarily caused by fracture-surface roughness. Due to shear across many α_p platelets, larger facets were formed in the ω-aged microstructure and the fracture-surface roughness was controlled by the prior-β grain size. On the other hand, in the α-aged microstructure, the α_p interparticle spacing, which was much smaller than the β grain size, controlled the fracture-surface roughness. This difference appears to cause the different closure responses in the two cases at $R = 0.1$. It is also important to discuss the high closure levels observed in the ω-aged microstructure in the Paris-law regime ($10^{-5} \le da/dN \le da/dN < 10^{-3}$ mm/cycle) of crack growth. Figure 14 shows a comparison of closure levels in the two microstructures over the entire range of applied ΔK levels. The closure levels are plotted in terms of $(K_{cl} - K_{min})/K_{min}$, in order to show by what factor K_{cl} exceeded K_{min} during FCG. It is interesting to note that, initially, both microstructures exhibited comparable closure levels at the begining of the decreasing ΔK

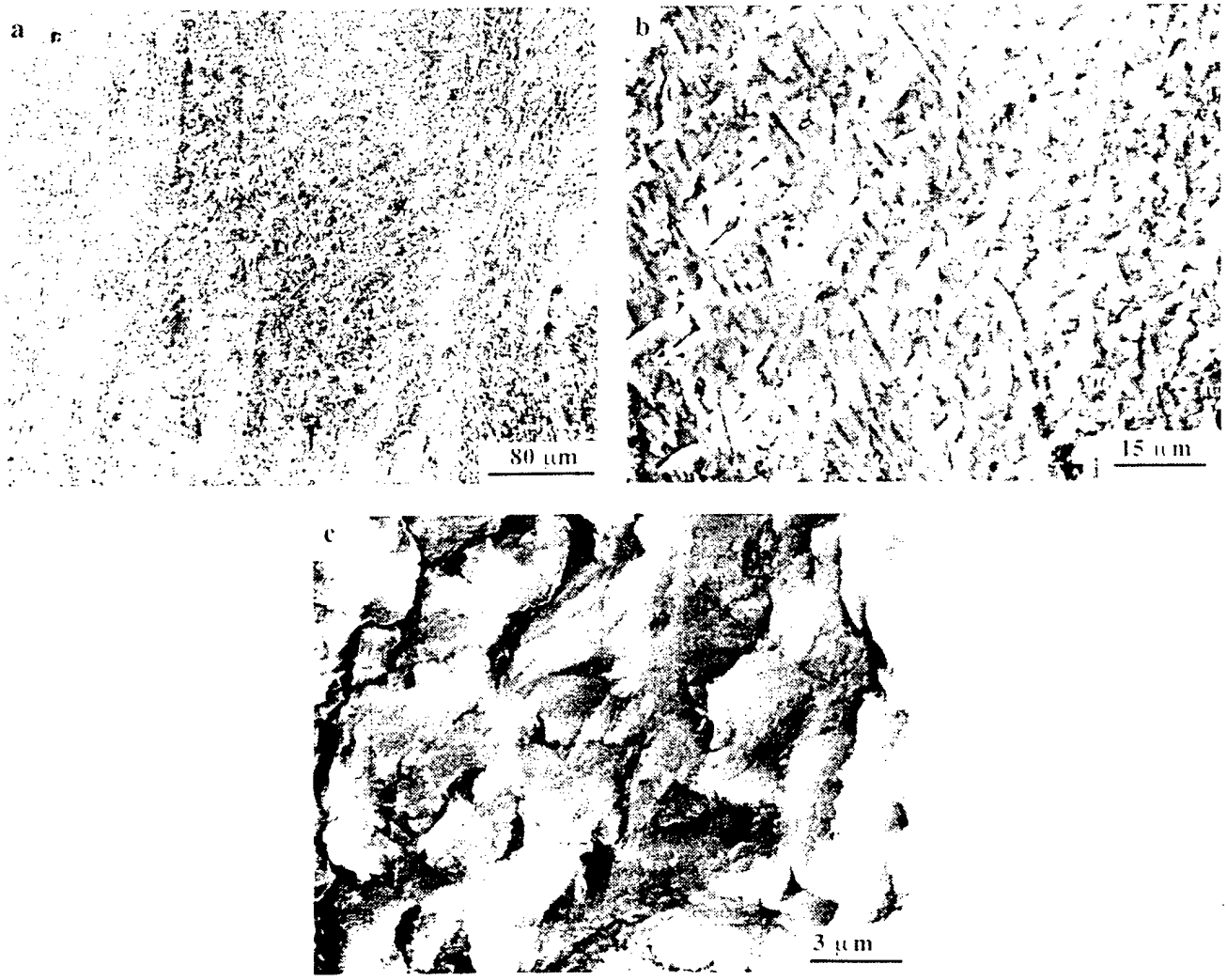

Fig. 10—Fracture topography in the α-aged microstructure in the near-threshold region: (*a*) at a low magnification, (*b*) showing well-defined traces of α_p particles, and (*c*) at a high magnification revealing features having sizes of the order of α_p interparticle distances.

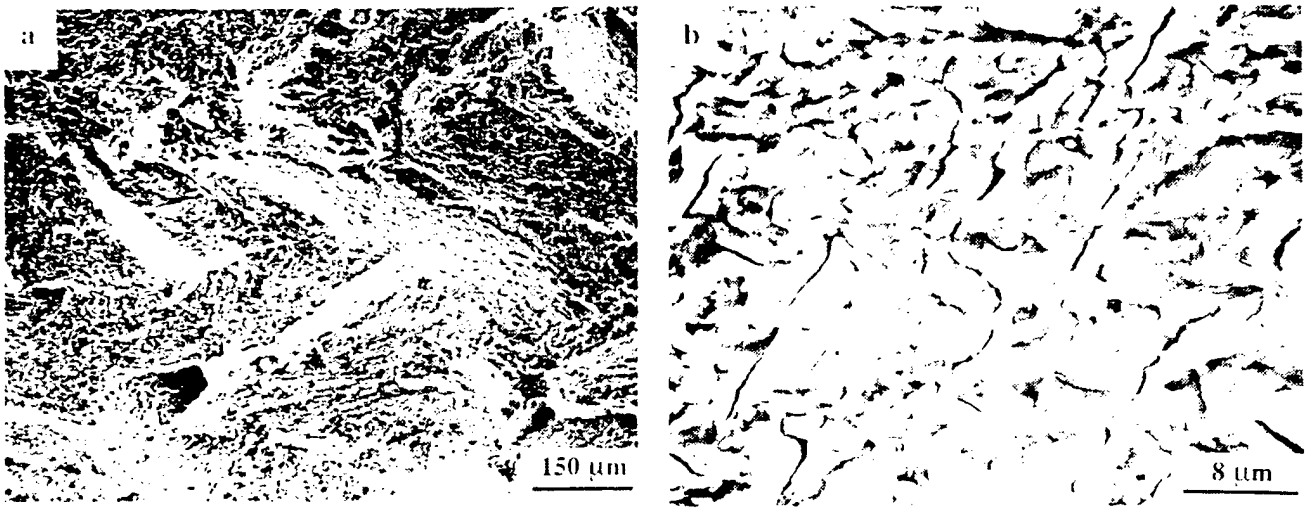

Fig. 11—Fracture topography in the ω-aged microstructure in the near-threshold region: (*a*) at a low magnification revealing the roughness features and (*b*) revealing the traces of α_p particles.

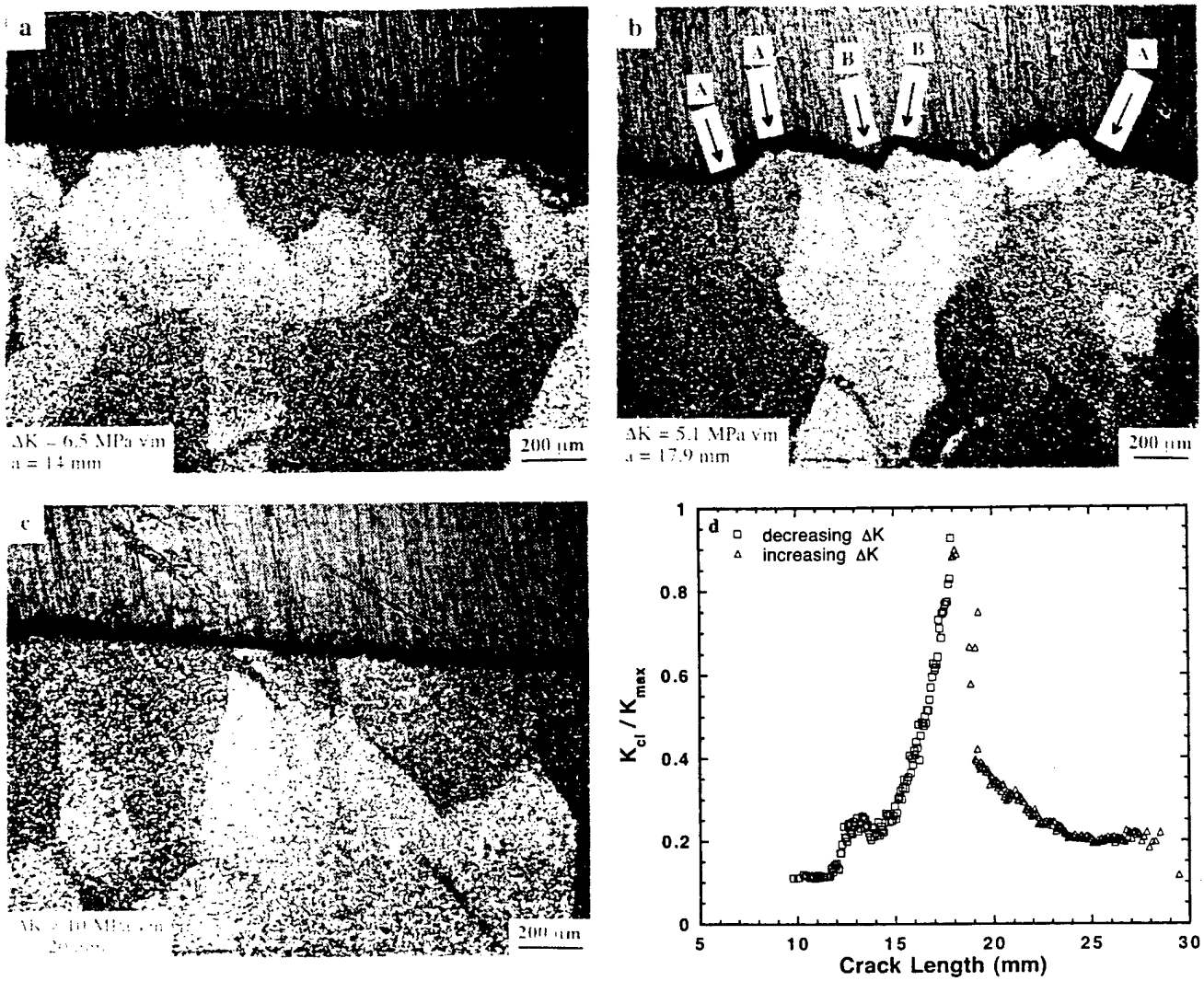

Fig. 12—Crack path profiles and normalized closure levels as a function of crack length in the ω-aged microstructure: (*a*) decreasing ΔK test, ΔK = 6.5 MPa$\sqrt{m}$, a = 14 mm; (*b*) threshold region, ΔK = 5.1 MPa$\sqrt{m}$, a = 17.9 mm; (*c*) increasing ΔK test, ΔK = 10 MPa$\sqrt{m}$, a = 20 mm; and (*d*) K_{cl}/K_{max} plotted as a function of crack length in the ω-aged microstructure at R = 0.1.

tests. However, due to the high fracture-surface roughness that formed in the near-threshold region, a significantly higher closure level was seen in the ω-aged microstructure. The ($K_{cl} - K_{min}$) values are about 5 and 8 times K_{min} for the α-aged and the ω-aged microstructures, respectively. However, during the increasing ΔK part after ΔK_{th}, the closure levels are no longer similar in the two microstructures. The closure levels are significantly higher in the ω-aged microstructure than in the α-aged microstructure. This is understandable, since the fracture-surface roughness that was formed near the threshold can continue to interfere with the opening and closing of the crack, even after the crack had propagated significantly under increasing ΔK conditions. The presence of closure ($K_{cl} > K_{min}$), even at R = 0.5 in the ω-aged microstructure, can be rationalized. The average height of asperities in the near-threshold region of the ω-aged microstructure was found to be about 125 μm (Figure 13), whereas the maximum crack-mouth opening displacement (CMOD) in the near-threshold region at R = 0.5 was 70 μm. The maximum crack opening level is clearly smaller than the average height of the asperities. Therefore, partial closure of cracks, even at R = 0.5, is expected. On the other hand, in the α-aged microstructure, the height of the fracture-surface asperities seems to correspond to the average α_p interparticle distance, *i.e.*, 1.8 μm. This is much smaller than the minimum CMOD encountered in the near-threshold region, which was 28 μm. Therefore, the fracture-surface roughness levels provide a rationale for the different closure levels observed at R = 0.1 and 0.5, in the two microstructures.

G. *Fatigue Fracture Mechanisms in the Paris-Law Region*

The fracture modes observed in the Paris-law regime ($10^{-5} \le da/dN \le 10^{-3}$ mm/cycle) of crack growth at R = 0.1 are shown in Figures 15 and 16 for the α-aged and ω-aged microstructures, respectively. In the α-aged microstructure, considerable secondary cracking perpendicular to the crack-propagation direction was observed (Figure 15(a)). The secondary cracks did not correlate to the dimensions of α_p particles. As suggested by Yoder *et al.*,[37] the secondary cracks might have occurred along slip bands. However, it

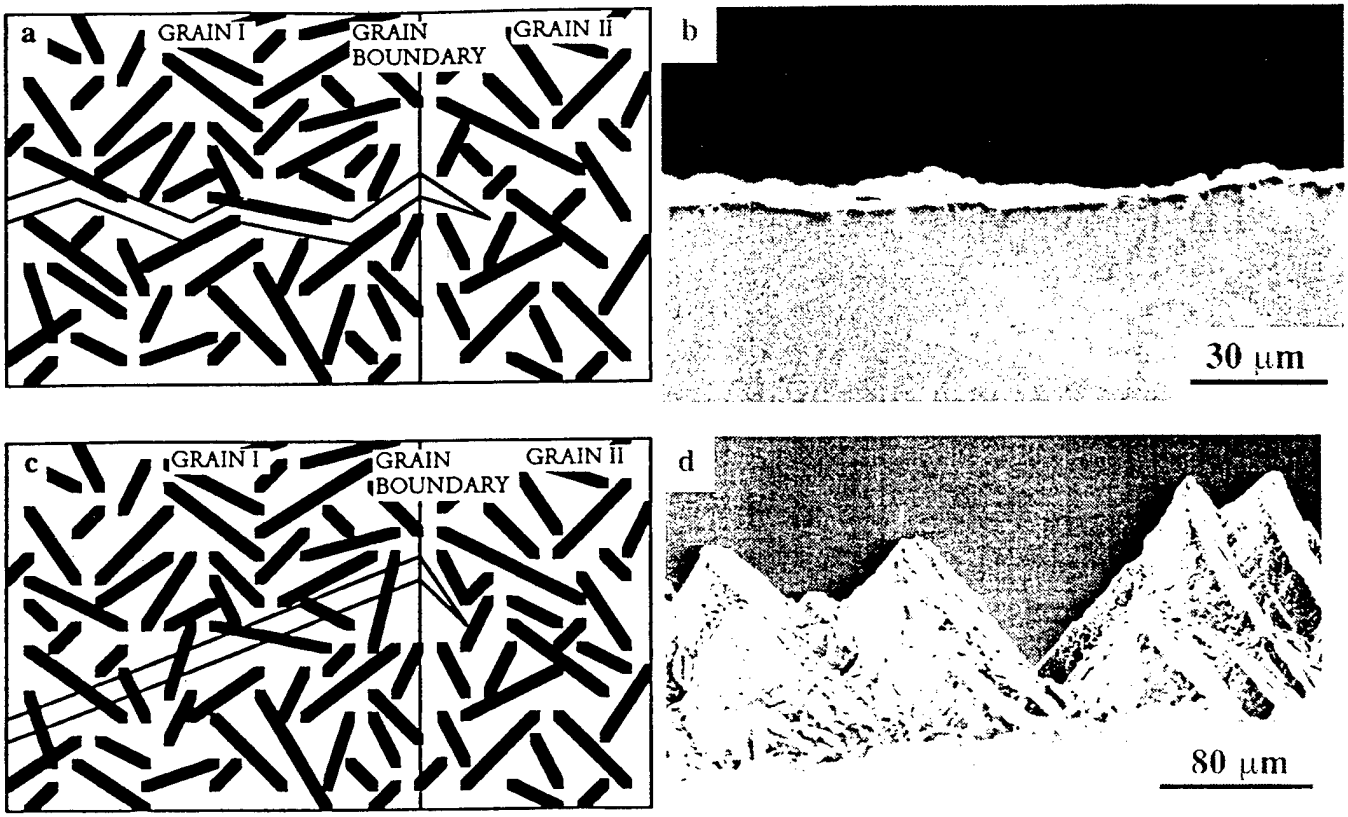

Fig. 13—Aschematic of the fatigue crack propagation mechanism in (*a*) α-aged and (*c*) ω-aged microstructures. The crack path profiles in the near-threshold region; these microstructures are shown in (*b*) and (*d*), respectively.

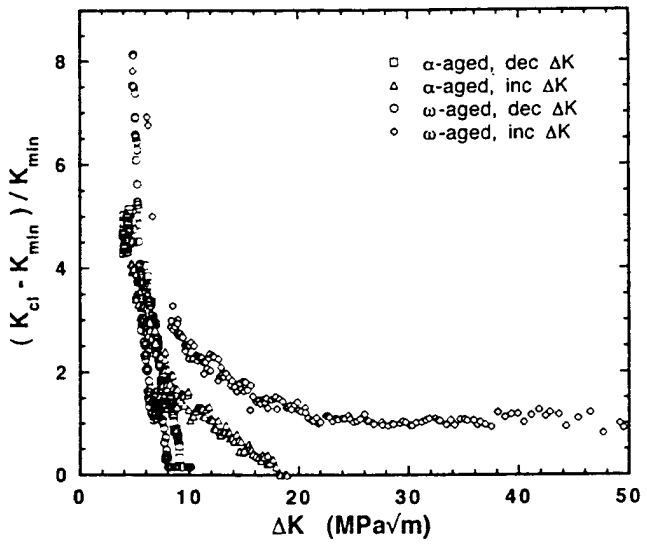

Fig. 14—The relative crack closure level ($(K_{cl} - K_{min})/K_{min}$) plotted as a function of ΔK, for the α-aged and ω-aged microstructures.

is not possible to conclude whether secondary cracks occurred at the α_p/β interfaces or along the slip bands. Besides secondary cracks, fatigue striations were also observed at high ΔK levels (Figure 15(b)). In the ω-aged case, on the other hand, there was almost no secondary cracking, with the exception of a few cracks at random locations, in the Paris-law regime (Figure 16(a)). At a higher magnification, (Figure 16(b)), the fracture surface appeared to consist of coarse slip steps accompanied by striation-like features. It was not possible to resolve the striations.

The monotonic crack-tip plastic-zone sizes ($r_m = (1/3\pi)(K_{max}/\sigma_{ys})^2$, where σ_{ys} is the yield stress) in the Paris-law ΔK regime ($10^{-5} \leq da/dN \leq 10^{-3}$ mm/cycle) were estimated to be greater than at least 16 μm in both microstructures. Therefore, the crack-tip plastic zone was larger than the average α_p interparticle distance. It is possible that this is the reason why α_p traces were absent in the fracture surfaces in this regime in both the microstructures. Even though the fracture-surface roughness in the Paris-law regime in the ω-aged microstructure was low, the fracture-surface roughness introduced in the near-threshold region influenced the crack closure during crack growth in this regime during increasing ΔK tests. Therefore, a significant effect of R on the crack growth rate resulted in high ΔK levels in the ω-aged microstructure. Such an effect was absent in the α-aged microstructure due to the very small roughness features in near-threshold region.

IV. CONCLUSIONS

1. A strong effect of stress ratio on fatigue-crack growth behavior, in particular, on the crack growth rates, was observed in the ω-aged condition of a Ti-10V-2Fe-3Al alloy when compared to the α-aged condition of the alloy.
2. The stress-ratio effect could, to a large extent, be explained on the basis of roughness-induced crack closure. When there was a high level of closure (ω-aged microstructure), the crack growth rates were strongly

Fig. 15—Fracture topography in Paris-law regime as observed in the α-aged microstructure at (*a*) a low magnification and (*b*) a high magnification.

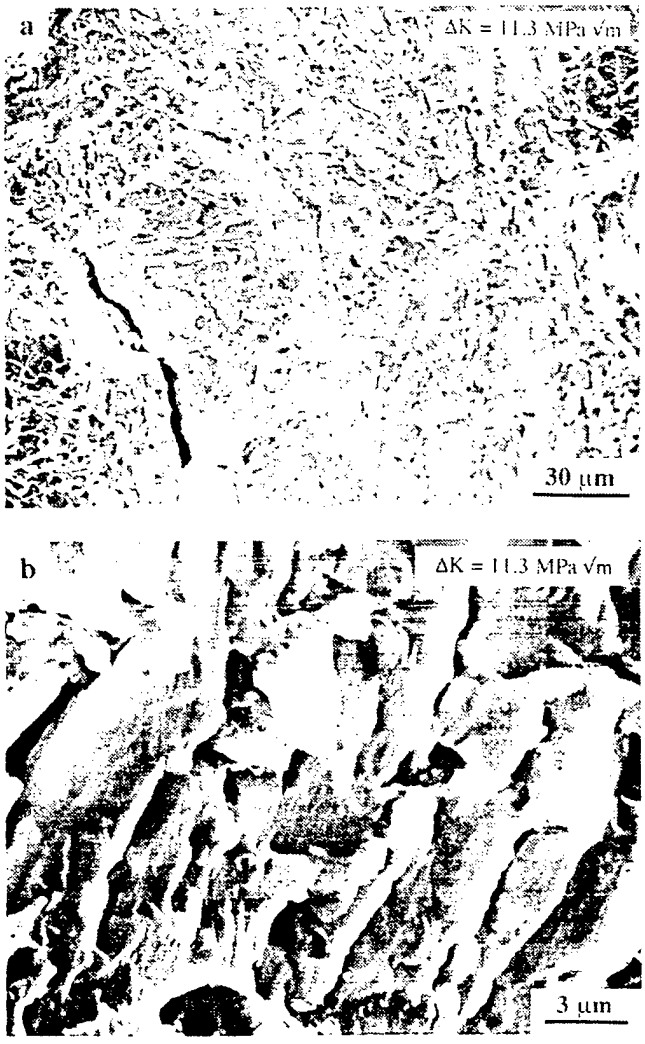

Fig. 16—Fracture topography in the Paris-law regime as observed in the ω-aged microstructure at (*a*) a low magnification and (*b*) a high magnification.

dependent on the stress ratio. When there was low closure (α-aged microstructure), the crack growth rates were almost independent of the stress ratio.

3. The fracture-surface roughness features near the threshold in the ω-aged microstructure were found to correspond to the prior-β grain size. In the α-aged microstructure, however, fracture-surface roughness features corresponded to the α_p interparticle spacing. The prior-β grain size and the α_p interparticle spacing were the microstructural units controlling crack growth rates in the ω-aged and the α-aged microstructures, respectively. This suggestion is consistent with the microstructural characteristics, deformation modes, and the crack-path profiles observed during fatigue-crack growth.

ACKNOWLEDGMENTS

The authors sincerely acknowledge the support of the Structural Materials Program, Air Force Office of Scientific Research (AFOSR, Washington, DC) through Grant No. F49620-96-1-0102. The authors appreciate the interest and encouragement of Drs. C.H. Ward and S. Wu of this organization. The provision of material by TIMET is gratefully acknowledged. In particular, the authors thank C. Clay and P. Allen, TIMET, in this regard.

REFERENCES

1. R.R. Boyer and G.W. Kuhlman: *Metall. Trans. A*, 1987, vol. 18A, pp. 2095-2103.
2. G. Terlinde, H. J. Rathjen, and K.H. Schwalbe: *Metall. Trans. A*, 1986, vol. 17A, pp. 1037-49.
3. G. Terlinde, T.W. Duerig, and J.C. Williams: *Metall. Trans. A*, 1983, vol. 14A, pp. 2101-15.
4. C.C. Chen and R.R. Boyer: *JOM*, 1979, vol. 31, pp. 33-39.
5. D. Eylon, A. Vassel, Y. Combres, R.R. Boyer, P.J. Bania, and R.W. Schultz: *JOM*, 1994, vol. 46, pp. 14-15.
6. R.R. Boyer: *JOM*, 1980, vol. 32, pp. 61-65.
7. M.H. Campagnac and A. Vassel: *Designing with Titanium*, Proc. Int. Conf., The Institute of Metals, London, 1986, pp. 261-66.
8. T.W. Duerig, J.E. Allison, and J.C. Williams: *Metall. Trans. A*, 1985, vol. 16A, pp. 739-51.
9. T.W. Duerig and J.C. Williams: *Beta Titanium Alloys in the '80s*, Proc. Symp. Sponsored by the Titanium Committee of AIME, R.R. Boyer and H.W. Rosenberg, eds., TMS, Warrendale, PA, pp. 19-67.
10. G.W. Kuhlman: *Microstructure/Property Relationships in Titanium Aluminides and Alloys*, Y.W. Kim and R.R. Boyer, eds., TMS, Warrendale, PA, 1991, pp. 465-91.

11. S. Suresh and R.O. Ritchie: *Metall. Trans. A*, 1982, vol. 13A, pp. 1627-31.
12. S. Suresh and R.O. Ritchie: *Fatigue Crack Growth Threshold Concepts*, Conf. Proc., D. Davidson and S. Suresh, eds., TMS-AIME, Warrendale, PA, 1984, pp. 227-61.
13. P.K. Liaw: *Mechanics of Fatigue Crack Closure*, ASTM STP 982, J.C. Newman, Jr. and W. Elber, eds., ASTM, Philadelphia, PA, 1988, pp. 62-92.
14. W.J. Evans and A.W. Beale: *Forging and Properties of Aerospace Materials*, Proc. Int. Conf. organized by Activity Group Committee 2, The Metals Society, London, 1978, pp. 170-91.
15. R.J. Bucci and P.C. Paris: *J. Mater.*, 1972, vol. 7, pp. 402-09.
16. A. Yuen, S.W. Hopkins, G.R. Leverant, and C.A. Rau: *Metall. Trans. A*, 1974, vol. 5, pp. 1833-42.
17. P.E. Irving and C.J. Beevers: *Metall. Trans. A*, 1974, vol. 5, pp. 391-98.
18. S. Dubey, A.B.O. Soboyejo, and W.O. Soboyejo: *Acta Mater.*, 1997, vol. 45 (7), pp. 2777-87.
19. J.M. Larsen: Ph.D. Thesis, Carnegie Mellon University, Pittsburgh, PA, 1987.
20. G.T. Gray III and G. Lutjering: *Proc. 2nd Int. Conf. Fatigue and Fatigue Thresholds*, C.J. Beevers, ed., EMAS Pub. Inc., West Midlands, U.K., 1984, vol. II pp. 707-16.
21. K. Sadananda and A.K. Vasudevan: *Fracture Mechanics: 25th volume*, ASTM STP 1220, F. Erdogan, ed., ASTM, Philadelphia, PA, 1995, pp. 484-501.
22. *Annual Book of ASTM Standards*, ASTM, Philadelphia, PA, 1993, vol. 03.01, sec. 3, pp. 679-706.
23. *Quantitative Microscopy*, R.T. DeHoff and F.N. Rhines, eds., McGraw-Hill Book Company, New York, NY, 1968, pp. 45-73 and 77-123.
24. Y. Ohmori, H. Natsui, K. Nakai, and H. Ohtsubo: *Mater. Trans., JIM*, 1998, vol. 39 (1), pp. 40-48.
25. R.O. Ritchie: *Int. Met. Rev.*, 1979, vol. 24, pp. 205-30.
26. P.E. Bretz, J.I. Petit, and A.K. Vasudevan: *Fatigue Crack Growth Threshold Concepts*, D. Davidson and S. Suresh, eds., TMS-AIME, Warrendale, PA, 1984, pp. 163-83.
27. G.W. Kuhlman, A.K. Chakrabarti, T.L. Yu, R. Pishko, and G. Terlinde: in *Microstructure, Fracture Toughness and Fatigue Crack Growth Rate in Titanium Alloys*, A.K. Chakrabarti and J.C. Chesnutt, eds., TMS. AIME, Warrendale, PA, 1987, pp. 171-91.
28. S. Suresh: *Metall. Trans. A*, 1983, vol. 14A, pp. 2375-85.
29. K. Minakawa and J. McEvily: *Scripta Metall.*, 1981, vol. 15, pp. 633-36.
30. K.S. Ravichandran: *Int. J. Fract.*, 1990, vol. 44, pp. 97-110.
31. B.S. Hickman: *Trans. TMS-AIME*, 1969, vol. 245, pp. 1329-36.
32. T.W. Duerig, G.T. Terlinde, and J.C. Williams: *Metall. Trans. A*, 1980, vol. 11A, pp. 1987-98.
33. M. Niinomi and T. Kobayashi: *Iron Steel Inst. Jpn. Int.*, 1991, vol. 31, pp. 848-55.
34. D. DeFontaine, N.E. Paton, and J.C. Williams: *Acta Metall.*, 1971, vol. 19, pp. 1153-62.
35. J.C. Williams, D. De Fontaine, and N.E. Paton: *Metall. Trans.*, 1973, vol. 4, pp. 2701-08.
36. B.S. Hickman: *J. Mater. Sci.*, 1969, vol. 4, pp. 554-63.
37. G.R. Yoder, L.A. Cooley, and T.W. Crooker: *Metall. Trans. A*, 1977, vol. 8A, pp. 1737-43.

Appendix V

Mean Stress (Tensile) Effects on Fatigue Crack Growth Behavior of Some Structural Titanium Alloys

Mean Stress (Tensile) Effects on Fatigue Crack Growth Behavior of Some Structural Titanium Alloys: An Overview of Microstructural Issues

K. S. Ravichandran and S. K. Jha

Department of Metallurgical Engineering
135 South 1460 East Room 412
The University of Utah, Salt Lake City, UT 84112

ABSTRACT

An overview of the effect mean stress or stress ratio (R) of the fatigue cycle, on fatigue crack growth responses of some structural titanium alloys is performed. The fatigue crack growth data generated by the authors on some alloys, are considered in combination with the data of other alloys reported in literature. The alloys include those that are commercially used as well as some model alloys that were either employed in academic studies or were under development in the past. It has been found that the mean stress dependence in titanium alloys is brought about by two different mechanisms, namely, crack closure at low ΔK levels and static-mode-cracking contribution at high ΔK levels. It was observed that in general, a decrease in the tensile ductility of the alloy causes an increase in the sensitivity of fatigue crack growth rates to the mean stress. The microstructural and deformation characteristics that are responsible for this behavior are highlighted.

Fatigue Behavior of Titanium Alloys
Edited by R.R. Boyer, D. Eylon, and G. Lütjering
The Minerals, Metals & Materials Society, 1999

INTRODUCTION

Fatigue crack growth (FCG) behavior in structural titanium alloys has been studied extensively; a recent review [1] provides a comprehensive survey on this subject. Briefly, FCG has been found to be sensitive to microstructure [2-5], stress ratio (R) [6-15], environment [16, 17] and orientation [18, 19]. Of these, the effect of mean stress or stress ratio on fatigue crack growth received a great deal of attention, both in investigations of the past [6, 7] as well as more recent [12, 13], to name a few. This is understandable, since loading conditions in actual applications of titanium alloys mostly involve varying mean stress and stress amplitude, therefore requiring a good understanding of the effect of mean stress on fatigue crack growth.

The relatively earlier investigations focused on the mean stress effect at relatively higher growth rates, say, above about 10^{-5} mm/cycle. It was attempted to provide a rational for the increased growth rates at high mean stress levels, either in terms of empirical correlations [6, 8] or in terms of some form of "effective ΔK" driving the crack growth under various stress ratios [7]. The basic conclusion from these studies is that the increased growth rates at high stress ratios are due to the higher static stress intensity factor superimposed along with a cyclic stress intensity range, both acting to drive the crack.

In relatively recent investigations, however, attention has been mainly focused on crack growth at low growth rates, say, below about 10^{-5} mm/cycle, where several crack wake mechanisms such as oxide, plasticity or roughness induced crack closure [20] begin to influence the FCG behavior. Since crack closure generally occurs at low stress ratios due to smaller cyclic crack tip openings involved, the lower growth rates at low stress ratios (typically 0.1) is due to the partial shielding of the crack tip from the applied stress intensity range. Since this does not occur at high R, crack growth at high R is not affected. Therefore, it is suggested that when crack growth rates are compared in terms of actual ΔK experienced at the crack tip, i.e., ΔK_{eff}, very little effect of R on FCG is noticed. Some studies [10, 13] have shown that the effect of stress ratio can be either fully or partly explained by the crack closure mechanism. On the other hand there are also studies [10, 21] showing that crack closure does not completely explain the differences in growth rates at different mean stress levels.

The objective of the present work is to provide a comprehensive review of the FCG data as influenced by mean stress in different titanium alloys, in the light of some of our recent work [22, 23]. A recent study [24] identified varied mean stress effects on the smooth fatigue behavior of conventional titanium alloys. In this study, however, it is attempted to identify the microstructural factors responsible for the occurrence of a high mean stress or a low mean stress effect during fatigue crack growth in different titanium alloys.

In this work, the results of our study of fatigue crack growth behavior of (i) a beta (β) titanium alloy, Ti-10V-2Fe-3Al [22], and (ii) an alpha-2 (α_2) intermetallic titanium aluminide alloy, Ti-24Al-11Nb, based on Ti_3Al compound [23] are analyzed in the light of the data reported in literature on (iii) alpha-beta ($\alpha+\beta$) titanium alloys, Ti-6Al-4V [6, 7], (iv) an alpha (α) rich titanium alloy, Ti-8.6Al [10], (v) a near-α titanium alloy, Ti-8Al-1Mo-1V [8], and (vi) a gamma (γ) titanium aluminide intermetallic alloy, Ti-33.5Al-2.5Mn, based on TiAl compound [25]. The mean stress effect in each of these materials is assessed in terms of their microstructure, ductility and fracture mechanism during fatigue crack growth at room

temperature. Only tensile mean stress is considered, since for the range of mean stresses from zero to compressive, only very small differences in fatigue crack growth response when plotted in terms of ΔK, is normally found [7].

MATERIALS AND EXPERIMENTS

Materials and Heat Treatment

The Ti-10V-2Fe-3Al alloy, received as β-forged and hot rolled plates, were heat treated to produce two microstructural conditions. The first, the α-aged microstructure was obtained by solution treating in the $\alpha+\beta$ field, at 700°C for 2 hours, followed by water quenching. The microstructure was subsequently aged at 525°C for 8 hours, followed by water quenching. The resulting microstructure consisted of about 45% primary-α (α_p) particles in a transformed β-matrix consisting of smaller secondary-α (α_s) particles. The second, the ω-aged microstructure was obtained by following the same solution treatment, but aging at 260°C for 6 hours followed by water quenching. The microstructure had the same amount of α_p, but the matrix was enriched with fine, uniformly distributed ω-phase [22]. The mechanical properties of these microstructures are given in Table I.

The Ti-24Al-11Nb alloy, received as β-forged disc, was heat treated in the $\alpha_2+\beta$ field, at 1080°C for 2 hours, followed by air cooling. The microstructure was stabilized by heat treating at 593°C for 8 hours, followed by air cooling. The resulting microstructure had a distribution of primary-α_p particles (about 28% by volume) in a matrix of transformed β. Mechanical properties of this microstructure are given in Table I.

The Ti-6Al-4V alloy, reported in Ref. [7], was heat treated by annealing at 954°C for 1 hour, followed by water quenching. The material subsequently was aged at 704°C for 2 hours. The Ti-6Al-4V and Ti-8Al-1Mo-1V alloys reported in Refs. [6] and [8] were in the mill-annealed condition. This condition suggests that the microstructures were made of continuous and relatively fine α-phase with islands of β-phase. The available mechanical properties are given in Table I. The Ti-8.6 Al alloy, reported in Ref. [10] was processed by cross-rolling in multiple passes at 950°C, followed by recrystallization to obtain an equiaxed microstructure of α-grains. The γ-TiAl intermetallic alloy, Ti-33.5Al-2.5Mn was made by reaction sintering [25] followed by Hot-Isostatic Pressing (HIP). The microstructure was a duplex structure with $\alpha_2+\gamma$ lamellar colonies. The known mechanical properties of this alloy are given in Table I.

Conditions of Fatigue Crack Growth Testing

The fatigue crack growth data for alloys Ti-10V-2Fe-3Al and Ti-24Al-11Nb were generated using 8 mm thick compact tension (CT) specimens, following the ASTM standard E647. Crack growth was monitored automatically using compliance measurements. Tests were run at a frequency of 35 Hz. Both the increasing as well as decreasing ΔK tests were performed. Crack closure measurements were performed using crack opening displacement (COD) gages. Further details are provided in Ref. 22.

The Ti-6Al-4V alloy, reported in Ref. [7] was tested for fatigue crack growth behavior using 2 mm thick center-cracked tension (CCT) specimens at a frequency of 1-4 Hz. A few tests were done at 30 Hz and 1000 Hz, but no effect of frequency on crack growth or fracture modes was found. The method of crack growth monitoring was not reported.

Table I. Description of microstructures and mechanical properties of alloys considered

Material (Alloy Type) [Ref.]	Microstructure	E* (GPa)	YS* (MPa)	UTS* (MPa)	El.* (%)	Kq* (MPa$\sqrt{m}$)
Ti-10V-2Fe-3Al (β, α aged) [present work]	α_p+ α_s particles in β matrix	100	988	1066	13	> 60
Ti-10V-2Fe-3Al (β, ω aged) [present work]	α_p+ ω particles in β matrix	100	1028	1046	8.7	40
Ti-6Al-4V (α+β) [7]	α_p in transformed β matrix	110	916	NA	NA	66
Ti-6Al-4V-TL (α+β) [6]	Continuous α phase with β particles	110	1050	1071	12	59
Ti-8Al-1Mo-1V (near α) [8]	Continuous α with traces of β	110	NA	NA	NA	55
Ti-8.6Al (α) [10]	Equiaxed α grains (30 μm and 110 μm)	120	875	980	8-17	? (20-30)
Ti-24Al-11Nb (α_2, Ti_3Al) [present work]	Primary α_2 in transformed β matrix	120	505	578	1.4	20
Ti-33.5Al-2.5Mn (γ, TiAl) [25]	Duplex and Lamellar with α_2+ γ phases	170	373	NA	1	7.1-14

*E is elastic modulus; YS is yield strength; UTS is ultimate tensile strength; El. is elongation and Kq is fracture toughness.

The Ti-6Al-4V alloy, reported in Ref. [6] was tested for fatigue crack growth behavior, using 5 mm thick CT specimens, at a frequency of 2-25 Hz. Crack growth was monitored using an electrical potential technique. The Ti-8Al-1Mo-1V alloy, reported in Ref. [8] was tested for fatigue crack growth behavior, using 6.6 mm thick CCT specimens at a frequency of 5 Hz in an argon atmosphere. Crack growth was monitored using electrical potential technique. The Ti-8.6 Al alloy, reported in Ref. [10] was tested for fatigue crack growth behavior using 6 mm thick CT specimens at 30 Hz. Crack growth was monitored using an optical microscope. Crack closure measurements were made using back face strain (BFS) gage technique. The Ti-33.5Al-2.5Mn intermetallic alloy was tested [25] for fatigue crack growth behavior using 6 mm

thick CT specimens. The frequency of testing and the method of crack length measurement was not reported.

Unless otherwise specified, almost all the tests were conducted at room temperature in laboratory environment using servo-hydraulic fatigue test systems equipped with feed-back control of the load. Therefore, the data can be considered as reliable and can be employed for comparisons of the effects of microstructure and material on the mean stress dependence of fatigue crack growth.

RESULTS AND DISCUSSION

Microstructure

Microstructures of the Ti-10V-2Fe-3Al in the α-aged condition and the Ti-24Al-11Nb alloy are shown in Figs. 1 (a&b). The microstructure of the ω-aged Ti-10V-2Fe-3Al was basically the same as in Fig. 1(a). However, the microstructure at TEM magnifications was very different, showing a distribution of fine ω-phase particles [22]. It is to be noted that in general, the tendency to brittle fracture by cleavage increases in the order: β phase, α phase, α_2 (Ti3Al) phase and γ (TiAl) phase, due a combination of factors such as crystallographic structure, atomic order and covalency of bonding along some crystallographic directions. This behavior is consistent with the general decrease in ductility in that order, as evident from Table I.

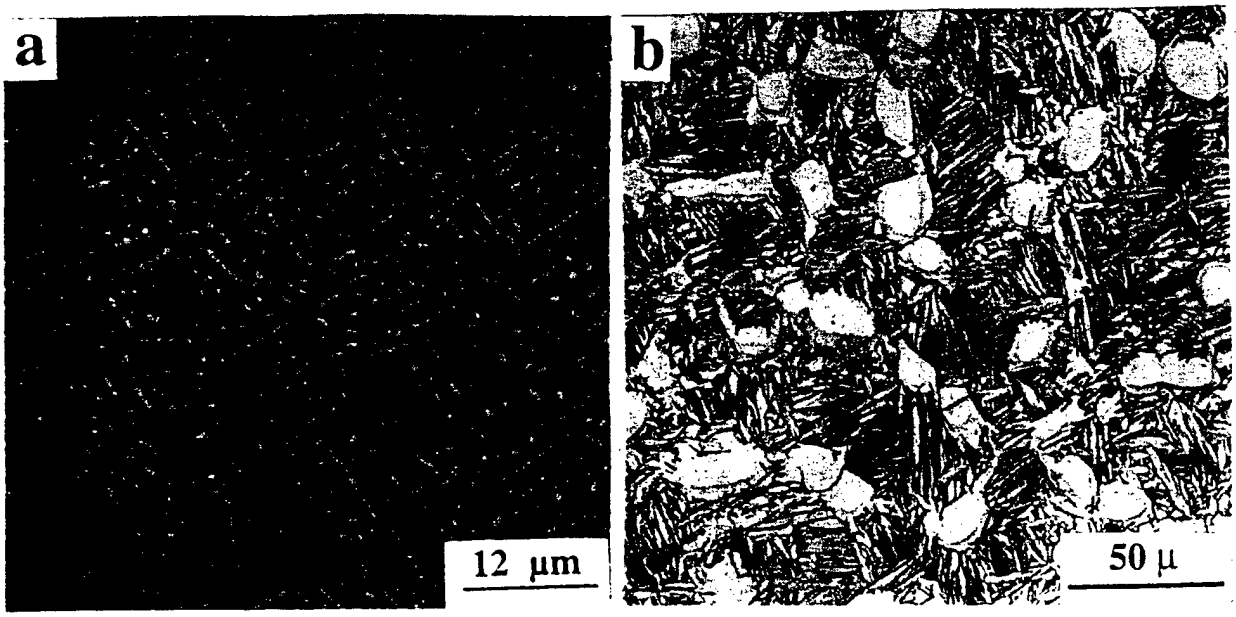

Fig. 1 Microstructures of (a) α-aged Ti-10V-2Fe-3Al and (b) Ti-24Al-11Nb alloy

Fatigue Crack Growth Behavior

Figure 2 illustrates the fatigue crack growth response of α-aged Ti-10V-2Fe-3Al, in terms of da/dN versus ΔK. It can be seen that there is only a very small effect of mean stress or stress ratio on crack growth rates, over most of the crack growth regime. However, at crack growth rates $< 10^{-6}$ mm/cycle, a very small effect of stress ratio is noted. In contrast, the

microstructure in the ω-aged condition showed a strong sensitivity to mean stress, over the entire crack growth regime (Fig. 3)

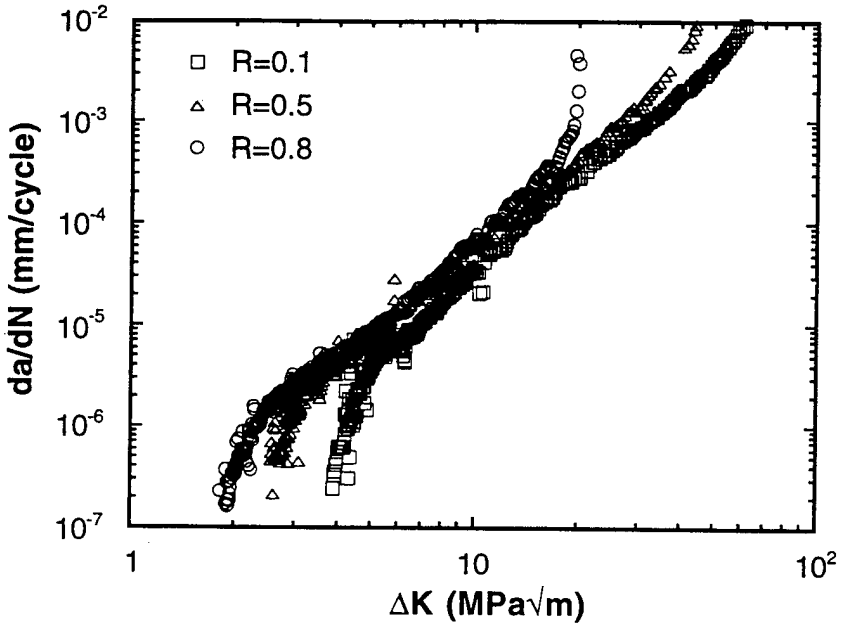

Fig. 2. Fatigue crack growth behavior of α-aged Ti-10V-2Fe-3Al

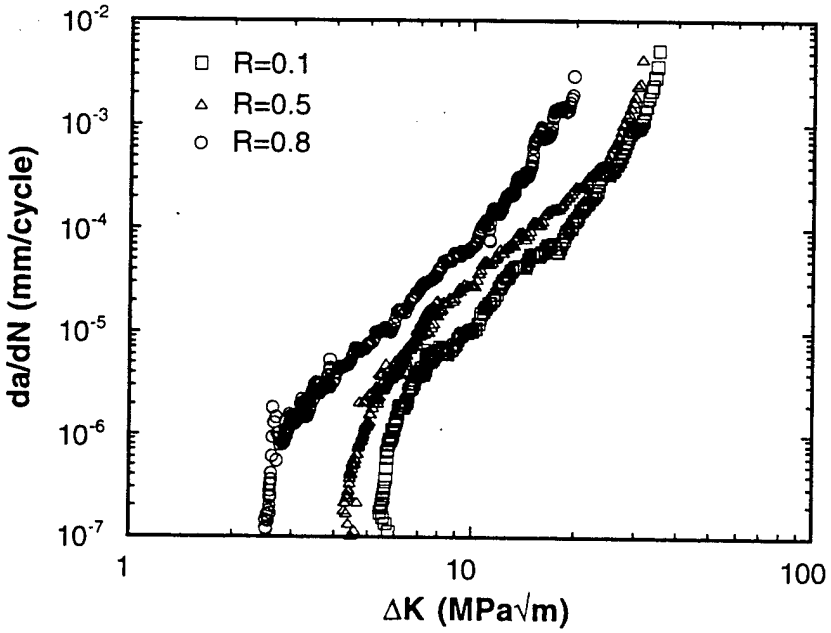

Fig. 3. Fatigue crack growth behavior of ω-aged Ti-10V-2Fe-3Al

Fatigue cracks growth rates for the α+β Ti-6Al-4V alloys are presented in figures 4, and 5 for mill annealed [6] and α+β heat treated [7] microstructures, respectively. Since the data are limited to whatever the growth rate ranges investigated in the original works, a complete comparison among them is difficult. However, from the limited data, it can be seen that there is a small amount of mean stress effect on crack growth rates at low and high ΔK levels. For instance, in the mill annealed microstructure (Fig. 4), the crack growth rates $\leq 10^{-4}$ mm/cycle were strongly dependent on stress ratio. Although in that study no crack closure data were reported, a recent study [13] documented the levels of crack closure at different stress ratios in

Ti-6Al-4V alloy with a different microstructure. It is inferred from the latter study that much of stress ratio effect is due to the occurrence of crack closure at low ΔK levels.

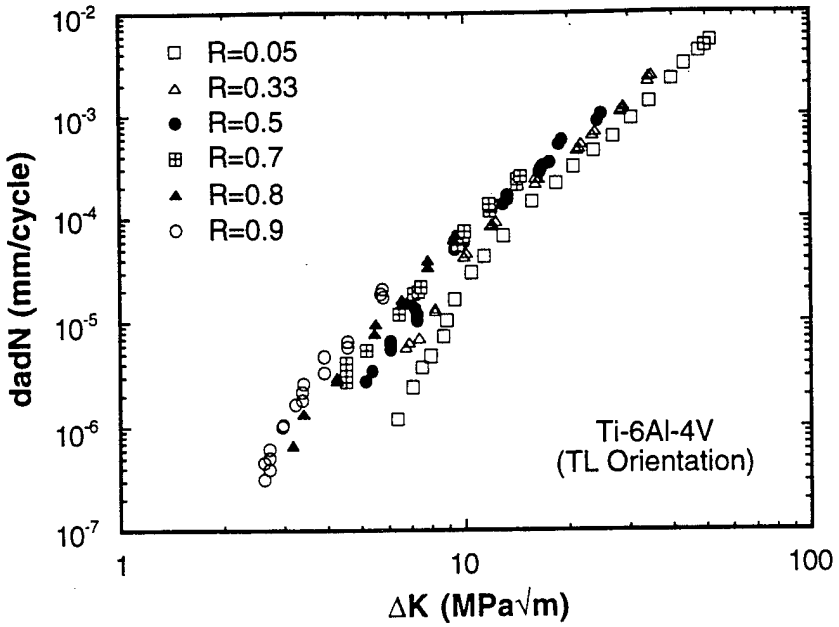

Fig. 4. Fatigue crack growth behavior of mill annealed Ti-6Al-4V [Ref. 6]

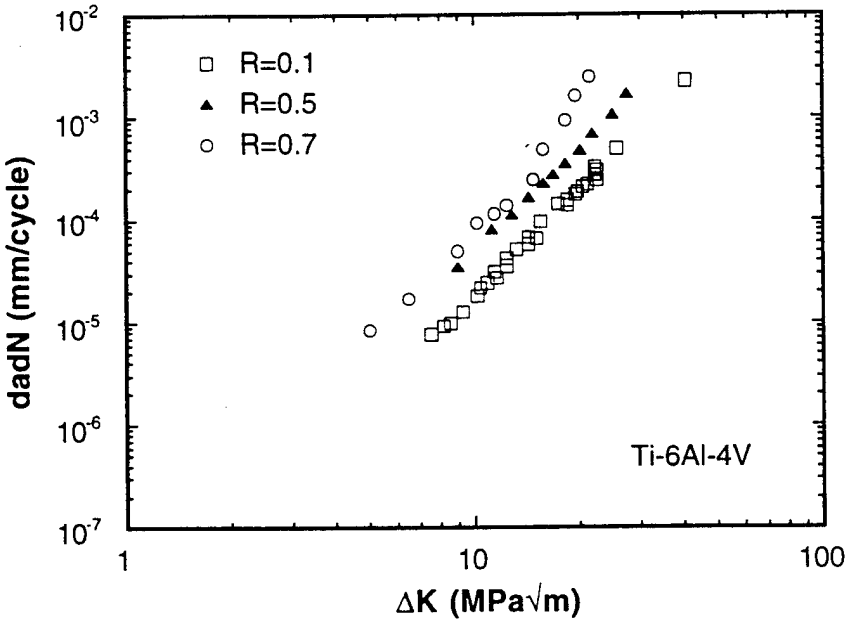

Fig. 5. Fatigue crack growth behavior of α+β heat treated Ti-6Al-4V [Ref. 7]

In Fig. 4, the crack growth rates above 10-4 are only mildly sensitive to stress ratio, and the effect is comparable between the mill annealed and the α+β heat treated microstructures. For example, the ΔK required to maintain a crack growth rate of 10^{-3} mm/cycles are about 31 and 25 MPa√m for R=0.1 and 0.5, respectively in the mill annealed Ti-6Al-4V, whereas they are about 32 and 25 MPa√m for R=0.1 and 0.5 respectively, in the α+β annealed Ti-6Al-4V. These values compare well also with the ΔK values of 32 and 22 for R=0.05 (or 0.125) and R=0.5 respectively, for the near-α titanium alloy, Ti-8Al-1Mo-1V[8] (Fig. 6). It is to be noted that Ti-8Al-1Mo-1V alloy contains more of α-stabilizing element and less of β-stabilizing

elements, therefore, the alloy is expected to have relatively more α, compared to the $\alpha+\beta$ titanium alloy, Ti-6Al-4V.

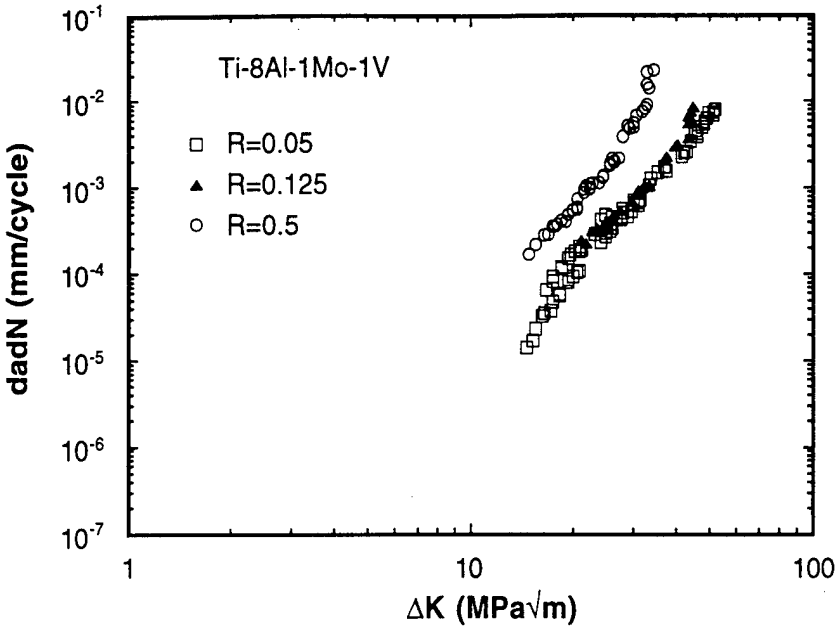

Fig. 6. Fatigue crack growth behavior of Ti-8Al-1Mo-1V alloy [Ref. 8]

It is, therefore, clear that the mean stress dependence of FCG in Ti-6Al-4V and Ti-8Al-1Mo-1V classes of alloys are nearly similar. The mean stress effect at low ΔK is largely promoted by crack closure. However, the small mean stress effect observed at high ΔK levels, appears to be promoted by the static modes of fracture, in addition to the cyclic crack growth.

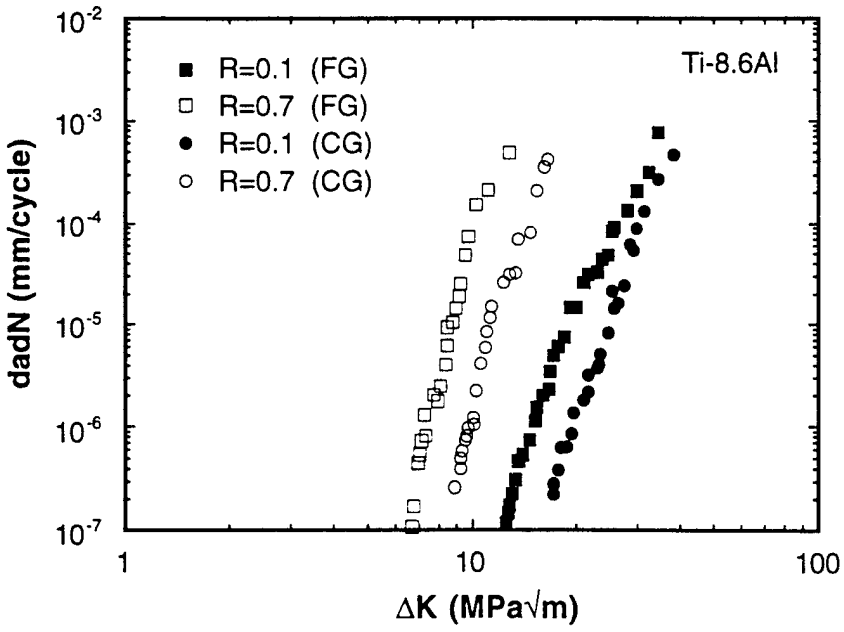

Fig. 7. Fatigue crack growth behavior of equiaxed Ti-8.6Al alloy [Ref. 10]
(FG = Fine Grain size, 30 μm; CG = Coarse Grain Size, 110 μm)

Fatigue crack growth behavior of the nominally single phase Ti-8.6Al alloy, with two grain sizes were studied in Ref. [10]. The data are shown in Fig. 7. Two observations can be made from the data. First, the magnitude of increase in growth rates at a given ΔK, when the stress ratio was increased from 0.1 to 0.7, is roughly the same for both grain sizes. Secondly, all the

da/dN versus ΔK curves show a higher slope compared to that seen for the β (Ti-10V-2Fe-3Al) and α+β (Ti-6Al-4V) and near-α (Ti-8Al-1Mo-1V) alloys. This suggests that for a given change in ΔK, the crack growth acceleration produced in Ti-8.6Al alloy is much higher than that in these alloys.

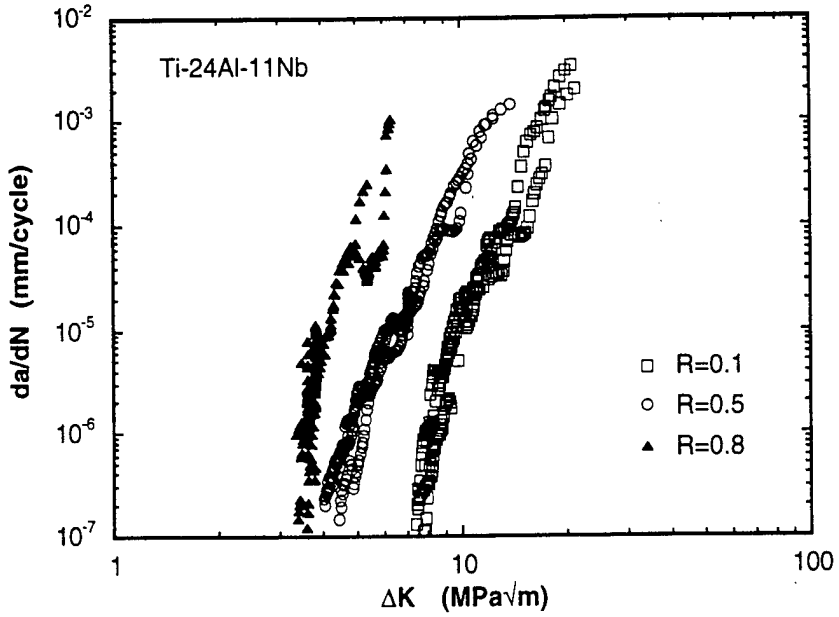

Fig. 8. Fatigue crack growth behavior of Ti-24Al-11Nb titanium aluminide alloy.

Fatigue crack growth behavior of a relatively more brittle titanium aluminide (Ti_3Al) alloy, Ti-24Al-11Nb is presented in Fig. 8. It can been seen that the effect of stress ratio on FCG rates is very stronger than that in the β, α+β, near-α and α alloys considered above. The microstructure of this material consisted of primary α_2 particles embedded in a $\alpha_2+\beta$ matrix (fig. 1b). The amount of β phase in this microstructure was very small (about 10%) [23]. Therefore, the primary phase, α_2 largely controlled the crack growth behavior as well as its dependence on stress ratio.

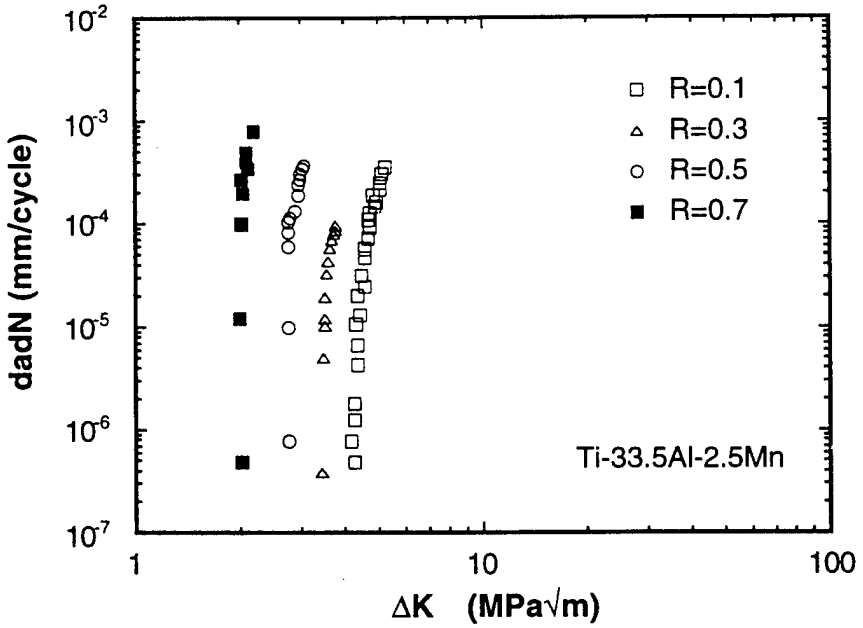

Fig. 9. Fatigue crack growth behavior of Ti-33.5Al-2.5Mn titanium aluminide alloy [Ref. 25]

The effect of stress ratio on FCG rates in the lamellar microstructure of a $\alpha_2+\gamma$ titanium aluminide intermetallic alloy was investigated in Ref. [25]. The brittleness of this alloy is at least comparable or greater that the Ti-24Al-11Nb alloy, as evidenced from the ductility and fracture toughness levels in Table I. The FCG data are presented in Fig. 9. It can be seen that the FCG curves at all stress ratios have very high slopes, suggesting the highest sensitivity of FCG rates to stress ratio, compared to all other alloys discussed here. It can also be inferred from this data that the stable crack growth before catastrophic failure is very limited compared to the other alloys discussed above. In part, this behavior is due to the low fracture toughness of this material (Table I). Similar observations have been reported [26] in investigations on a different alloy in this class.

The Role of Crack Closure on Mean Stress Dependence of Fatigue Crack Growth

It has been well established that the mean stress or stress ratio influences FCG in two primary ways. In the first type, the influence arises as a result of crack closure [13, 20, 27] especially at low ΔK levels, when the cyclic crack tip opening displacements are smaller than the crack wake aspects such as (i) oxide scale thickness (especially in corrosive or high temperature conditions, in the presence of an active environment); (ii) fracture surface roughness (caused by the zigzag nature of crack growth in coarse microstructures exhibiting a significant level of planar slip) and (iii) plastic stretching (largely in relatively low strength and high ductility materials, when tested under plane stress conditions). The second type of mean stress effect arises especially at high ΔK levels, where the crack wake interference is no longer present, but the static fracture modes ahead of the crack tip contributes to the crack advance [28-30]. In particular, this effect was noticed at high R levels in a temper-embrittled microstructure of a high strength steel [28] as well as during corrosion fatigue crack growth of a high strength aluminum alloy [30]. This effect can be identified when crack growth rates at different stress ratios differ from each other, even when plotted in terms of da/dN versus ΔK_{eff}.

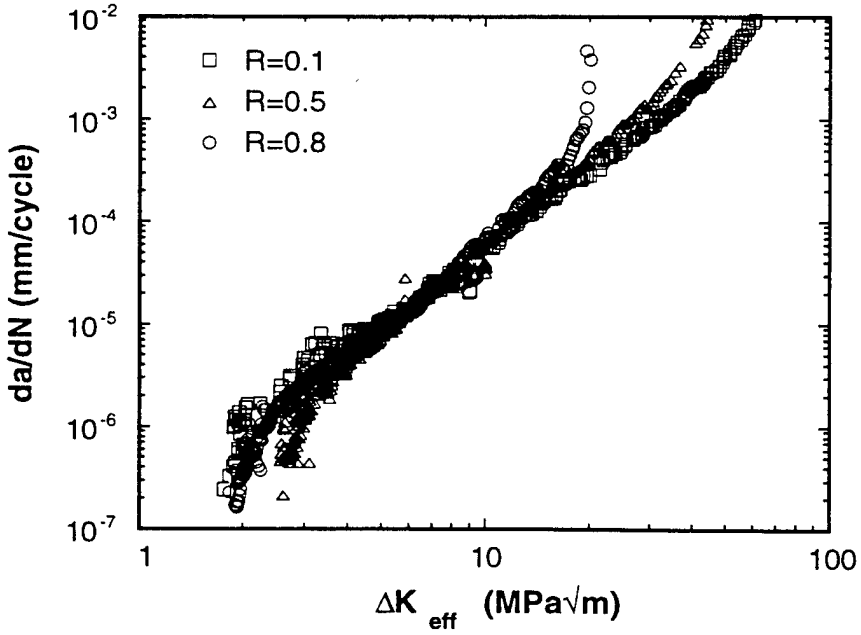

Fig. 10. Fatigue crack growth behavior of α-aged Ti-10V-2Fe-3Al in terms of da/dN versus ΔK_{eff}

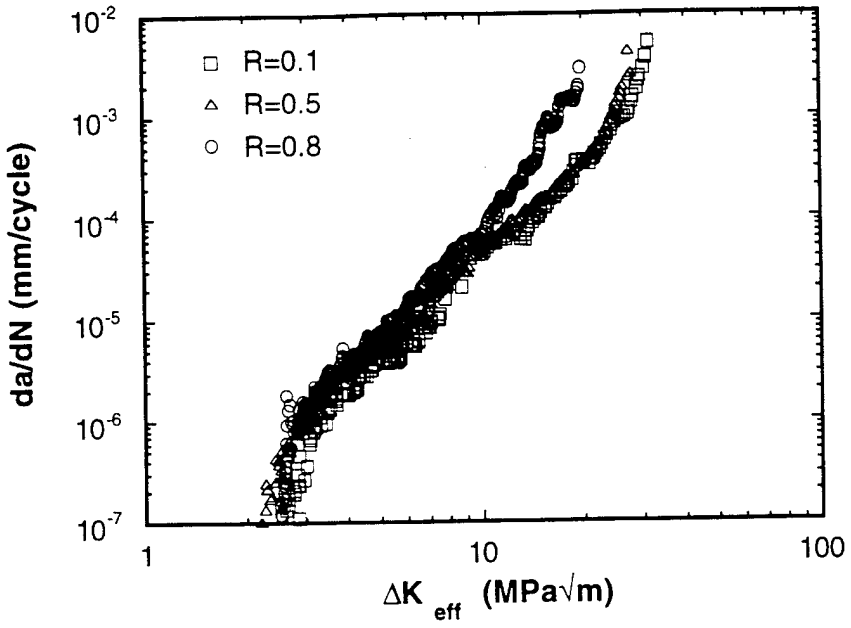

Fig. 11. Fatigue crack growth behavior of ω-aged Ti-10V-2Fe-3Al in terms of da/dN versus ΔK_{eff}

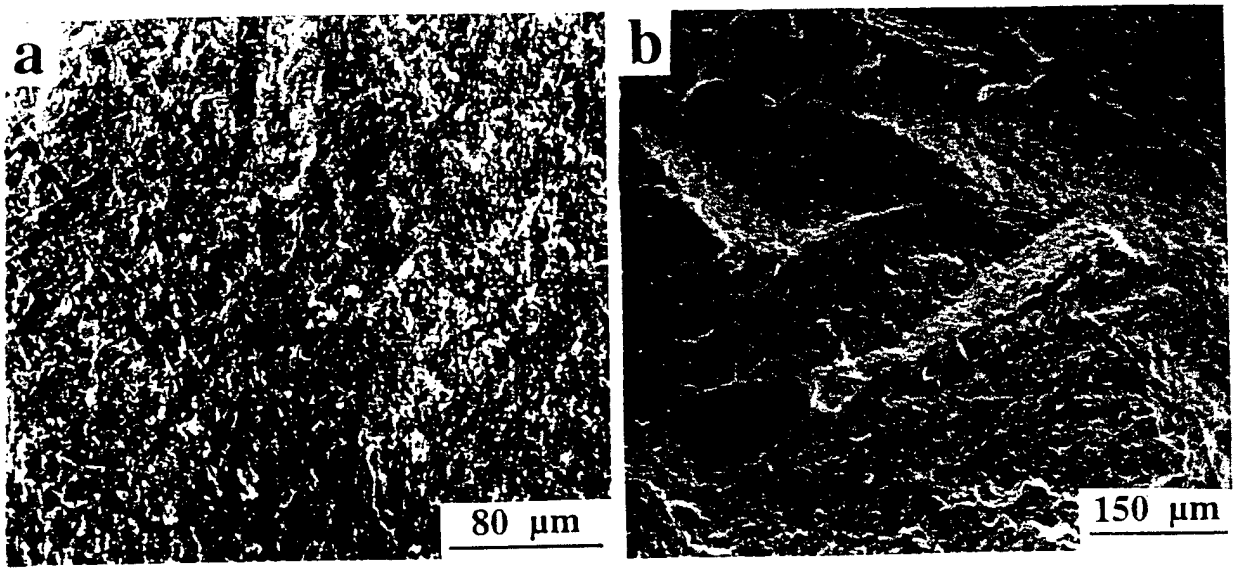

Fig. 12 Mechanisms of fracture during fatigue crack growth in Ti-10V-2Fe-3Al alloys; (a) α-aged and (b) ω-aged microstructure.

In order to differentiate the effects of crack closure and static fracture mode contributions to the stress ratio effect in the titanium alloys considered here, the available data are presented in Figs. 10 through 13 in terms of da/dN versus ΔK_{eff}. Figure 10 illustrates the FCG behavior of α-aged Ti-10V-2Fe-3Al alloy. It can be seen that the FCG rates at all stress ratios are almost the same. A comparison of this data with that in Fig. 2 indicates that the apparent stress ratio effect seen in Fig. 2, although small, is entirely due to crack closure. The very small difference between the FCG rates of R=0.1 and of higher stress ratios, in the near-threshold region is not significant. The interpretation based on crack closure also applies to the ω-aged Ti-10V-2Fe-3Al alloy microstructure as well (Fig. 11). However, in this microstructure, the effect of crack closure on FCG is much higher than that observed in the α-aged Ti-10V-2Fe-3Al alloy

microstructure. The only exception is the relatively higher FCG rates above a growth rate of 10^{-4} mm/cycle in the R=0.8 test data. The K_{max} corresponding to this stage is 50 MPa$\sqrt{m}$, which is very close to the fracture toughness of this material. It is possible that some contribution from static fracture modes occurred during crack growth at this high K_{max} levels, in view of the reduced fracture toughness of the ω-aged microstructure, compared to that of the α-aged (Table I). The topography of fracture is shown in Figs. 12 (a) and (b) for the α-aged and the ω-aged Ti-10V-2Fe-3Al alloy, respectively. The mechanisms of fracture were nearly the same at all ΔK levels in each of the microstructures. It is evident from these figures that the absence of crack closure in the α-aged microstructure is due the relatively flat fracture surface whereas the presence of crack closure in the ω-aged microstructure is due to the rough fracture surface, consistent with the mechanism of roughness induced crack closure in titanium alloys [31].

The Role of Static Fracture Contribution on the Mean Stress Dependence of Fatigue Crack Growth:

The inability of the phenomenon of crack closure in explaining the stress ratio dependence of FCG, in other alloys (Ti-8.6Al and Ti-24Al-11Nb) is illustrated in Figures 13 and 14. Figure 13 shows the FCG data for two grain sizes of Ti-8.6Al alloy, in terms of da/dN versus ΔK_{eff}. It can be seen that even in the absence of the crack closure effect, the FCG curves at R=0.1 and R=0.7 are separated significantly. In the original work [10], this difference in the crack growth behavior due to stress ratio was hypothesized to occur from the differences in slip reversibility. For instance, at low R, a higher ΔK required to maintain a given crack growth could result from the increased slip reversibility along crystallographic planes ahead of the crack tip, simply because the range of ΔK was higher, compared to that at high R. However, the aspect of contribution from static modes of crack extension to crack growth at high R was not suggested. It is plausible that this effect occurred during crack growth at high R in this material, as evidenced by the presence of large percentage of cleavage facets on fracture surfaces of the specimens of a similar material [31].

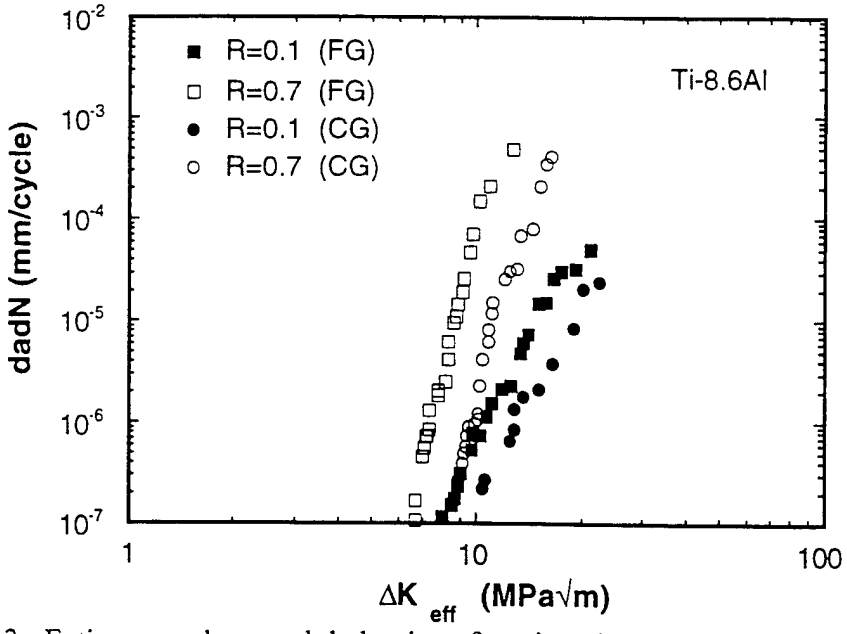

Fig. 13. Fatigue crack growth behavior of equiaxed Ti-8.6Al alloy [Ref. 10] (FG = Fine Grain size, 30 μm; CG = Coarse Grain Size, 110 μm)

Figure 14 illustrates the effect of stress ratio on fatigue crack growth behavior in terms of da/dN versus ΔK_{eff} for the relatively brittle titanium aluminide intermetallic alloy, Ti-24Al-11Nb. A mean stress effect in the da/dN versus ΔK_{eff} behavior, that is quite larger compared to the other materials considered above, is evident. In particular, while the FCG data of R=0.1 and R=0.5 are somewhat closer, the R=0.8 data is significantly separated from these data. Similar effects were observed in other microstructural forms and sizes of the same material [23]. Fracture surface observations (Fig. 15) indicated that the fracture mode was cleavage, with very little evidence of ductility on the fracture surface. This is consistent with the very low ductility of the material (Table I). It is therefore suggested the accelerated crack growth at high stress ratios is due to the increased contribution from static mode of crack extension, in addition to cyclic crack growth.

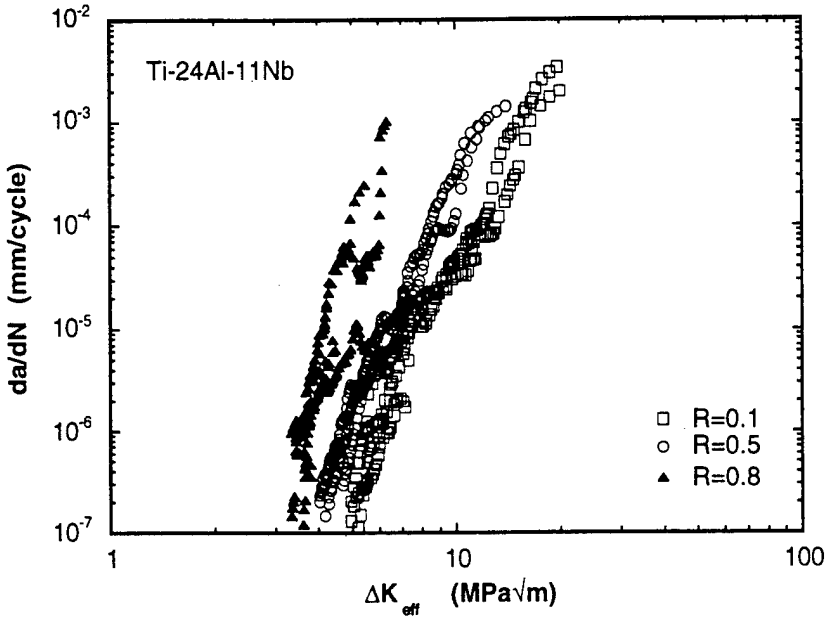

Fig. 14. Fatigue crack growth behavior of equiaxed Ti-24Al-11Nb alloy.

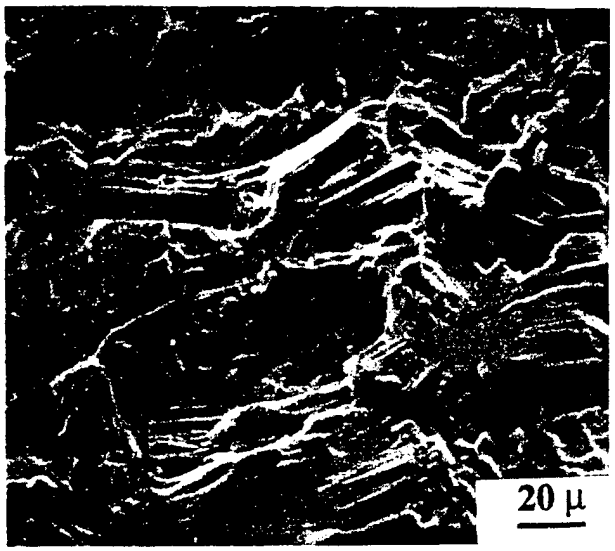

Fig. 15 Mechanism of fracture during fatigue crack growth in Ti-24Al-11Nb alloy

Relationship Between Alloy Type and Mean Stress Effect

The relationship between alloy type and the mean stress dependence of FCG brought about by the mechanisms other than "crack closure" can be understood by either comparing the low R crack growth data in terms of da/dN versus ΔK_{eff} or by evaluating the high R data, which is independent of crack closure. Figures 16 and 17 illustrate the comparisons of available FCG data in terms of ΔK_{eff} for R=0.1 and in terms of ΔK for R=0.7-0.8, respectively. The data are presented as a function of $\Delta K^2/E$, where E is the elastic modulus of the material. This parameter is equivalent to the "strain energy release rate range, ΔG," and provides a common basis for comparison of behavior of materials with different elastic modulus values. The normalization of ΔK with E was employed [32] to show that fatigue crack growth of different metallic systems, in the Paris-Law regime simply differed according to the respective elastic characteristics of the material, consistent with the principles of linear elastic fracture mechanics.

Both the data presented in Figures 16 and 17 indicate that the slopes of da/dN versus ΔK (or ΔK_{eff}) curves generally increase with a decrease in the "macroscopic ductility" of the material as measured in tension or the fracture toughness. In particular, FCG behavior of the β and $\alpha+\beta$ alloys are almost the same at R=0.7-0.8. This suggests that there is no difference in crack growth between them as caused by the static modes of crack extension. Therefore, these can be identified as materials that do not show the mean stress effect by the static-fracture mode contribution during crack growth. On the other hand, the FCG behavior of alloys: Ti-8.6Al, Ti-24Al-11Nb and Ti-33.5Al-2.5Mn appear to form a different group, in that, the slope of the da/dN versus ΔK curves as well as growth rates for a given ΔK increase with alloys in that order. The alloys in this group are generally known [33, 34] to exhibit significantly different deformation behavior, compared to the group of β and $\alpha+\beta$ titanium alloys. The major difference arises from the crystallographic, microstructural and deformation characteristics of these alloys. For instance, the Ti-8.6Al alloy has been known [33] to exhibit planar slip, due to the presence of "short-range-order" involving Ti_3Al particles. The tendency for planar slip is even higher for the Ti-24Al-11Nb alloy, due to its ordered DO_{19} crystal structure, where deformation is mainly known to occur by superdislocations, localized to narrow bands [34]. In the case of Ti-33.5Al-2.5Mn alloy, although the microstructure is two phase ($\alpha_2+\gamma$), the intrinsic ductility of γ phase is very limited [35]. Therefore, in these alloy systems, the relaxation of crack tip stress is very limited and the deformation is limited to narrow localized slip bands. Further, because of the limited homogeneous deformation, these alloys also show an increased susceptibility to brittle fracture by cleavage during fatigue crack growth [36]. Under these conditions, the laboratory air environment at room temperature can increase the rate of fatigue crack growth. In fact, alloys similar to Ti-24Al-11Nb and Ti-33.5Al-2.5Mn in terms of phase content are known [37, 38] to exhibit either frequency-dependent FCG behavior or crack growth at constant load in room temperature laboratory air. This suggests that a high planarity of slip and the presence of a modest embrittling environment such as moist laboratory air can lead to crack extension under constant load. This mechanism is applicable to the FCG at high mean stress levels in these alloy system. Although this phenomenon is also commonly observed in conventional titanium alloys as well [39, 40], it appears that the intensity of it is much higher in the alloys: Ti-8.6Al, Ti-24Al-11Nb and Ti-33.5Al-2.5Mn. Because the average static "K" (K_{mean}) at high R is higher, static crack extension can be expected to occur, in addition to the cyclic crack extension produced by the cyclic stress intensity range (ΔK). The

increase in the slope of the da/dN versus ΔK curves, the sensitivity to mean stress and the cleavage fracture mode accompanying crack extension is consistent with this mechanism.

It is not clear how the static and cyclic modes of crack advance occurs at the same time. It is also not clear whether crack growth occurs cycle by cycle or after the accumulation of a specified number of cycles. Further, the question of what parts of the loading cycle cause the static and cyclic crack extensions during fatigue crack growth is yet to be resolved.

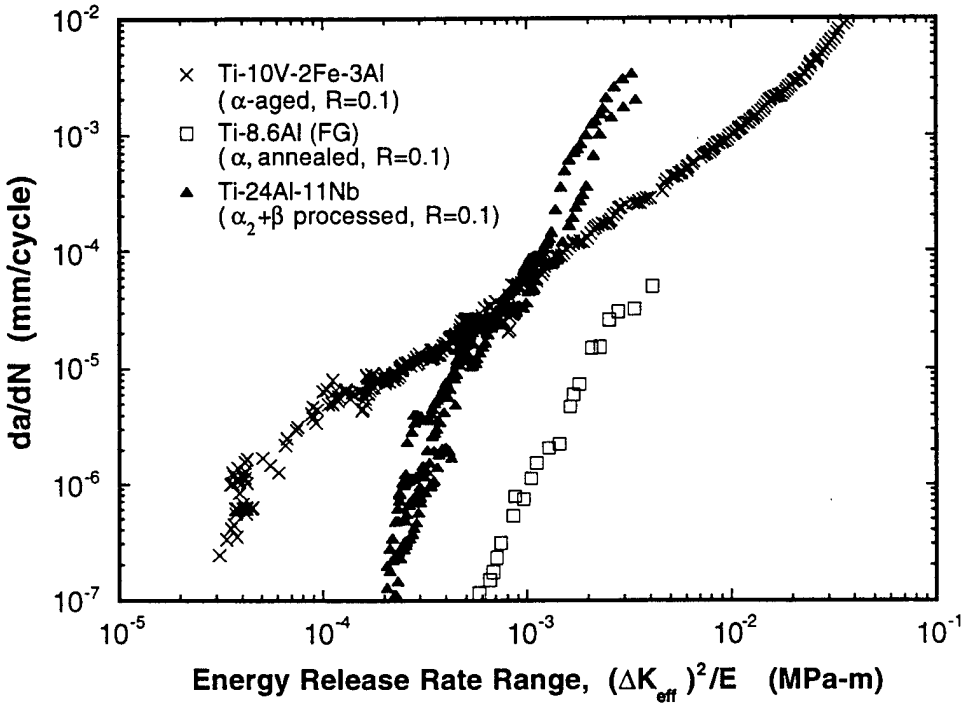

Fig. 16 Fatigue crack growth behavior at low stress ratio, R=0.1 plotted in terms of "effective (closure-free)" strain energy release rate range.

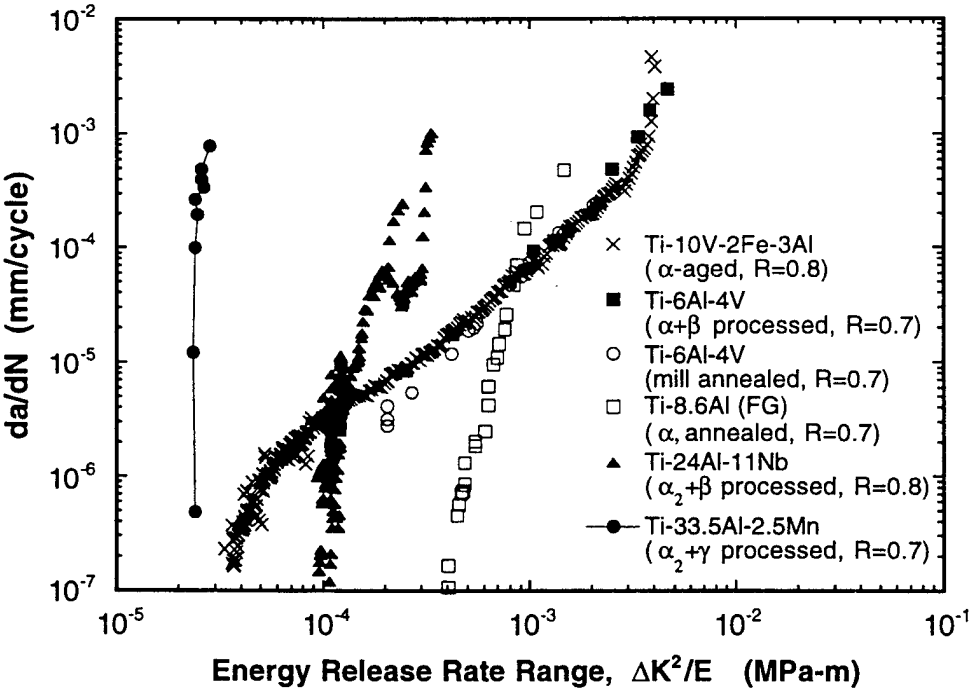

Fig. 17 Fatigue crack growth behavior at high stress ratios, R=0.7-0.8, plotted in terms of strain energy release rate range.

SUMMARY

From an overview of the literature data on fatigue crack growth behavior as a function of stress ratio, in the light of our work on some titanium alloys, the following observations can be made.

1. A significant part of the mean stress effect at relatively low ΔK levels are brought about by the mechanism of crack closure. Crack closure is responsible for this effect, whether or not a given alloy shows a susceptibility to static-mode cracking. Fracture surface roughness, promoted by the planar slip deformation characteristics appears to be largely responsible for this effect.

2. The presence or absence of crack closure, seem to depend on largely the microstructural condition of the alloy, as typified by the β alloy: Ti-10V-2Fe-3Al. A very low level of crack closure in the α-aged condition and a high level of crack closure in the ω-aged condition, resulted in weak and strong mean stress dependence of fatigue crack growth, respectively.

3. From the perspective of mean stress effect at high ΔK levels, brought about by the contributions from static-mode of crack extension, it is possible to group the alloys into two categories. In the first, the alloys belonging to the β and $\alpha+\beta$ class, with microstructures exhibiting relatively homogeneous deformation characteristics, show only a very small sensitivity to mean stress effect brought about by the static modes of crack extension. In the second, alloys (high α, α_2 and $\alpha_2+\gamma$) that either show a high degree of planar slip and/or macroscopically brittle behavior show a very high sensitivity to mean stress brought about by this mechanism. This is reflected from the increases in the slopes of the fatigue crack growth curves, corresponding to decreases in the macroscopic ductility or fracture toughness.

REFERENCES

1. J. K. Gregory, Handbook of Fatigue Crack Propagation in Metallic Structures, edited by A. Carpinteri, Elsevier Science B.V., 1994, p. 281
2. J. C. Chesnutt and J. A. Wert, Proc. Int. Symp. Fatigue Crack Growth Threshold Concepts, Edited by D. L. Davidson and S. Suresh, TMS-AIME, Warrendale, PA 1983, p. 83.
3. C. W. Brown and G. C. Smith, Proc. 1st Int. Conf. Fatigue Thresholds, edited by J. Backlund, A. F. Blom and C. J. Beevers, EMAS Publications Ltd., Vol. 1, 1981, p. 329
4. G. R. Yoder, L. A. Cooley and T. W. Crooker, Proc. 2nd Int. Conf. Fatigue and Fatigue Thresholds, edited by C. J. Beevers, EMAS Publishers Ltd., Vol. 1, 1984, p. 351
5. K. S. Ravichandran, Acta Metall., Vol. 39, 1991, p. 401
6. J. H. FitzGerald, Journal of Testing and Evaluation, Vol. 2, 1977, p. 343
7. A. Yuen, S. W. Hopkins, G. R. Leverant and C. A. Rau, Metallurgical Transactions, vol. 5, 1974, p. 1833
8. R. J. Bucci and P. C. Paris, Journal of Materials, Vol. 7, 1972, p. 402
9. M. A. Hicks, R. H. Jeal and C. J. Beevers, Fat. Engng. Mater. Struct., 6 (1983) 51.
10. G. T. Gray III and G. Lutjering, Proc. 2nd Int. Conf. on Fatigue and Fatigue Thresholds, edited by C. J. Beevers, EMAS Ltd., Vol. II, 1984, p. 707
11. J. L. Robinson and C. J. Beevers, Metal Science Journal, Vol. 7, 1973, p. 153

12. W. J. Evans and A. W. Beale in Proc. of Int. Conf. on Forging and Properties of Aerospace Materials, The Metals Society, 1997, p. 170
13. S. Dubey, A.B.O. Soboyejo and W. O. Soboyejo, Acta Materialia, Vol. 45, 1997, p. 2777
14. A. L. Dowson, A. C. Holis and C. J. Beevers, Int. J. Fatigue, Vol. 14, 1992, p. 261
15. J. K. Gregory and L. Wagner, Proc. 4th Int. Conf. Fatigue and Fatigue Thresholds, edited by H. Kitagawa and T. Tanaka, Vol. I, 1990, p. 191
16. D. L. Davidson and J. Lankford, Metallurgical Transactions, Vol. 15A, 1984, p. 1931
17. D. B. Dawson and R. M. N. Pelloux, Metallurgical Transactions, Vol. 5, 1974, p. 723
18. R. I. Jaffee and G. Lutjering in Microstructure and Fatigue Crack Growth in Titanium Alloys, edited by J. C. Chesnutt, A. K. Chakraborty, TMS-AIME, 1987, p. 193
19. A. W. Sommer and F. H. Froes and D. Eylon in Proc. 5th Int. Conf. Titanium, edited by G. Lutjering, U. Zwicker and W. Bunk, Vol. 4, 1984, p. 2235
20. S. Suresh and R. O. Ritchie, Small Fatigue Cracks, edited by R. O. Ritchie and J. Lankford, The Metallurgical Society, Warrendale, PA, 1986, p. 227
21. M. Peters, K. Welpmann and H. Doker, Proc. 5th Int. Conf. on Titanium, edited by G. Lutgering et. al., Vol. IV, 1985, p. 2267
22. S. K. Jha and K. S. Ravichandran, this volume
23. K. S. Ravichandran, Unpublished Research, University of Utah, 1998
24. J. Lindemann and L. Wagner, Mat. Sci. Engng., Vol. A234-236, 1997, p. 1118
25. H. Mizukoshi and K. Shibue, Journal of the Japan Institute of Metals, Vol. 56. 1992, p. 342
26. J. M. Larsen, B. D. Worth, S. J. Balsone, A. H. Rosenberger and J. W. Jones, Fatigue'96, Proc. Int. Conf. on Fatigue and Fatigue Thresholds, Vol. III, Elsevier Science Ltd., Oxford. U.K., 1996, p. 1719
27. J. K. Gregory and L. Wagner, Fatigue'90, Prof. 4th Int. Conf. on Fatigue and Fatigue Thresholds, Edited by H. Kitagawa and T. Tanaka, Vol. I, 1990, p. 191
28. R. O. Ritchie and J. F. Knott, Acta Metall., Vol. 21, 1974, p. 639
29. R. O. Ritchie and J. F. Knott, Mater. Sci. Engng., Vol. 14, 1974, p. 7
30. J. C. Radon, Metal Science, Vol. 13, 1979, p. 411
31. M. D. Halliday and C. J. Beevers, J. Testing and Evaluation, Vol. 9, 1981, p. 195
32. J. M. Larsen, PhD thesis, Department of Metallurgical Engineering and Materials Science, Carnegie-Mellon University, PA, 1987
32. P. K. Liaw, T. R. Leax and W. A. Logsdon, Acta Metall., Vol. 31, 1983, p. 1581
33. J. E. Allison and J. C. Williams Proc. 5th Int. Conf. Titanium, edited by G. Lutjering, U. Zwicker and W. Bunk, Vol. 4, 1984, p. 2243
34. D. Banerjee, A. K. Gogia, T. K. Nandy, K. Muraleedharan and R. S. Mishra, in Structural Intermetallics, edited by R. Darolia, J. J. Lewandowski, C. T. Liu, P. L. Martin, D. B. Miracle and M. V. Nathal, The Metallurgical Society of AIME, Warrendale, PA, 1993, p. 19.
35. Y. W. Kim, JOM, Vol. 41, 1989, p. 24
36. B. D. Worth, J. M. Larsen, S. J. Balsone and J. W. Jones, Metall. Trans., Vol. 28A, 1997, p. 825
37. P. B. Aswath and S. Suresh, Metall. Trans., Vol. 22A, 1991, p. 817
38. R. Gnanamoorthy, Y. Mutoh and Y. Mizuhara, Mater. Sci. Engng., Vol. A203, 1995, p. 348
39. D. A. Meyn, Metallurgical Transactions, Vol. 5, 1974, p. 2405
40. G. R. Yoder, C. A. Griffis and T. W. Crooker, Trans. ASME, J. Engng. Mater. Tech., October 1974, p. 268